

**Trace element mineral analysis in high pressure
metamorphic rocks from Trescolmen,
Central Alps**

Dissertation
zur Erlangung des Doktorgrades
der Mathematisch-Naturwissenschaftlichen Fakultäten
der Georg-August-Universität zu Göttingen

vorgelegt von
Thomas Zack
aus Bremen

Göttingen 1999

D7

Referent:

Priv. Doz. Dr. Stephen F. Foley

Korreferent:

Prof. Toby Rivers

Tag der mündlichen Prüfung:

27. Januar 2000

Summary	3
Zusammenfassung	5
Chapter 1. Introduction	8
1.1 Geology of the study area	8
1.2 Structure of thesis	11
Chapter 2. Fluid infiltration at 2.0 GPa in eclogites from Trescolmen: Constraints from Cs-Rb-Ba systematics in phengite and amphibole	12
2.1 Introduction	12
2.2 Evidence for fluid infiltration under eclogite facies conditions	13
2.3 Analytical techniques	15
2.4 Results	19
2.5 Discussion	21
2.5.1 <i>Protolith constraints from LIL element concentrations</i>	21
2.5.2 <i>Fluid exchange between eclogites and metapelites</i>	24
2.5.3 <i>Implications for subduction zone environments</i>	26
2.6 Conclusions	28
2.7 Appendix to Chapter 2	29
Chapter 3. Trace element abundance in eclogitic rutile	30
3.1 Introduction	30
3.2 Analytical procedures	31
3.2.1 <i>Electron microprobe</i>	31
3.2.2 <i>Laser ablation microprobe</i>	34
3.3 Evaluation of results	35
3.3.1 <i>Mass balance calculation for eclogite sample 50-13</i>	37
3.3.2 <i>Element ratios for eclogite 50-13</i>	40
3.3.3 <i>Comparison of element ratios between rutile und whole rock</i>	41
3.4 Applications	42
3.4.1 <i>Provenance constraints by single grain analyses of detrital rutiles</i>	42
3.4.2 <i>Role of rutile in subduction zones</i>	44

Chapter 4. Evaluating hydrous eclogites from Trescolmen for their use of deriving trace element partitioning values for subduction zone modelling	47
4.1 Introduction	47
4.2 Analytical methods	48
4.3 Whole rock geochemistry	50
4.4 Mineral chemistry	54
4.4.1 <i>Clinopyroxene</i>	56
4.4.2 <i>Garnet</i>	61
4.4.3 <i>Zoisite, clinozoisite and allanite</i>	62
4.4.4 <i>Other hydrous phases (amphibole, phengite, paragonite, talc, apatite)</i>	63
4.5 Mass balance calculations	64
4.6 Mineral/mineral partitioning systematics	67
4.6.1 <i>Evaluating the use of samples for trace element equilibration studies</i>	67
4.6.2 <i>Trace elements buffered by single phases</i>	73
4.6.3 <i>Amphibole/clinopyroxene partitioning</i>	74
4.6.4 <i>Zoisite/clinopyroxene partitioning</i>	77
4.6.5 <i>Mineral/clinopyroxene partitioning of other hydrous phases</i>	78
4.7 Mechanisms of trace element equilibration	80
4.7.1 <i>Equilibration processes</i>	80
4.7.2 <i>Reasons for lack of trace element equilibration</i>	80
4.8 Concluding remarks	82
Chapter 5. References	84
Acknowledgments	94
Lebenslauf	95

Summary

This study focuses on the trace element behaviour in high pressure metamorphic rocks. The eclogite locality Trescolmen in the Adula Nappe was found to be an ideal natural laboratory that preserves a wealth of information about former conditions under high pressure. The specific question was to derive key parameters for the trace element behaviour during dehydration reactions operating in subducting oceanic crust (residence sites of various trace elements, partition coefficients between high pressure phases, processes influencing trace element mobility). Of broader interest is the question how the advent of an analytical technique (here laser ablation ICP-MS) opens up new applications in different fields of the geosciences.

Representative eclogites and surrounding metapelites from Trescolmen were investigated by optical microscopy (phase determination, textural information, selection of phases for trace element analysis), XRF, solution-ICP-MS and whole rock laser ablation-ICP-MS (all three methods for whole rock analysis), electron microprobe (high contrast backscattering imaging, major and trace element quantitative analysis, thin section element mapping) and laser ablation ICP-MS (cleaning procedures for thin section analysis, defocussed laser beam for chalcophile and siderophile elements, He as carrier gas for light element analysis). Special attention was taken to test and optimize analytical procedures for the measurement of a range of trace elements (Li, Be, B, Rb, Sr, Y, Zr, Nb, Mo, Sn, Sb, Cs, Ba, Ce, Nd, Sm, Hf, Ta, W, Pb, Th, U) in different metamorphic phases (clinopyroxene, garnet, amphibole, phengite, paragonite, zoisite, clinozoisite, talc, apatite, rutile).

It was found that eclogites from Trescolmen have major and trace element whole rock signatures comparable to mid ocean ridge basalts (MORB) and even span the whole range of chemical variety observed in these rock types, from Mg-rich gabbroic protoliths to Fe and Ti-rich basalts. Therefore these samples can be used as direct analogues of the uppermost basaltic layer of subducting oceanic crust. Furthermore phengites in the eclogites preserve Cs-Rb-Ba pattern possibly imprinted on the protoliths by a low temperature sea floor alteration. A geological scenario for the Adula Nappe in an advanced continental rifting environment has been developed where the geochemical findings of this study are combined with the close association of eclogites with continental metasediments and the lack of ultramafic rocks in the northern and middle Adula Nappe.

Petrographic observation and backscattered imaging reveal a rich inventory of textural relationships indicating the infiltration of H₂O-rich fluids during the early stages of uplift, still under eclogite-facies conditions. Here, fluids lead to the formation of hydrous phases like paragonite replacing kyanite and amphibole overgrowing an older generation of eclogite-facies minerals. Additionally, the formation of large, homogeneous omphacite is best explained by mass transfer processes which are characteristic for a free fluid. Healed cracks in garnet cores with a chemical composition identical to eclogite-facies garnet rims are also strong evidence for the existence of a free fluid that caused hydrofracturing in garnets.

A number of trace elements exhibit a strong preference for certain phases in eclogites so that only one minor or accessory phase can dominate the budget of various trace elements in a whole rock. The most extreme examples where more than 70% of the whole rock budget is accommodated in one phase are found to be Cs, Rb and Ba in phengite, Ti, Nb, Sb, Ta and W in rutile, Zr and Hf in zircon, Y and heavy rare earth elements (HREE) in garnet as well as Sr, light rare earth elements (LREE), Pb, Th and U in zoisite (or allanite, if present).

A subsuite of four eclogite samples was discovered to show a close approach towards equilibrium both for major as well as trace elements, demonstrated by large, homogeneous crystals and consistent trace element partition coefficients between all high pressure phases. For the interpretation of trace element distribution in high pressure rocks it is an important finding that all four samples are foliated eclogites that have a chemical signature of basalts whereas samples with the clearest signs of trace element disequilibrium are recorded in massive metagabbroic eclogites. Therefore a fine-grained or even glassy protolith and a thorough deformation are the most important prerequisites for the approach of trace element equilibrium in metamorphic rocks. A free fluid during metamorphism is probably also an important parameter, but without deformation not a sufficient criterion.

All results in this study are evaluated in the light of their implications for the understanding of subduction zone processes. It is now possible to realistically model the trace element composition of fluids liberated from dehydrating subducting slabs. In earlier attempts only the fluid composition in equilibrium with major phases in eclogite parageneses have been calculated. Since this study shows the importance of minor and accessory phases for the trace element balance in eclogites (e.g. Ba in phengite, Sb in rutile, Pb in zoisite), the earlier models must be extended by including these phases. It can be reached in taking trace element partition coefficients from eclogites demonstrating equilibrium parageneses as found in the four samples of this study. If and how fluids can be transferred from the subducting oceanic crust into the overlying mantle wedge is an ongoing controversy. Eclogite samples from Trescolmen show clear evidence for the existence of a free moving fluid under high pressure conditions, therefore ruling out the possibility of fluid immobility in eclogites as assumed from oxygen isotope studies. The favoured process promoting fluid mobility and enhancing trace element equilibration is the operation of continuous or discontinuous deformation, which can be assumed to exist between the subducting oceanic crust and the overlying mantle.

The results of this study allow conclusions beyond the field of high pressure metamorphic rocks. It is demonstrated that the highly fluid-mobile elements Cs, Rb and Ba have concentrations in high pressure phases that can be best explained by very low amounts of fluid-rock interactions. This is significant with respect to the fact that highly sensitive Cs-Rb-Ba systematics can be used to detect episodes of low amounts of fluid throughflux in rocks that did not show any recordable evidence when analyzed with the less sensitive oxygen isotope method. Applications in the area of ore deposit exploration are therefore possible where low amounts of fluid throughflux need to be detected. Furthermore it was found that trace element concentrations in rutile of eclogites and metapelites have significant differences. Under sedimentary conditions, rutile is known to be a very stable mineral, but was not seen to be very characteristic. The analysis of trace elements in rutile of heavy mineral concentrates has now the prospect that specific source areas of sediments can be worked out on this basis, which is an important question in the area of petroleum geology.

Zusammenfassung

Diese Studie befaßt sich mit der Spurenelementverteilung in metamorphen Hochdruckgesteinen. Die Eklogitlokalität Trescolmen (Adula Decke) ist ein ideales natürliches Laboratorium, das eine Vielzahl an Informationen über ihre zurückliegenden Hochdruckbedingungen konserviert hat. Im engeren Sinne war das Ziel dieser Arbeit, Schlüsselfragen über das Spurenelementverhalten bei Dehydrierungsreaktionen in subduzierenden Ozeanplatten zu beantworten (z.B. die Aufenthaltsorte verschiedener Spurenelemente in verschiedenen Mineralphasen, die Verteilungskoeffizienten zwischen Hochdruckphasen, welche Prozesse beeinflussen die Spurenelementmobilität). Im weiteren Sinne war die Frage von Interesse, wo die Einführung einer Analysenmethodik, in diesem Fall die Laser Ablations ICP-MS, neue Anwendungen in den verschiedenen Bereichen der Geowissenschaften eröffnet.

Repräsentative Proben von Eklogiten und den umgebenden Metapeliten aus dem Gebiet von Trescolmen wurden untersucht mittels: optischer Mikroskopie (Phasenbestimmung, Texturinformation, Auswahl der Phasen für die Spurenelementuntersuchung), RFA, Lösungs-ICP-MS, Gesamtgesteins-Laser Ablation-ICP-MS (die letzten drei Methoden dienen der Gesamtgesteinsanalyse), Elektronen Mikrosonde (hochauflösende Rückstreuelektronenbilder, quantitative Analyse von Haupt- und Spurenelementen, Elementverteilung in kompletten Dünnschliffen) und Laser Ablation-ICP-MS (unter Beachtung besonderer Reinigungsschritte für Analysen an Dünnschliffen, Benutzung eines defokussierten Laserstrahls für siderophiler und chalkophiler Elemente, Einsatz von He als Trägergas bei der Analyse leichter Elemente). Besondere Aufmerksamkeit galt dabei dem Testen und Optimieren von analytischen Methoden, die der Messung einer Vielzahl von Spurenelementen (Li, Be, B, Rb, Sr, Y, Zr, Nb, Mo, Sn, Sb, Cs, Ba, Ce, Nd, Sm, Hf, Ta, W, Pb, Th, U) in verschiedenen metamorphen Phasen dienen (Klinopyroxen, Granat, Amphibol, Phengit, Paragonit, Zoisit, Klinozoisit, Talk, Apatit, Rutil).

Es stellte sich heraus, daß Eklogite aus Trescolmen Haupt- und Spurenelementkonzentrationen aufweisen, die vergleichbar sind mit Mittelozeanischen Rückenbasalten (MORB) und die somit die gesamte chemische Variation dieser Gesteine nachzeichnen, von Mg-reichen gabbroischen Protolithen bis hin zu Fe- und Ti-reichen Basalten. Daher können diese Proben als direkte Analoge der obersten basaltischen Schicht einer subduzierenden Ozeankruste angesehen werden. Weiterhin hat sich gezeigt, daß Phengite in den Eklogiten Cs-Rb-Ba Muster aufweisen, die möglicherweise den Protolithen während einer Niedrigtemperatur-Ozeanboden-Metamorphose aufgeprägt wurden. Für die nördliche und mittlere Adula-Decke ist es zum einen bemerkenswert, daß ultramafische Gesteine nahezu vollständig fehlen, und zum anderen, daß Eklogite in enger Beziehung zu kontinentalen Metasedimenten vorkommen. Diese Phänomene wurden in Einklang gebracht mit den geochemischen Resultaten dieser Studie und daraus ein geologisches Szenario der Adula-Decke in einem fortgeschrittenen kontinentalen Dehnungsbereich entwickelt.

Petrographische Beobachtungen und Rückstreuelektronenbilder erschließen ein reichhaltiges Inventar von strukturellen Beziehungen, welche eine Infiltrierung der Eklogite durch H₂O-reicher Fluide während eines frühen Hebungstadiums der Adula-Decke, noch unter Hochdruckbedingungen, dokumentiert. Hierbei führen diese Fluide zur Bildung wasserhaltiger Phasen wie Paragonit, der Disthen ersetzt, und Amphibol, der eine ältere Generation von eklogitfaziellen Mineralen überwächst. Weiterhin wird die Bildung großer, homogener Omphazite am besten durch

Massentransferprozesse erklärt, die charakteristisch sind für ein freies Fluid. Geheilte Risse in Granatkernen mit einer identischen chemischen Zusammensetzung wie eklogitfazielle Granatränder sind auch ein deutlicher Hinweis auf die Existenz eines freien Fluides.

Eine Anzahl von Spurenelementen zeigt eine starke Präferenz für bestimmte Phasen in Eklogiten, so daß nur ein akzessorisches Mineral das Budget verschiedener Spurenelemente dominieren kann. Die extremsten Beispiele, bei denen mehr als 70% des Gesamtgesteinsbudgets in einer Phase angereichert sind, stellen Cs, Rb und Ba in Phengit, Ti, Nb, Sb, Ta und W in Rutil, Zr und Hf in Zirkon, Y und schwere Selten Erden Elemente (HREE) in Granat sowie Sr, leichte Selten Erden Elemente (LREE) Pb, Th und U in Zoisit (oder Allanit, sofern vorhanden) dar.

Eine Gruppe von vier Eklogitproben wurde gefunden, die eine große Annäherung an Gleichgewichtsbedingungen sowohl auf Haupt- als auch auf Spurenelementniveau aufzeigen, dokumentiert durch große, homogene Kristalle und konsistenter Spurenelementverteilungen zwischen allen Hochdruckphasen. Für die Interpretation von Spurenelementverteilungen in Hochdruckgesteinen ist es eine wichtige Entdeckung, daß alle vier Proben foliierte Eklogite sind, die chemische Signaturen von Basalten aufweisen, während die deutlichsten Hinweise auf Ungleichgewichtsbedingungen in massiven, metagabbroischen Eklogiten nachgewiesen werden konnten. Daher sind die wichtigsten Voraussetzungen für die Einstellung von Gleichgewicht in metamorphen Gesteinen ein feinkörniger oder sogar glasiger Protolith und eine durchgehende Deformation. Ein freibewegliches Fluid während der Metamorphose ist wahrscheinlich auch ein wichtiger Parameter, jedoch ohne gleichzeitig stattfindender Deformation kein hinreichendes Kriterium.

Alle Ergebnisse dieser Studie sind ausgewertet worden im Hinblick auf Auswirkungen für das Verständnis von Subduktionszonenprozessen. Es ist jetzt möglich, realistische Modelle der Spurenelementzusammensetzung von Fluiden zu modellieren, die in dehydrierenden subduzierenden Platten freigesetzt werden. In früheren Ansätzen konnte nur die Fluidzusammensetzung, die im Gleichgewicht mit den Hauptphasen von Eklogitparagenesen steht, berechnet werden. Da diese Studie die Bedeutung akzessorischer Phasen für die Spurenelementbilanz in Eklogiten unterstreicht (z.B.: Ba in Phengit, Sb in Rutil, Pb in Zoisit), müssen frühere Modelle durch die Hinzunahme dieser Phasen erweitert werden. Dies kann erreicht werden durch die Benutzung von Spurenelementverteilungskoeffizienten zwischen Haupt- und akzessorischen Phasen, die sich aus den vier Gleichgewichtsproben dieser Studie ableiten lassen. Ausgangspunkt für eine noch andauernde Kontroverse sind die Fragen, ob und wie Fluide von der abtauchenden Ozeanplatte in den darüberliegenden Mantelkeil überführt werden. Eklogitproben von Trescolmen zeigen deutliche Hinweise auf die Existenz eines frei beweglichen Fluids während der Hochdruckphase und schließen daher die Möglichkeit von Fluidimmobilität in Eklogiten aus, wie durch Isotopenstudien bisher vermutet wurde. Der favorisierte Prozess, der die Fluidmobilität begünstigt und darüberhinaus die Einstellung von Spurenelementgleichgewichten beschleunigt, ist das Auftreten von kontinuierlicher oder diskontinuierlicher Deformation, was an der Grenzfläche zwischen abtauchender Ozeanplatte und überliegendem Mantel als wahrscheinlich angesehen werden kann.

Aus den Ergebnissen dieser Arbeit lassen sich Rückschlüsse ziehen auf Bereiche, die über das Gebiet der Metamorphose von Hochdruckgesteinen hinausreichen. So konnte gezeigt werden, daß die hoch fluidmobilen Elemente Cs, Rb und Ba Verteilungsmuster in Mineralphasen aufweisen, die am besten dadurch erklärt werden können, daß sehr niedrige Fluid-Gesteins-Interaktionen stattgefunden haben. Dieses ist in sofern bedeutsam, als das

sich mit Cs-Rb-Ba-Systematiken Reaktionen von durchströmenden Fluiden im Gestein nachweisen lassen, für die die klassische Sauerstoffisotopenanalyse nicht sensitiv genug ist. Anwendungen zum Aufspüren von niedrigen Fluiddurchflüssen z.B. im Bereich der Lagerstättenexploration sind daher denkbar. Weiterhin stellte sich heraus, daß Spurenelementkonzentrationen in Rutilen von Eklogiten und Metapeliten signifikante Unterschiede aufweisen. Unter Sedimentationsbedingungen stellt Rutil ein sehr stabiles Mineral dar, jedoch wurde es bisher als wenig charakteristisch angesehen. Es gibt durch die Analyse der Spurenelemente in Rutilen von Schwermineralfraktionen aus Sedimenten nun die Möglichkeit, unterschiedliche Herkunftsgebiete dieser Sedimente herauszuarbeiten, welche auf dem Gebiet der Erdölgeologie eine wichtige Fragestellung darstellt.

Chapter 1. Introduction

1.1 Geology of the study area

Trescolmen is situated 10 km southwest of the San Bernardino Pass, Switzerland, and is between 2000 and 2500 m in elevation. Being a part of the Adula nappe, it belongs to the basement and overlying sediments of the Penninic Unit (the former passive margin of Europe) in common with several other eclogite-bearing units (Tauern Window, Dora Maira, Monte Rosa, Gran Paradiso; Froitzheim et al., 1996).

In Trescolmen, numerous metre-sized eclogite boudins occur within garnet mica schist over an area of about one square kilometre (Fig. 1). The tholeiitic composition of the eclogites is compatible with a MORB-like protolith (Santini, 1992), permitting at least two different tectonic scenarios. On the one hand, slices of true oceanic crust could have been imbricated and tectonically disrupted during the Alpine collision, forming exotic blocks surrounded by pelitic material of continental affinity (Santini, 1992). Alternatively, tholeiitic magmas could have been emplaced into/onto the thinned passive continental margin during the rifting stage as dikes, tuffs and/or lava flows. The latter possibility has been proposed for the Tauern eclogites on the basis of detailed lithostratigraphy (Kurz et al., 1998) and fits better with the almost complete lack of ultramafic assemblages in the Middle Adula nappe. These two scenarios will be further explored in Chapter 4. In any case, the Trescolmen eclogites are similar in composition to modern oceanic crust and must have undergone a similar PT-history to oceanic crust that is subducted underneath modern volcanic arcs.

The PT history for Trescolmen has been studied in great detail (Heinrich, 1986; Meyre et al., 1997, 1999). An early (pre-eclogitic) epidote-amphibolite facies metamorphic stage can be inferred from the presence of calcic amphibole and epidote inclusions in grossular-rich cores of large garnets in the eclogites (Heinrich, 1986). The eclogite facies conditions themselves can be subdivided into at least two different stages. Peak pressure conditions (ca. 2.4 GPa, 600°C) are recorded in metapelites by the rare subassemblage Mg-glaucophane + kyanite (Meyre et al., 1999) and by an early foliation in the eclogites (Meyre et al., 1997). The second stage of eclogite facies metamorphism, indicated by various signs of water influx described in detail in Chapter 2, is estimated to have taken place under slightly lower pressure conditions (ca. 1.8 to 2.0 GPa, 650°C, Meyre et al., 1997, corresponding to the Trescolmen stage of Meyre & Puschignig, 1993). Numerous irregular quartz-bearing veins crosscutting eclogite bodies are ascribed to this stage. Formation under eclogite-facies conditions is confirmed by the presence of euhedral omphacite needles in these veins (Heinrich, 1986). Other vein-filling minerals include kyanite, apatite, phengite and rutile. The high pressure event was followed by rapid exhumation and accompanied by regional metamorphism under amphibolite to greenschist facies conditions (Zapport and Leis metamorphic stages respectively; Meyre & Puschignig, 1993). Compared to other localities in the Adula nappe, eclogite bodies at Trescolmen are much less affected by amphibolite facies overprinting. Amphibolite rinds are restricted to the outermost margin of eclogite boudins, in some cases being only a few millimetres thick. Amphibolite overprinting of eclogites is characterised by

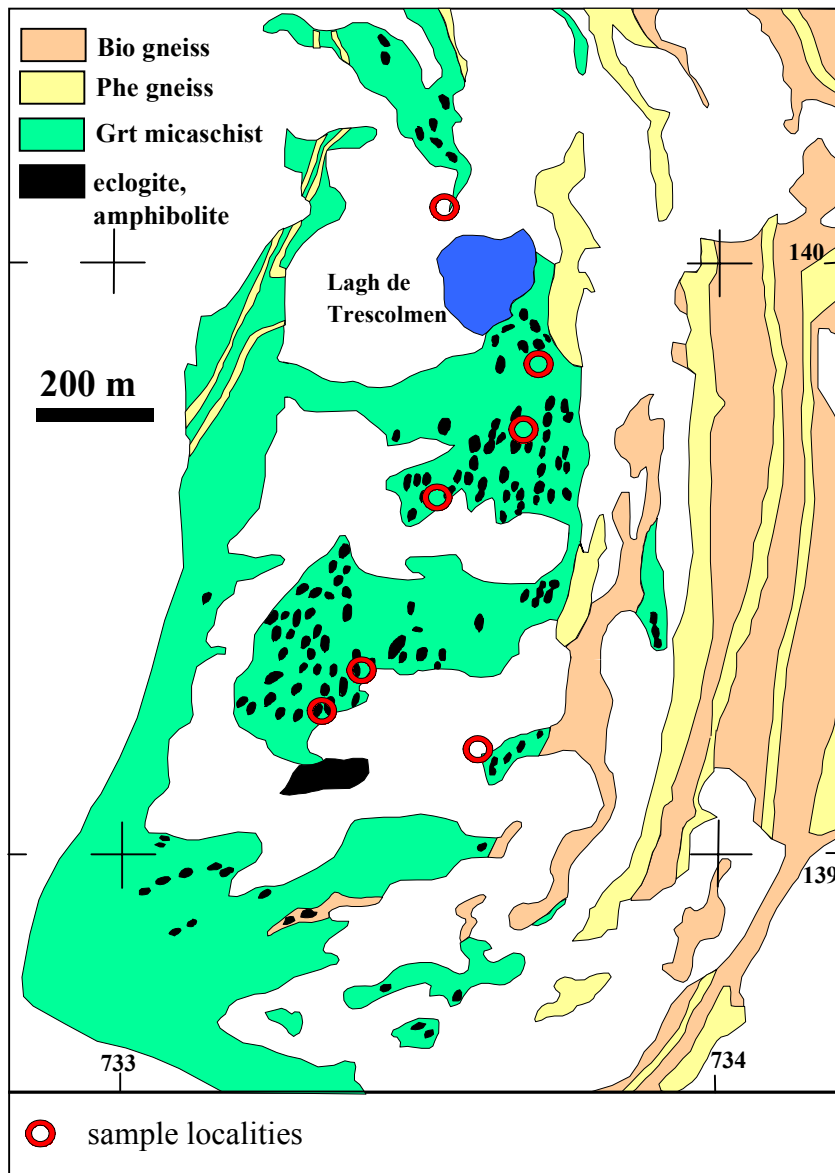


Fig. 1 Geological map of the area around the Lagh de Trescolmen, modified after Meyre & Frey (1998). Eclogite samples used in this thesis are marked by open circles, precise localities of these samples are also given as Swiss coordinates in Table 1.

formation of symplectitic intergrowths of green hornblende + plagioclase \pm diopside replacing omphacite and by overgrowth of garnet by chlorite \pm epidote (Heinrich, 1982).

The good preservation of eclogite bodies in Trescolmen is explained by a combination of limited fluid availability from the surrounding metapelites (the amount increases farther south beyond the biotite-in isograd; Heinrich, 1982) and limited deformation during amphibolite facies conditions, with a significant amount of deformation of the metapelite having already taken place under eclogite facies conditions (Meyre & Puschig, 1993; Meyre et al., 1999).

Eclogites from Trescolmen all contain the mineral assemblage clinopyroxene, garnet, amphibole, rutile, quartz, apatite and zircon. Eclogites and garnet micaschists from Trescolmen are generally coarse grained and characterized by unaltered minerals, making them ideal candidates for laser ablation microprobe studies, for which grain sizes of at least 20 μm are required for analysis. Additional phases which occur in several samples are kyanite, sulphides (pyrite and chalcopyrite), phengite, paragonite, zoisite, clinozoisite, allanite and talc. Garnet mica schists contain the assemblage phengite, garnet, quartz, rutile, apatite and zircon, with additional paragonite and kyanite in some

samples. Amphibolite facies overprinting in the metapelites produced phengites with lower celadonite content, biotite and staurolite (Meyre et al., 1998). We relate rutile in the garnet mica schists to the eclogite-facies assemblage and ilmenite to the amphibolite-facies overprint, based on the observation that ilmenite replacing rutile is most abundant in those parts of garnet mica schists rich in biotite formed by amphibolite-facies overprinting.

The samples were collected from the area surrounding Lagh de Trescolmen, with localities indicated by Swiss coordinates in Table 1. Only a few samples were taken directly from outcrops (Ad25, 59-1, 59-5). The other samples are from angular blocks, the largest up to one metre in size (52-1, 77-5), all originating from the immediate surrounding. Samples 59-1 and 59-5 are from the same outcrop, where talc inclusions in amphibole can be observed in some parts (59-5) of a one metre large boudin. Of these, only a sample from a talc-free area (59-1) was chosen for LAM analyses. CHM30a and CHM30b are from the same block (CHM30), representing phengite-rich and zoisite-rich domains, respectively. These samples are separated by a maximum distance of about 40 cm (original size of the block). Ad25 and CHM30a are from rock chips of already published eclogite samples (Ad25-9-3: Heinrich, 1986; CHM30: Meyre et al., 1997).

Table 1. Phase assemblages and abundances of investigated samples. Modal abundances are based on whole thin section element mapping (Ad25, CHM30b, 50-13, 59-5, 77-5; see Chapter 3) or on visual inspection with a petrographic microscope (remaining samples).

	Ad25	CHM30a	CHM30b	50-2	50-13	50-14	52-1	55-3	55-4	59-1	59-5	77-5
Clinopyroxene (CPX)	43	xx	48	xx	56	xx	xx	xx	xx	xx	18	44
Garnet (GRT)	32	xx	29	xx	36	xx	xx	xx	xx	xx	55	26
Amphibole (AMP)	10	o	2.1	o	1.6	tr	o	x	x	x	24	3.9
Phengite (PHE)	3.9	o	-	o	5.5	-	o	o	-	-	-	1.2
Zoisite (ZOI)	5.8	o	8.4	-	-	-	-	-	-	-	-	9.2
Allanite (ALL)	-	-	-	tr	tr	-	tr	tr	-	-	-	-
Clinozoisite (CZO)	-	-	-	-	-	-	-	-	-	-	-	7.1
Kyanite (KYA)	1.6	o	3.5	-	tr	-	-	-	-	o	1.0	o
Quartz (QZ)	3.1	o	8.3	o	tr	o	o	o	o	o	tr	7.3
Rutile (RUT)	0.5	tr	1.2	o	1.1	o	o	tr	tr	tr	tr	1.0
Apatite (APA)	0.02	tr	-	tr	0.5	o	tr	tr	tr	-	-	0.08
Talc (TLC)	-	-	-	-	-	-	-	-	o	-	1.4	-
Paragonite (PAR)	-	-	-	tr	tr	x	tr	-	-	-	-	-
Foliation	+	-	-	+	+	-	+	-	-	-	-	+
Grain size	-	++	++	-	+	+	+	++	+	++	++	+
Sample localities	139810	139650	139650	139310	139310	139310	139250	140150	140150	139715	139715	139300
(Swiss coordinates)	773690	733550	733550	773410	773410	773410	773375	733560	733560	733665	733665	733620

Abbreviations for modal abundances: tr <1%, o 1-10%, x 10-20%, xx >20%, - not identified; for foliation: - massive, + foliated; for matrix grain size (relative ordering): - small, + medium, ++ large.

1.2 Structure of thesis

The subjects of the following three chapters are centered around detailed *in-situ* trace element measurements of eclogites and garnet mica schists from the eclogite locality Trescolmen. One important result of this thesis is the finding that certain minor and accessory phases dominate the whole rock budget of various trace elements. This is the basis of interpreting the data accumulated in this study in a structured way.

Chapter 2 concentrates on Cs-Rb-Ba systematics in phengites, which dominates the whole rock budget of these fluid mobile trace elements. It is demonstrated that the *in-situ* analysis of these elements can be used to find evidence of a pre-metamorphic low-T alteration event in the eclogites and to detect very low fluid-rock interactions under eclogite-facies conditions. Additionally, this part also documents various petrographic signs of fluid infiltration into the eclogites.

Chapter 3 describes for the first time the importance of rutile for the trace element budget of a number of chalcophile and siderophile trace elements like Sb, Sn, Mo and W. Rutile is also an important phase for Nb and Cr, and this is discussed in respect to the use of trace element signatures in detrital rutiles for provenance studies. In this contribution, the instrumental capacities of a modern electron microprobe is used extensively, so that detailed information is given in the fields of trace element analysis, modal abundance calculations and textural studies.

In Chapter 4, textural, major and trace element information is evaluated for the specific purpose of calculating equilibrium partition coefficients between high pressure phases to derive a comprehensive data set for modelling subduction zone processes. For the analysis of ppb-concentrations in thin section samples special cleaning procedures and optimizations of the laser ablation microprobe are described. The role of the former protolith and the deformation history of the eclogites is emphasized for the attainment of a close approach to equilibrium in metamorphic rocks.

Chapter 2. Fluid infiltration at 2.0 GPa in eclogites from Trescolmen: Constraints from Cs-Rb-Ba systematics in phengite and amphibole

2.1 Introduction

There is a growing body of evidence that points to the subducting slab as the source for H₂O and a wide range of elements and isotopes in subduction zones (Cs, Rb, Ba and U, McCulloch & Gamble, 1991; ¹⁰Be, Tera et al., 1986; Sb and As, Noll et al., 1994; Pb, Li and B isotopes, Moriguti & Nakamura, 1998). This implies that the subducting slab stores these elements at least to the depth at which partial melting in the mantle wedge occurs beneath volcanic arcs. Depending on the magnitude of a possible lateral component of material transport into the melting zone (Davies & Stevenson, 1992), this corresponds to a slab depth of 60 to 130 km (2.0-4.0 GPa). One complex of questions centres around the problem which minerals host these elements in the slab (Peacock, 1993; Poli & Schmidt, 1998), and whether their subsequent release takes place through dehydration and/or partial melting reactions (Ringwood, 1974).

In the case of H₂O-rich fluids as the transport agent, equally important questions arise as to how these fluids migrate out of the slab into the overlying mantle wedge. The scale and nature of fluid movement under high pressure conditions is not well constrained. Several recent studies of eclogites have concluded, on the basis of observed heterogeneities in fluid inclusions and oxygen isotopes, that fluid flow is restricted under high pressure conditions to the decimetre scale (e.g. Philippot & Selverstone, 1991; Nadeau et al., 1993; Getty & Selverstone, 1994). Where fluids have clearly been mobilised in high pressure veins, they have similar major element and oxygen isotope signatures to their immediate surroundings (Cartwright & Barnicoat, 1999).

In regional metamorphic systems, oxygen isotopes have been used extensively to derive quantitative parameters concerning fluid flow on a regional scale i.e. fluid-rock ratio, integrated fluid flux, direction of fluid flow (Taylor, 1977; Bickle & McKenzie, 1987; Baumgartner & Rumble, 1988; Ferry & Gerdes, 1998). With this technique, evidence for large scale fluid flow has been found in several different tectonic environments, e.g. in ancient accretionary wedges (Catalina Schist terrane: Bebout & Barton, 1989; Bebout, 1991), hydrothermally altered oceanic crust (Muehlenbachs, 1986), contact aureoles around crystallising magma bodies and localised fractures as well as shear zones (Oliver, 1996). In contrast, areas of limited fluid circulation are probably more common, but are rarely suited to the calculation of fluid fluxes by the oxygen isotope technique (for an exception, see Matthews et al., 1996), since oxygen is a major element in both the fluid and the surrounding rock. As a result, at low fluid-rock ratios the oxygen isotopes of the infiltrating fluid are buffered by the surrounding rock body, and large quantities of fluid are required to buffer the oxygen isotopic composition of the infiltrated rock body.

More sensitive techniques must be developed in order to test if calculated low fluid fluxes in many high pressure rocks mean that only small amounts of fluid penetrated the system, or that fluid was incapable of leaving the system. Trace elements that are highly enriched in fluids compared to their source rock are well suited for the detection and

quantification of low fluid-rock ratios. As emphasised by Banner & Hanson (1990), the lower the fluid-rock ratio the more appropriate are the elements with low partition coefficients ($D^{\text{Min/Fluid}}$). Such elements should be fluid-mobile and typical of incompatible element enrichments in island arc source regions.

Investigations of fluid-rock interactions among fluid-mobile elements are hampered by their susceptibility to late stage alteration effects, by analytical problems due to their low concentrations, and by a scarcity of experimentally determined $D^{\text{Min/Fluid}}$ values. The first problem can be overcome by analysing carefully-chosen single mineral grains in-situ with a microprobe method (e.g. ion microprobe or LAM-ICP-MS) rather than analysing whole rocks (for an example, see Foley et al., 1996). The latter two problems can be minimised by choosing the LIL elements Cs, Rb and Ba as examples of fluid-mobile elements (for Ba, see Nabelek & Labotka, 1993) since they are relatively easy to analyse and an increasing number of experimental studies of their partitioning behaviour are emerging (Beswick, 1973; Volfinger, 1976; Brenan et al., 1995; Melzer et al., 1998; Melzer & Wunder, 1999).

Samples from Trescolmen were found to be suitable samples for exploring the application of the in-situ trace element technique to questions about fluid-rock interaction in eclogitic parageneses. These rocks show a pronounced re-equilibration stage under high pressure conditions (Meyre et al., 1997) that seems to imply fluid infiltration at high pressure, similar to the paragonite-bearing coesite eclogites from Dabie Shan (Okay, 1995). In this chapter the evidence for fluid infiltration under high pressure conditions is first documented and the importance of phengite in controlling the Cs, Rb and Ba contents in high pressure rocks is shown. Construction of a Cs-Rb-Ba discrimination diagram allows constraints to be placed on a likely protolith of the Trescolmen eclogites and estimation of the magnitude of fluid-rock interaction under high pressure conditions.

2.2 Evidence for fluid infiltration under eclogite facies conditions

Eclogite from Trescolmen is characterised by the abundant and varied occurrence of high pressure hydrous phases (Table 1). *Phengite* is present in most of the analysed samples and forms part of the equilibrium parageneses. It displays a preferential alignment parallel to the early omphacite foliation (Fig. 2a), suggesting that it was stable under peak pressure conditions. In contrast, there is evidence for recrystallization of phengite in other samples (e.g. CHM30), where it occurs in local quartz segregations. *Zoisite* is generally less abundant than phengite and is also mostly aligned in the omphacite foliation. *Talc* was found only in the most Mg-rich eclogites. In a 3 m wide eclogite body (locality of samples 59-1 and 59-5), talc is concentrated near the eclogite-pelite contact but is rare inside the eclogite body, where it is restricted to small aggregates that may represent former veins (59-5). *Paragonite* is commonly closely associated with phengite. However, paragonite also occurs as a replacement product of kyanite (Fig. 2b). All stages of replacement can be observed in a single thin section (e.g. 50-14), from fresh kyanite without paragonite, through kyanite with a thin rim of paragonite and paragonite enclosing corroded relics of kyanite, to clusters of inclusion-free paragonite. Barroisitic and tremolitic *amphiboles* are found in a range of textural relationships with respect to the other eclogitic phases. Barroisitic amphibole generally forms large anhedral porphyroblasts that are either aligned with the foliation or grow irregularly over it (Heinrich, 1986; Meyre et al., 1997), and contain inclusions of all other high pressure phases. At the outcrop scale it appears that barroisitic

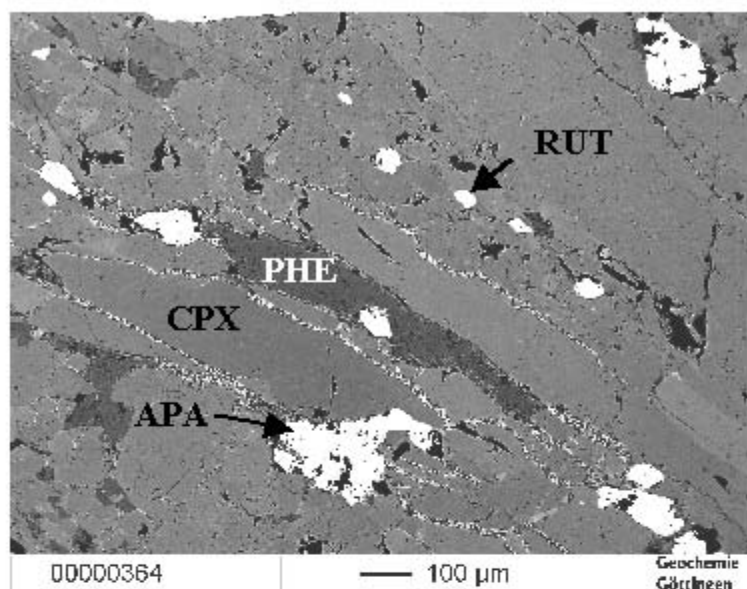
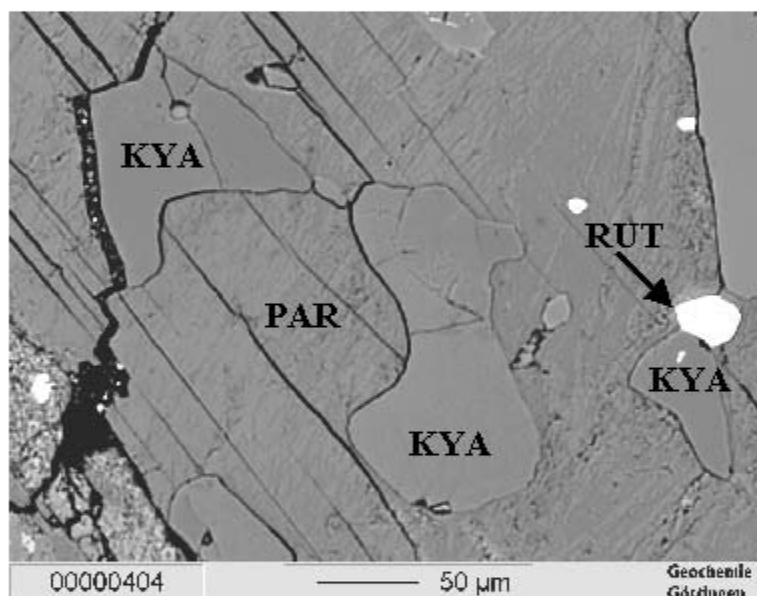
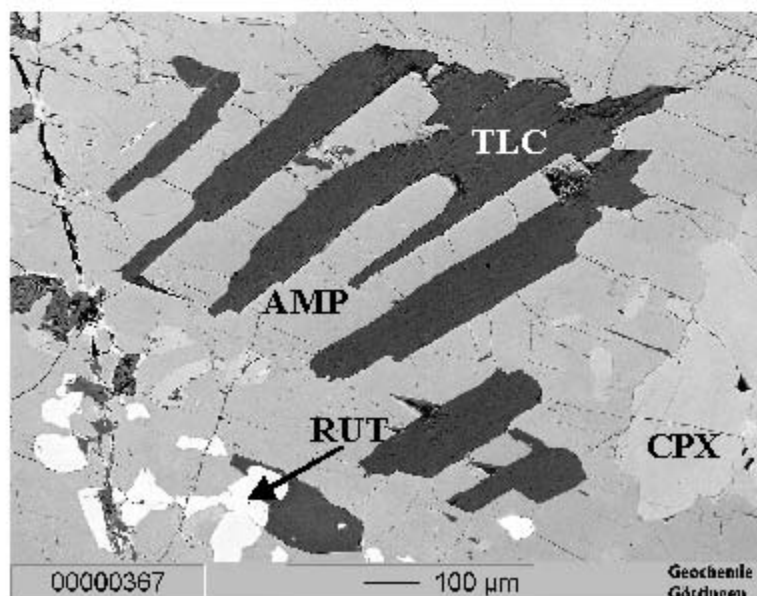


Fig. 2 Backscattered images of textural relations among hydrous high pressure phases in eclogites.

a) Phengite (PHE) grain parallel to the eclogite foliation defined by the preferred orientation of omphacite (CPX) and rutile (RUT). Also visible are two apatite crystals (lower middle and upper right). Sample 50-13.



b) Several resorbed kyanite (KYA) crystals (all with the same optical orientation) surrounded by paragonite (PAR). Sample 50-14.



c) Relict talc (TLC) grain occurring in the centre of 1 mm large tremolitic amphibole (AMP). Also visible are several diopsidic clinopyroxenes (CPX) and rutile. Sample 59-5.

amphibole poikiloblasts are more concentrated near the rims of some eclogite bodies, but these bodies are not large enough to exhibit an unambiguous trend, and the cores of the eclogite bodies are never devoid of amphibole. Of special interest is the partial replacement of talc by tremolitic amphibole (Fig. 2c) in the vein-like areas described above. In general, it is easy to chemically and texturally distinguish the large, pale green, high-pressure barroisitic and tremolitic amphiboles from the later, dark green amphibolite-facies hornblendes, occurring with other low-pressure phases in a fine-grained symplectitic intergrowth.

From these observations, it is inferred that hydrous fluid influx under high pressure conditions is required to explain the following water-consuming reactions:



In mafic systems both reactions can take place at pressures between 1.8 and 2.2 GPa (Fig. 3; Meyre et al., 1997) under H₂O saturated conditions. If the interpretation of talc formation in veins in sample 59-5 is correct, a fluid influx to produce the talc veins must have taken place at even higher pressure. Talc breakdown may have taken place according to the fluid-conserving reaction



Using TWQ and the database of Berman (1990), the stable occurrence of talc in relation to omphacite and tremolitic amphibole is restricted to a pressure greater 2.2 GPa at 650°C (see Fig. 3 for details).

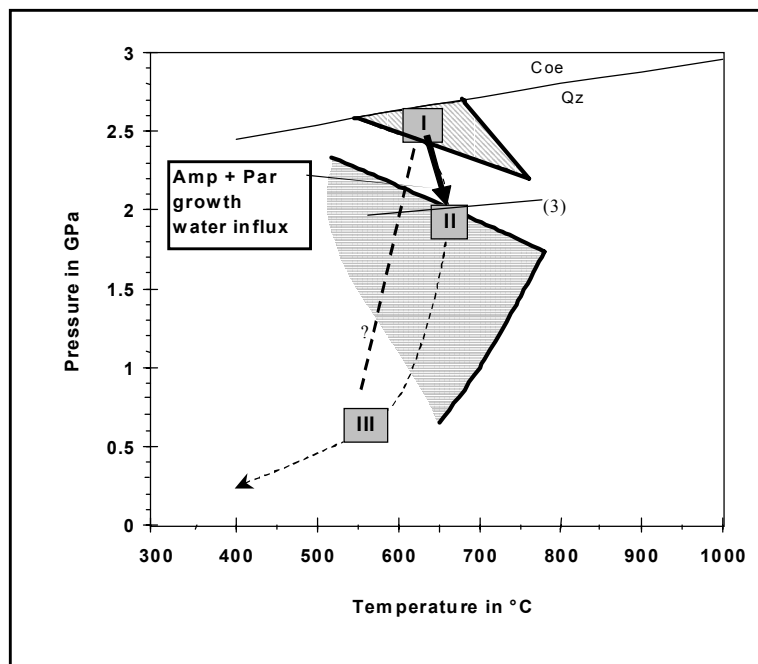


Fig. 3 *PT path for the area of Trescolmen. Pre-peak path is not well established, but probably passed the epidote-amphibolite facies field. Peak pressure conditions are defined by the “peak-pressure stage” (field I), followed by the “Trescolmen stage” (field II) and by the the “Zapport stage” (field III). A pressure difference of about 0.4 GPa between the peak-pressure and the Trescolmen stage is implied by the significant offset of stability fields for the subassemblage glaucophane + kyanite (horizontal hatched field; characteristic for the peak pressure stage) and paragonite + omphacite (cross hatched field; characteristic for the Trescolmen stage). Fluid flux into eclogite bodies occurred between field I and II (thick black arrow), either facilitating Trescolmen deformation or being enhanced by it. Reaction (3), as given in the text, was calculated with activity models ($a_{tr} = 0.57$; $a_{di} = 0.64$; $a_{tlc} = 1$) outlined by Will et al. (1998) and the thermodynamic data base of Berman (1990).*

Fluid flux into eclogite bodies occurred between field I and II (thick black arrow), either facilitating Trescolmen deformation or being enhanced by it. Reaction (3), as given in the text, was calculated with activity models ($a_{tr} = 0.57$; $a_{di} = 0.64$; $a_{tlc} = 1$) outlined by Will et al. (1998) and the thermodynamic data base of Berman (1990).

2.3 Analytical techniques

Major and minor element analysis were performed on a Cameca SX51 electron microprobe in Heidelberg and a JEOL 8900 RL electron microprobe in Göttingen, both equipped with 5 WDS spectrometers. The operating conditions for amphibole and phengite analyses were 15 kV acceleration voltage, 12 nA beam current on the Faraday cup and a 5 μm beam diameter. The matrix correction methods for the raw counts were PAP for the Heidelberg and phi-rho-zet for the Göttingen microprobe. Counting times on the peak were 15 seconds for the major elements and 30-120 seconds for Ba and Sr. This translates into detection limits (DL) of as low as 100 ppm for the longest counting times. The potential problem of overlapping of the Ti $K\alpha$ on Ba $L\alpha$ peaks was evaluated by analysing synthetic rutile. It was found to yield 0.6 wt. % apparent BaO for 100% of TiO_2 , and could therefore be neglected for the Ti-poor phases analysed in this study. Calculation of amphibole mineral formulae (Table 2) was done following the procedure of Schumacher (1997), using the average of possible minimum and maximum Fe^{3+} values.

Cs, Rb, Ba, and Sr were measured by laser ablation microprobe-ICP-MS (LAM) at Memorial University of Newfoundland. Details about the current laser source, mass spectrometer and data reduction can be found in Horn et al. (1997 and references therein). For this study, operating conditions were optimised by using laser pulse energies from 0.2-0.7 mJ for phengite and from 0.3-1.4 mJ (always at 10 Hz) for amphibole. The best performance was achieved with a defocused laser beam, having the focus some 100-400 μm above the sample surface. This reduces fractionation significantly, and in this study Ca/Si ratios did not change during a 1 minute ablation period. As a result, Si could be used as an internal standard for phengite and Ca for amphibole analyses without introducing a systematic error. Another advantage of the defocused beam is a more regular distribution of energy on the mineral surface, which leads to smooth ablation behaviour even for the large pulse energies applied to ablate some amphibole crystals.

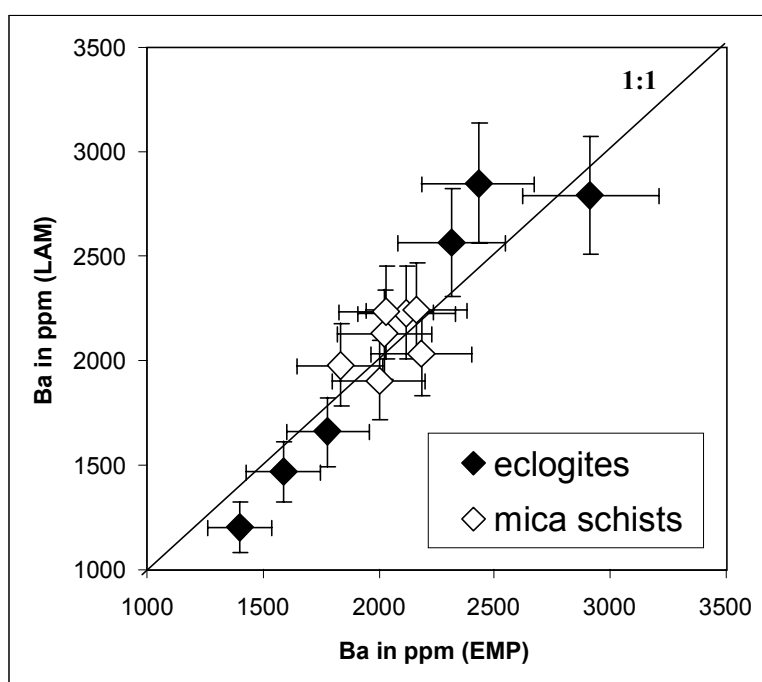


Fig. 4 Comparison of Ba concentration in phengite from electron (EMP) and laser (LAM) microprobe measurements. Error bars are 10% standard deviation. Notice the larger variation in Ba concentration of phengite in eclogites compared to mica schists.

Table 2. Amphibole compositions of Trescolmen eclogites. All major element concentrations measured by electron microprobe (in wt%), trace elements with * by LAM (in ppm). Mineral formulae calculated after the method of Schumacher (1997).

	Ad25	CHM30	50-2	50-13	50-14	52-1	55-3	55-4	59-1	59-5
SiO ₂	50.76	52.98	50.53	49.81	48.60	47.29	54.06	55.28	53.02	55.12
TiO ₂	0.25	0.12	0.28	0.26	0.28	0.39	0.14	0.055	0.14	0.091
Al ₂ O ₃	12.15	8.16	13.67	13.35	14.21	14.47	8.64	4.83	9.52	6.06
Cr ₂ O ₃	0.048	0.16	0.037	0.11	0.056	0.054	0.082	0.11	0.085	0.017
FeO	5.47	4.60	7.24	5.57	8.32	8.78	6.36	4.58	3.29	2.69
MnO	0.02	0.03	0.03	0.03	0.02	0.03	0.13	0.05	0.04	0.03
MgO	16.27	18.55	14.00	15.30	13.27	13.27	16.76	20.05	18.71	20.66
CaO	8.62	9.39	5.94	7.97	6.96	8.23	6.93	9.69	9.81	9.88
Na ₂ O	3.63	2.86	5.48	4.46	5.42	4.38	3.83	2.32	2.87	2.00
K ₂ O	0.33	0.29	0.34	0.40	0.060	0.47	0.26	0.44	0.059	0.048
Total	97.55	97.14	97.54	97.25	97.19	97.37	97.18	97.39	97.53	96.595
Si	7.037	7.336	7.032	6.955	6.864	6.718	7.464	7.618	7.272	7.577
Al(IV)	0.963	0.664	0.968	1.045	1.136	1.282	0.536	0.382	0.728	0.423
Al(VI)	1.023	0.667	1.274	1.152	1.229	1.141	0.870	0.403	0.810	0.559
Ti	0.026	0.013	0.029	0.027	0.030	0.042	0.015	0.006	0.014	0.009
Fe ³⁺	0.185	0.223	0.206	0.104	0.153	0.162	0.323	0.254	0.143	0.157
Cr	0.005	0.018	0.004	0.012	0.006	0.006	0.009	0.012	0.009	0.002
Mg	3.362	3.829	2.905	3.185	2.793	2.809	3.449	4.118	3.824	4.234
Fe ²⁺	0.399	0.250	0.582	0.520	0.788	0.839	0.334	0.207	0.199	0.039
Fe ²⁺	0.049	0.060	0.055	0.026	0.041	0.042	0.076	0.066	0.036	0.113
Mn	0.003	0.003	0.004	0.003	0.002	0.004	0.016	0.006	0.004	0.003
Ca	1.280	1.393	0.885	1.192	1.053	1.252	1.025	1.430	1.441	1.455
Na	0.668	0.544	1.057	0.779	0.904	0.702	0.883	0.498	0.519	0.428
Na	0.309	0.224	0.422	0.430	0.580	0.505	0.142	0.121	0.245	0.105
K	0.058	0.051	0.060	0.071	0.011	0.085	0.045	0.077	0.010	0.008
Cs *	0.011	<0.01	0.004	0.005	n.a.	<0.04	<0.01	<0.003	0.014	n.a.
Rb *	1.7	2.1	2.0	1.5	n.a.	3.1	1.1	1.4	2.9	n.a.
Ba *	2.1	4.5	5.5	3.7	n.a.	7.5	0.9	1.8	3.8	n.a.
Sr *	15	33	175	82	n.a.	173	42	63	85	n.a.

Table 3. Phengite compositions of Trescolmen eclogites and metapelites. All major and some trace element concentrations measured by electron microprobe (in wt% except Ba and Sr in ppm), trace elements with * analysed by LAM (in ppm).

	eclogites						garnet mica schists						
	Ad25	CHM30	50-2	50-13	52-1	55-3	50-1	50-9	59-4	58-3	60-2	61-1	81-1
SiO ₂	50.32	51.17	52.29	51.71	50.77	50.42	50.69	50.15	49.60	50.35	50.29	50.37	51.41
TiO ₂	0.45	0.35	0.35	0.35	0.50	0.34	0.40	0.40	0.40	0.38	0.46	0.40	0.32
Al ₂ O ₃	28.08	26.23	26.10	27.10	27.28	24.90	28.36	28.43	28.55	28.42	29.20	27.46	26.92
Cr ₂ O ₃	0.070	0.37	0.020	0.083	0.015	1.34	0.031	n.a.	n.a.	0.016	0.026	n.a.	n.a.
FeO	1.02	1.34	1.51	0.97	1.63	1.50	1.34	2.19	1.84	2.53	1.83	1.45	1.23
MnO	0.017	0.012	b.d.	b.d.	b.d.	0.019	b.d.	0.011	0.02	b.d.	b.d.	0.018	0.022
MgO	3.65	4.26	4.34	4.09	3.91	4.12	3.39	2.86	2.92	2.81	2.85	3.56	4.00
CaO	0.021	0.026	b.d.	b.d.	b.d.	0.013	b.d.	b.d.	0.01	b.d.	b.d.	b.d.	b.d.
Na ₂ O	0.88	0.77	0.46	0.49	0.58	0.56	0.67	0.68	0.62	0.60	0.61	0.45	0.54
K ₂ O	9.77	9.62	10.59	10.62	10.50	10.29	9.96	9.61	9.81	9.75	9.96	10.12	10.00
Ba	1401	2915	2317	1589	2431	1780	2027	2034	1833	2002	2165	2117	2185
Sr	228	506	376	393	490	323	431	475	528	274	225	385	520
Total	94.45	94.43	95.91	95.60	95.46	93.69	95.13	94.62	94.02	95.11	95.49	94.11	94.72
Si	3.351	3.408	3.446	3.414	3.366	3.419	3.356	3.342	3.320	3.341	3.321	3.375	3.413
Ti	0.023	0.017	0.017	0.017	0.025	0.017	0.020	0.020	0.021	0.019	0.023	0.020	0.016
Al	2.203	2.058	2.027	2.109	2.132	1.990	2.213	2.233	2.274	2.222	2.273	2.168	2.107
Cr	0.004	0.019	0.001	0.004	0.001	0.072	0.002		0.001	0.001	0.001		
Fe	0.057	0.075	0.083	0.054	0.091	0.085	0.074	0.122	0.100	0.140	0.101	0.081	0.068
Mn	0.001	0.001				0.001		0.001				0.001	0.001
Mg	0.363	0.422	0.427	0.403	0.386	0.416	0.335	0.284	0.283	0.278	0.281	0.355	0.396
Ca	0.001	0.002				0.001							
Na	0.113	0.099	0.059	0.063	0.074	0.073	0.086	0.087	0.074	0.077	0.078	0.058	0.070
K	0.830	0.817	0.890	0.894	0.888	0.890	0.841	0.817	0.854	0.825	0.839	0.865	0.847
Cs *	12.8	6.7	9.0	11.9	7.4	12.2	19.9	11.8	13.1	12.7	12.6	11.4	11.4
Rb *	476	387	361	351	321	519	390	361	359	401	378	350	387
Ba *	1198	2790	2567	1462	2827	1659	2144	2231	1964	1931	2277	2228	2035
Sr *	160	646	444	310	470	231	478	444	422	299	239	319	584

Precise data on Cs, Rb and Ba are relatively easy to achieve in phengite analyses, with pit sizes of less than 40 μm in regular thin sections being sufficient. A comparison of measured Ba concentrations derived from electron microprobe and LAM analyses shows excellent agreement (Fig. 4) and precludes any significant systematic matrix effect influencing the LAM analyses. On the other hand, Cs contents in amphibole were mostly below detection limit. Although eclogite-facies mineral phases in Trescolmen are commonly very coarse grained, mineral inclusions and microfractures along cleavage planes generally limit pit sizes to 40-60 μm . If inclusions or microfractures were analysed accidentally, they were excluded from data reduction by careful inspection of each measurement in time-resolved mode. In a few cases (e.g. in sample 55-4, a thick section 80 μm thick), pit diameters of up to 140 μm could be drilled (at 1.4 mJ and 400 μm defocusing distance) for 18 sec on inclusion-free areas of some amphiboles. Even under these ideal conditions, however, the Cs concentration in amphibole in this sample was below the calculated detection limit (<3 ppb).

2.4 Results

All analysed phengites (Table 3) are characterised by their high celadonite (Cel) content (37-47 mol % in eclogites and 33-41 mol % in garnet mica schists) and low paragonite (Pg) content (Na/Na+K ratio between 0.05-0.2). These components are negatively correlated (in accordance with data from Heinrich, 1983). Phengite in metapelites can be distinguished from phengite in metabasitic eclogites in being less enriched in celadonite at a given value of X_{Pg} . Large variations in X_{Cel} and X_{Pg} can be also found within single large crystals, with the highest celadonite and lowest paragonite component in the core. Detailed WDS-element mapping reveals that at least the NaK-1 exchange is not a growth zoning pattern but rather a late diffusion process, probably related to the amphibolite facies overprinting, with Na gain in phengite at the expense of K. This occurs at grain boundaries as well as along cleavage planes. Despite these chemical variations, none of these parameters is correlated with the Ba content. Instead microprobe traverses from unzoned cores to the diffusionally reset margins show no Ba zonation, at least within the precision of the analyses (5-10% at the 2000 ppm level). Since repeated Rb and Cs analyses with the LAM also show the same limited variation within a single sample, we conclude that the very slight amphibolite overprinting did not severely alter the LILE composition of the investigated phengite.

Both chemical variations among amphiboles in different samples and chemical zonation in single large amphibole porphyroblasts can be pronounced (Heinrich, 1983; Heinrich, 1986). For this study, variations in the large M4- and A-sites are of interest. In general, Na (M4) in the amphibole cores is strongly coupled to the jadeite content of nearby omphacite. Na (M4) and Na+K (A-site) in amphibole cores are positively correlated at a 1:1 ratio. However, this correlation breaks down for the amphibole rims, where the A-site occupancy (by Na + K) increases with decreasing Na(M4) content. Since these variations can be very pronounced in the A-site (from 0.2 to 0.6 a.p.f.u. in a single porphyroblast), it can be expected that the LIL elements Cs, Rb and Ba will also show distinct zoning. Unfortunately the rim areas of amphiboles always show symplectitic intergrowth with quartz and could not be analysed with the defocused beam set up in this study. Since amphibole core compositions are strongly coupled with the composition of coexisting omphacite, coeval crystallisation of both phases is indicated (Heinrich, 1986).

The best evidence for phengite and amphibole core compositions representing a single crystallisation stage comes from the strong coupling of Ba partitioning between phengite and amphibole (expressed as the partition coefficient $D_{Ba}^{Amp/Phe}$). This partition coefficient can vary by a factor of 5 (0.0005-0.0028). The spread in values is strongly coupled the chemistry of the different amphiboles. An example is shown in Fig. 5 and explained as follows. The Ba atom can be best accommodated in the large A-sites of both phengite and amphibole. As the A-site of phengite is almost completely filled (Na+K = 0.87-0.92), the composition of phengite can be expected to exert a constant influence on Ba incorporation into its crystal structure. On the other hand, amphiboles of different samples show a large variation in composition in their A-site occupancies (K+Na = 0.13-0.46). Incorporation of Na + K in the A-site of amphibole appears to favour Ba incorporation into this site, suggesting that a charge difference of +1 due to replacement of Na or K by Ba in the partially filled site can be more easily balanced than a difference of +2 in a largely vacant A-site. Additionally, amphiboles with the highest abundance of atoms on the A-site also have the highest abundance of Al(4), which facilitates charge balancing of trace elements in various crystal sites (Brumm et

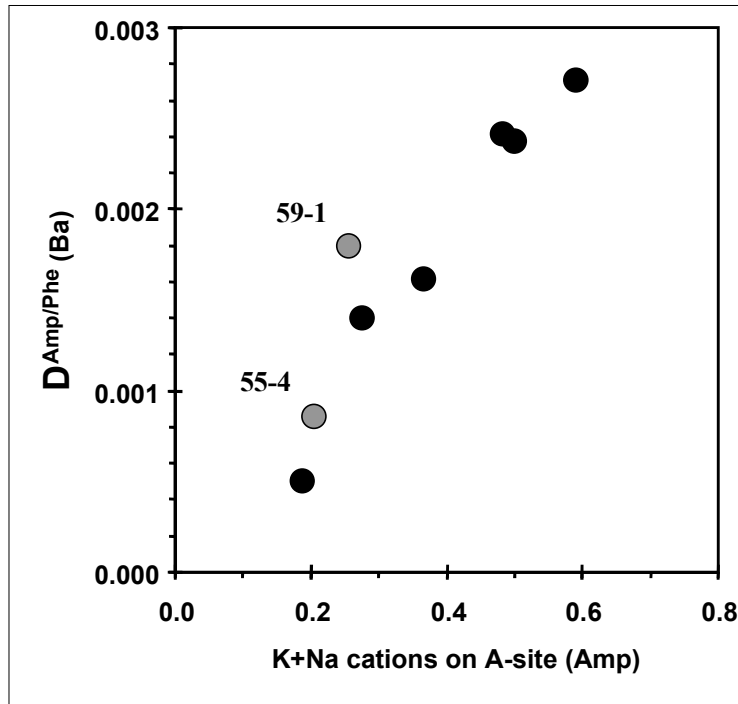


Fig. 5 Influence of amphibole crystal structure (here A-site occupancy) on the partitioning behaviour of Ba between amphibole and phengite ($D_{Ba}^{Amp/Phe}$). Black diamonds: phengite-amphibole pairs from different eclogite samples; gray squares: phengite-amphibole partitioning between amphiboles of phengite-free samples (59-1 and 55-4) and an average phengite from surrounding metapelite.

al., in prep.). Therefore, the observed positive correlation between $D_{Ba}^{Amp/Phe}$ and A-site occupancy in amphibole is to be expected and is interpreted as evidence for attainment of equilibrium between phengite and amphibole.

Analyses of garnet, clinopyroxene, zoisite and apatite in several samples show that these phases do not incorporate Cs and Rb in significant amounts (always below detection limit; at least <0.2 ppm). Cs and Rb were detected in amphibole (0.004-0.03 ppm and 1.1-3.1 ppm respectively), paragonite (0.05-0.6 ppm and 3-22 ppm respectively) and phengite (6.7-13 ppm and 320-520 ppm respectively). For the phases in Trescolmen eclogites, Ba concentrations increase in the order: garnet (0.007-0.08 ppm) < apatite (ca. 0.07 ppm) ≤ clinopyroxene, zoisite (0.04-0.15 ppm) < amphibole (0.9-7.5 ppm) < paragonite (180-370 ppm) < phengite (1200-2800 ppm). These data, combined with estimates of the modal abundances, reveal that in phengite-bearing samples more than 99% of Cs, Rb and Ba are concentrated in phengite (Fig. 6). Therefore phengite has to be considered the principal carrier of Cs, Rb and Ba in eclogites as well as in high pressure metapelites (see also Domanik et al., 1993; Sorensen et al., 1997), even if phengites are generally low in modal abundance. In phengite-free rocks, paragonite (sample 50-14) or amphibole (samples 55-4 and 59-1) are the principal carriers for Cs, Rb and Ba, but total LIL element concentrations are much lower in these rocks.

Strong selective partitioning of trace elements in high pressure metamorphic rocks has been reported previously (e.g. Hickmott, 1992). On the basis of the results of this study, this conclusion can be extended to phengite, in which the large ion lithophile elements Cs, Rb and Ba are highly concentrated in phengite compared to all other mineral phases. As another example, Sr abundance in sample 50-13 is controlled by the accessory mineral apatite. However, although the dominance of apatite in controlling the Sr budget is not as extreme as phengite for the Cs, Rb and Ba budget (Fig. 6), as amphibole, clinopyroxene and phengite can all accommodate significant amounts of Sr.

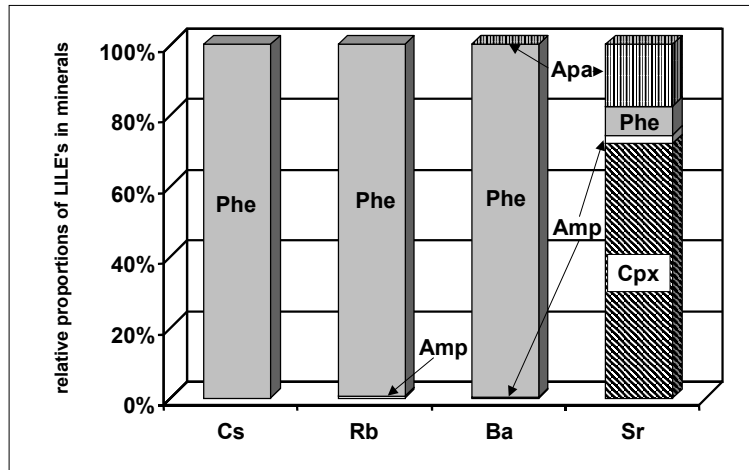


Fig. 6 Mass balance of LIL elements in eclogites exemplified for one sample (50-13). All mineral trace element compositions measured by LAM-ICP-MS, mineral modes are estimated by element mapping of one whole thin section (288,000 points, recalculated to wt% and normalized to 100%): garnet 38, clinopyroxene 58, amphibole 2, phengite 1.5, apatite 0.5. Other phases not considered include rutile, quartz and kyanite (together <5%).

LIL element concentrations (measured by LAM) of all phases in eclogites have been integrated with measured modal abundances to yield estimates of LIL concentrations in the rocks as a whole. These estimates can be compared to whole rock LILE data (measured by solution-ICP-MS) in order to establish a reliable mass balance for eclogitic rocks. For Ba, a complete mass balance with all primary mineral phases cannot always be achieved. In samples lacking phengite, the Ba concentrations in the whole rock are higher than the concentrations and mineral proportions measured for the Ba-richest phase (i.e. paragonite or amphibole). Solution-ICP-MS analysis of the Ba concentration for the whole rock sample 59-1 yielded a concentration of 1.72 ppm, whereas the reconstructed composition with 20 modal % amphibole (3.8 ppm Ba) as the only significant Ba phase results in a calculated concentration of 0.76 ppm Ba. Although care was taken to select rock chips with no visible sign of alteration, it can clearly be seen from this result that significant proportions of Ba (>50% in the case of 59-1) can be introduced by late stage products such as the amphibolite-facies symplectites.

2.5 Discussion

2.5.1 Protolith constraints from LIL element concentrations

We have plotted data for basalts that have undergone low and high temperature alteration, fresh volcanic rocks, pelagic sediments and 'average' composition continental crust in a Rb/Cs vs. Ba/Rb diagram (Fig. 7). This diagram was chosen because it is suitable to: (1) delimit specific fields for a range of protoliths that cannot be differentiated otherwise (e.g. fresh against altered MORB); (2) compare the eclogite data with their possible protoliths; and (3) investigate how fluid processes during metamorphism can be traced by changing LIL element ratios. The field of fresh MORB and OIB is restricted to mantle values of about 0.0126 for Cs/Rb and 11.3 for Ba/Rb (Hofmann & White, 1982; McDonough & Sun, 1995). In contrast, low-T (< ca. 300°C) altered MORB spans a large field away from fresh MORB towards higher Cs/Rb (up to 0.08) and lower Ba/Rb ratios (down to 0.3), indicating enrichments in the order Cs>Rb>Ba (Staudigel & Hart, 1983; Staudigel et al., 1996). High-T (> ca. 300°C) altered gabbros from ODP 149 (Seifert et al., 1997) partially overlap with low-T altered MORB, but show a cluster of significantly lower

Cs/Rb ratios than fresh MORB at constant mantle Ba/Rb ratios. Oceanic sediments have systematically high Cs/Rb ratios of >0.05 (Ben Othman et al., 1989; Plank & Langmuir, 1998). Ba/Rb ratios of oceanic sediments are less distinctive, having higher and lower values than primitive mantle, but with a concentration towards higher Ba/Rb values. The high Cs/Rb ratios of pelagic sediments and continental crust have been described by Ben Othman et al. (1989). Nevertheless the average composition of the continental crust (Taylor & McLennan, 1985) has significantly lower Cs/Rb (0.034) values than pelagic sediments. In summary it seems that fresh, low- and high-T altered basalts and sediments do indeed occupy distinctive fields in a Cs/Rb vs. Ba/Rb plot, although with considerable overlap.

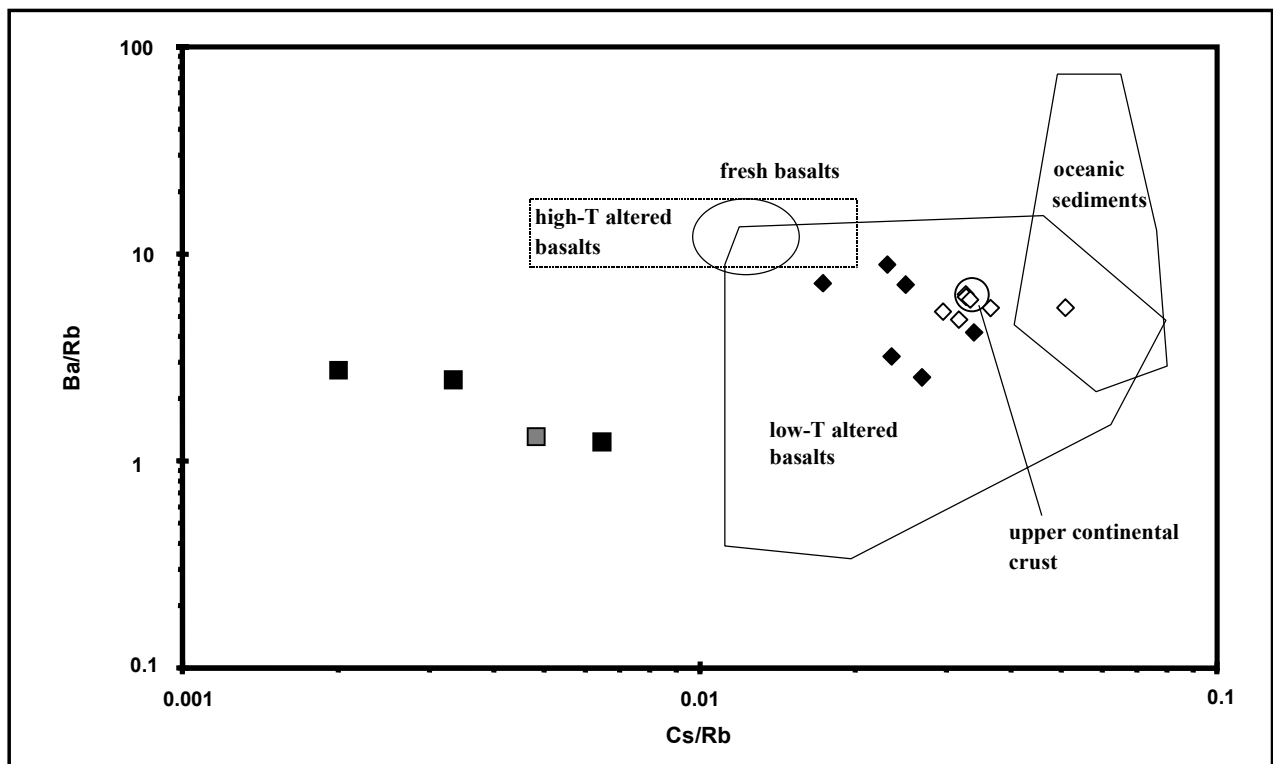


Fig. 7 Ba/Rb vs Cs/Rb plot illustrating phengite composition close to likely protoliths (black diamonds: phengite from eclogites; white diamonds: phengite from mica schists). Coexisting amphiboles of phengite-bearing samples: black squares. Amphibole from phengite-lacking eclogite (59-1; gray square) has comparable ratios to other amphiboles. Data sources for fields outlined in Figs .7 and 8: fresh basalts (N-MORB, E-MORB, OIB)- Sun & McDonough (1989); low-T altered basalts- Jochum & Verma (1996), Staudigel & Hart (1983), Staudigel et al. (1996); high-T altered basalts- Seifert et al. (1997); oceanic sediments (only pelagic clay-rich samples)- Ben Othman et al. (1989), Plank and Langmuir (1998); upper continental crust- Taylor and McLennan (1985).

As important as it is to define distinct fields in discrimination diagrams, it is equally necessary to explain the mechanisms that generate different fractionation effects between element ratios. In the case of the well-studied low-T alteration trends in the oceanic crust, Berger et al. (1988) found that elements with the smallest absolute ionic

hydration energy have the highest affinity towards minerals when in contact with circulating fluids. It is likely that adsorption of trace elements on the mineral surface is the dominant mechanism, so that in terms of effective partition coefficients, $D^{\text{Min/Fluid}}$ are in the order Cs>Rb>Ba (in accordance with increasing absolute ionic hydration energies). It can be speculated that the same mechanism may explain the distinctively higher Cs/Rb values of pelagic sediments in relation to the continental crust. Thus, even though Plank & Langmuir (1998) proposed that the trace element contents of pelagic sediments may be a good approximation to the average continental crust due to homogenisation of different sources, sediments from continental sources might preferentially adsorb Cs from oceanic seawater. This would lead to a higher Cs/Rb ratio of pelagic sediments compared to continental crust sources, as implied by the available data sources.

In marked contrast, high-T alteration trends seem to be controlled by the size of the crystallographic sites occupied by the LIL elements in the reacting minerals and valence of the elements (Blundy & Wood, 1994; Beattie, 1994). In the only experimental study of mineral/fluid partitioning behaviour of Rb and Cs, Volfinger (1976) showed that $D^{\text{Min/Fluid}}$ values at 400-800°C are in the order Cs<Rb for all minerals analysed (sanidine, muscovite and biotite). This is identical with results from melting studies of biotite, muscovite (Icenhower and London 1995), phlogopite (LaTourrette et al., 1995; Foley et al., 1996; Melzer & Wunder, 1999) and amphibole (Zack et al., 1997). They all showed that $D^{\text{Min/L}}$ was in the order Cs<Rb≅Ba, with the largest atom (Cs) always being the least suitable element to accommodate in these crystal structures. Nevertheless more $D^{\text{Min/Fluid}}$ studies for Cs, Rb, Ba as well as high quality geochemical data for high-T altered oceanic layer 3 sections like ODP 149 and ophiolite sections are needed. The relative paucity of these data has to be taken into account when applying discrimination diagrams of LIL elements.

With these caveats in mind, plotting our phengite data in the Cs/Rb vs. Ba/Rb diagram (Fig. 7) offers some new insights into the protolith history of hydrous eclogites as well as their subsequent metamorphic history. All phengites from eclogite samples plot inside the low-T altered MORB field, whereas 6 out of 7 phengites from the surrounding metapelite plot very close to the values of the upper continental crust (Taylor & McLennan, 1985). Phengites mirror Rb/Cs and Ba/Rb ratios of their host rock (being >90% of the whole rock budget for these elements). Therefore it seems that these element ratios in the metamorphic rocks of Trescolmen still preserve the compositions of their likely protoliths. We can conclude that at least all 6 of the analysed, phengite-bearing eclogites record the LILE pattern of the original MORB-type protoliths affected by low-T alteration, e.g. at a shallow crustal level. This is in accordance with the conclusions of Miller et al. (1988) who interpreted elevated $\delta^{18}\text{O}$ values in most eclogites from Koralpe and Saualpe as evidence for a low-T ocean floor alteration effect. Similarly, Putlitz et al. (1997) proposed that the upper sections of the oceanic crust are preferentially incorporated in orogenic belts, based on oxygen isotope studies of metabasalts in the Cyclades.

Sample 50-1, a mica schist with a Cs/Rb ratio higher than the upper continental crust value, is the only sample taken from the contact with an eclogite boudin. In this sample, the grain sizes of phengite and garnet in the mica schist are larger than further away from eclogite bodies (Heinrich, 1982). The large grain sizes and the presence of quartz segregations in close association point to recrystallisation in the presence of a fluid, e.g. in the pressure shadow of the eclogite boudins. According to the discussion above concerning partition coefficients of Cs and Rb, a high-T fluid should be enriched in Cs over Rb in relation to coexisting minerals. The high Cs/Rb ratio of 50-1 can therefore be explained by phengite crystallising from or in equilibrium with a high-T fluid. Here, the fluid could have been used up during phengite growth so that the high Cs/Rb ratio was imprinted on the phengite-

Since phengite in eclogites and metapelites both record the LIL element signature of their likely protoliths, phengite or another K-rich phase such as biotite with large stability fields must have been stable during the whole metamorphic cycle. For instance, biotite forms under amphibolite conditions in both pelitic and basaltic systems and has an upper stability limit of about 1.5-2.0 GPa (Stüwe & Powell, 1995; Schmidt, 1993). Phengite is stable under blueschist and eclogite facies conditions and breaks down only by partial melting (Schmidt, 1996). Following the assumed prograde PT path for Trescolmen, amphibolite facies biotite would have transformed to phengite with increasing pressure by a complex range of continuous reactions. Interestingly, H₂O is consumed by this process (Heinrich, 1982; Schmidt, 1993), so that LILE would not be mobilised into any fluid during these reactions. If a K-rich phase were not always present in eclogites during the metamorphic cycle, the LIL elements would not have been fixed, but would instead show the ratios of the surrounding metapelites (see below). Nevertheless, some mobilisation of potassium is indicated by the presence of phengite in kyanite-quartz veins and in the coarse-grained mica schists in contact with eclogite boudins. However, the effect is qualitatively minor; for example, randomly oriented phengites in quartz segregations of one eclogite sample (CHM30) have a Cs/Rb ratio strongly differing from that of metapelite (Fig. 7) and may represent very local recrystallisation.

2.5.2 *Fluid exchange between eclogites and metapelites*

In contrast to the phengite-bearing eclogites, the samples lacking phengite and containing amphibole as the dominant LILE phase have Cs/Rb ratios lower than any likely protolith at the given Ba/Rb ratio (Fig. 7). It becomes apparent that there must have been a modification of the original LILE pattern of these samples if we take into consideration the reconstructed whole rock content. Assuming a modal abundance of 20% for amphibole and 3% for phengite where present, we have plotted reconstructed Ba contents vs. Ba/Rb ratio in Fig. 8. In accordance with their LILE ratios, the Ba contents of the phengite-bearing samples plot in the field of altered basalts. On the other hand, the three analysed samples without phengite (55-4, 59-1 and 50-14) have Ba contents about an order of magnitude lower than any likely protolith. In these samples, some Ba (along with Rb and Cs) depletion is therefore inferred to have occurred.

Another important observation is that amphibole from the samples lacking phengite has very similar LIL element contents to the amphibole coexisting with phengite. If we preclude a mere coincidence, the implication is that *all* amphibole is in equilibrium with phengite, the phase dominating the LILE budget in eclogites and metapelites. Sample 59-1 was taken from the centre of an eclogite body about 2 m in diameter. No phengite was observed anywhere in the whole body. We therefore conclude that the LILE contents of the amphibole were controlled by a fluid buffered by phengite in the adjacent metapelite, suggesting at least a metre scale fluid mobility. The absolute water influx may have been very low. Given a weight abundance of amphibole between 10 to 30% with the amphibole having 2 wt% H₂O, the H₂O influx required for the amphibole growth need not have exceeded 0.2 to 0.6 wt% H₂O. Nevertheless, the total fluid required to develop similar LIL element patterns in all eclogitic amphiboles must have been higher in order to permit amphibole growth from a fluid with constant composition that did not become depleted by the take-up of LIL elements into the amphibole structure (as suggested for phengite in sample 50-1). To quantify this process, an approach similar to the widespread modeling of stable isotope interactions can be

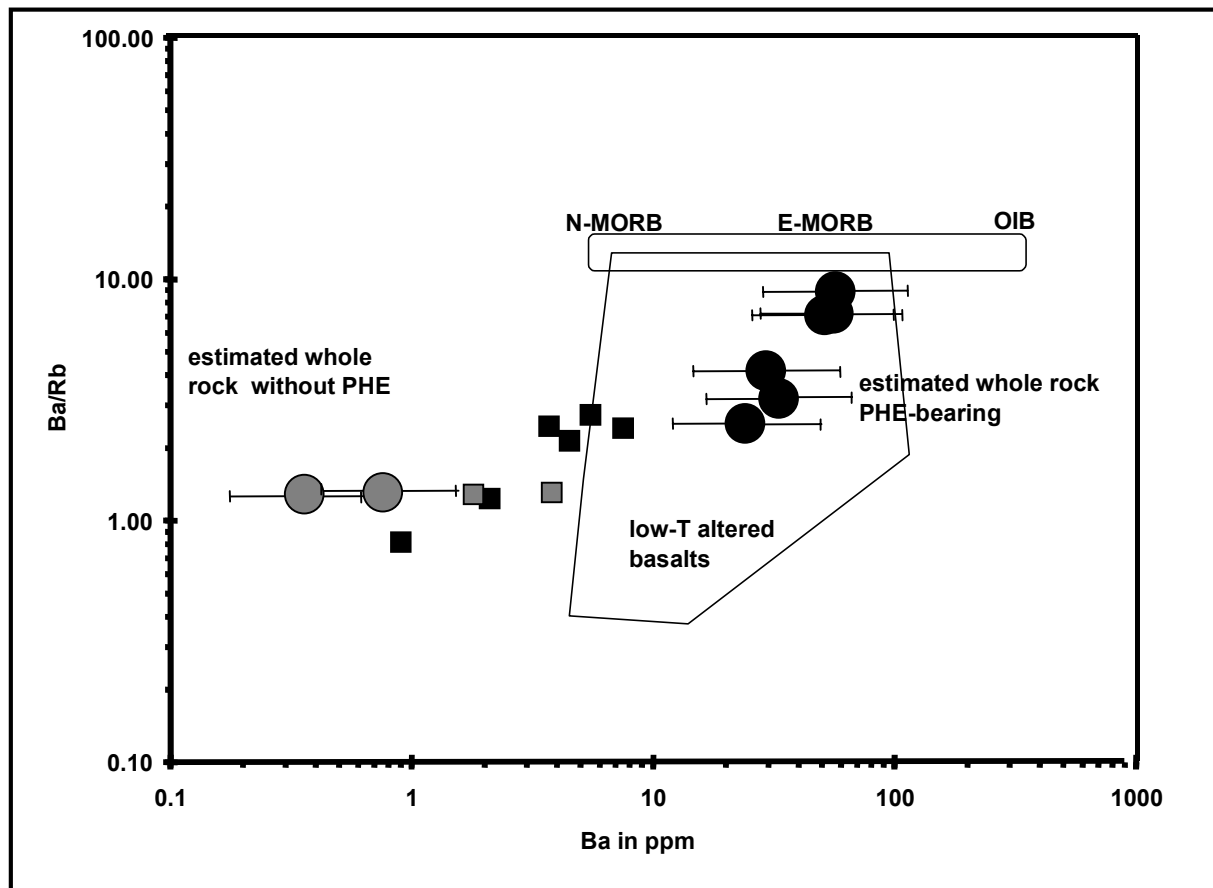


Fig. 8 *Ba/Rb vs Ba* plot illustrating (1) similar amphibole composition of phengite-bearing and -lacking eclogites (for symbols see Fig. 7); (2) reconstructed whole rock composition of phengite-bearing samples consistent with low-*T* altered basalt, and phengite-free samples lying outside any field of likely protolith, implying depletion through fluid-rock interaction. Black circles- reconstructed whole rock composition of phengite-bearing eclogites assuming 2% phengite (error bars showing maximal variability with 1-3% phengite); gray circles- reconstructed whole rock composition of phengite-lacking eclogites assuming 20% amphibole (error bars showing maximal variability with 10-30% amphibole).

used. Equations for modelling trace elements in open systems are taken from Nabelek (1987; his equation 10). Depletion in LILE concentration of amphibole-bearing eclogite by a metapelite-derived fluid can be modelled using the following assumptions: (1) an average phengite composition from the 6 analyzed mica schists, and $D^{\text{Phe/Fluid}}$ values as estimated in the appendix were used to calculate the composition of the fluid in equilibrium with the metapelite (15 ppm Cs, 75 ppm Rb and 740 ppm Ba); (2) after 0.6 wt% H₂O influx, the LILE elements from the metapelite-derived fluid are completely stored in the amphibole (resulting in a whole rock composition of 0.093 ppm Cs, 0.45 ppm Rb and 4.5 ppm Ba); and (3) treating amphibole as the dominant phase controlling LILE in the absence of phengite, assuming a constant amount of 30% modal amphibole in the eclogite and using $D^{\text{Amp/Fluid}}$ values as estimated in the appendix, yields whole rock partition coefficients (0.00012, 0.006 and 0.0009 for Cs, Rb and Ba, respectively). With these data the composition of amphibole from sample 59-1 could be reproduced with a minimum open system W/R ratio of 0.01.

The minimum calculated W/R ratio of about 0.01 is based on the assumption that all LILE elements were transported into the eclogite from the surrounding metapelite. This model would be in accordance with the petrographic observation that amphibole growth was triggered by fluid influx (reaction 2). A higher W/R ratio would be needed if the current LILE contents of amphibole were attained by leaching by a throughflowing fluid at high pressure from amphibole previously containing the higher LILE of the protolith. To quantify this kind of fluid/rock interaction, the same assumptions as above were made except that the starting composition of the eclogite was a moderately low-T altered basalt (0.34 ppm Cs, 17.7 ppm Rb, 10.2 ppm Ba). In this scenario, the amphibole composition of sample 59-1 could be reproduced at open system W/R ratios of at least 0.03. More extreme parameters such as more strongly altered basalt or a higher modal amount of amphibole would result in higher W/R ratios.

An upper W/R ratio can be derived from the LILE systematics of eclogitic and metapelitic phengite. Even though metapelitic and eclogitic phengites do not occupy distinct fields in Fig. 7, both rock types can be clearly distinguished by their spread of Cs, Rb and Ba concentrations (Fig. 4). Phengite in 6 metapelite samples, taken representatively from the whole area of Trescolmen, show an extremely homogeneous composition (11.2, 370 and 2110 ppm for Cs, Rb and Ba, with standard deviations of 5-7 %). In contrast, phengite in eclogites shows a much wider range of Cs, Rb and Ba concentrations (6.7-12.8, 320-520 and 1200-2800 ppm for Cs, Rb and Ba, standard deviation of 6 samples 22-34 %). The heterogeneous composition of different eclogites can only be preserved if element exchange between metapelites and eclogites was restricted. This restricted exchange can be modelled in terms of W/R interaction between a phengite-bearing eclogite and a metapelite-derived fluid, giving an upper limit for a W/R ratio. For the following we assume that: (1) the eclogite with the phengite composition furthest away from metapelitic phengite was taken (CHM30) with a calculated whole rock composition (1 modal % of phengite) of 0.067 ppm Cs, 3.9 ppm Rb and 27.8 ppm Ba; (2) the metapelite-derived fluid is used in the same way as for the amphibole calculations; (3) phengite is the only phase controlling LILE, resulting in whole rock partition coefficients of 0.008, 0.05 and 0.023 for Cs, Rb and Ba using $D^{\text{Phe/Fluid}}$ values as estimated in the appendix. Under such conditions a W/R ratio of greater than 0.1 would have obliterated LILE ratios of any likely low-T altered basalt protolith and produced phengite compositions identical to the phengites in the mica schist samples.

2.5.3 *Implications for subduction zone environments*

The geochemical pattern of the hydrous eclogites from Trescolmen permits their use as a case study for the behaviour of low-T altered basalts undergoing subduction. We have shown evidence for fluid migration under high pressure conditions (>1.8 GPa). The total amount of fluid could have been very low. Nevertheless one scenario can be excluded: If fluid from the surrounding metapelites was just enough to form amphibole, the resulting Cs/Rb ratio (ca. 0.2) would be almost two orders of magnitude higher than observed (0.004 for sample 59-1). The most efficient mechanism to explain the observed LILE pattern of the eclogitic amphiboles is pervasive fluid circulation equivalent to open system behaviour. The fluid in equilibrium with the surrounding metapelites infiltrates the eclogite bodies, in case of 59-1 at least on a metre scale. The calculated W/R ratio is extremely low (from 0.01 to 0.1).

W/R ratios of as low as 0.01 are in accordance with observed oxygen isotope heterogeneities on a decimetre scale in eclogites from the Tauern Window in a structurally similar setting (Getty & Selverstone, 1994), since oxygen isotope changes would be too small to be measurable. Fluid-rock ratios of 0.01 will cause only minor changes in $\delta^{18}\text{O}$ values even for interaction between two extremely different compositions (e.g. fluids in equilibrium with carbonate sediments interacting with mantle-derived basalts would shift $\delta^{18}\text{O}$ by 0.2 ‰). Fluid interaction between less extreme compositions such as oceanic pelites and low-T altered basalts (Trescolmen case) would result in almost undetectable changes in the $\delta^{18}\text{O}$ values, even for W/R ratios of 0.1. Experimental results of Watson & Lupulescu (1993) indicate non-wetting behaviour of aqueous fluids in clinopyroxene-rich systems which seems to be in contrast with our findings. Nevertheless, the strong anisotropy induced in rocks undergoing plastic deformation may facilitate fluid influx, as discussed for mylonitised marbles by Holness (1997). This effect is likely to dominate in most eclogites from Trescolmen, where a penetrative foliation is locally defined by partly aligned amphiboles.

Since fluids are able to infiltrate eclogitic rocks under high pressure, it is concluded that fluids can also leave this system. The ability of very small volumes of fluid to penetrate eclogitic systems is a prerequisite of many models addressing the large-scale behaviour of subduction zones, although the migration mechanisms and potential problems with fluid migration are seldom considered. The existence of volcanoes above subducting slabs of variable depths (from ca. 120 km to >400 km), together with systematic geochemical changes in these volcanic rocks, has been explained by a steady, though decreasing amount of fluid flux from the subducting slab wedge into the underlying mantle (Woodhead & Johnson, 1993; Ishikawa & Nakamura, 1994; Ryan et al., 1995; Ishikawa & Tera, 1997; Shibata & Nakamura, 1997; Moriguti & Nakamura, 1998). Most of this fluid component (as high as 99% in the case of the Izu arc) is thought to originate from the upper part of the altered oceanic crust, based on Li-B-Pb isotope systematics (Moriguti & Nakamura, 1998). The amount of fluid available from continuous and discontinuous dehydration reactions has been modelled by Poli & Schmidt (1995) and Schmidt & Poli (1998). In cold subduction zones, only about 0.1 wt% of H_2O is produced per 50 km depth, mostly from the continuous reactions $\text{lawsonite} + \text{diopside} + \text{garnet}_1 \rightarrow \text{garnet}_2 + \text{coesite/stishovite} + \text{H}_2\text{O}$, and $\text{phengite} \rightarrow \text{K-rich clinopyroxene} + \text{enstatite} + \text{coesite} + \text{H}_2\text{O}$ (Schmidt & Poli, 1998). These small amounts of fluids must be able to leave their eclogitic source rocks in a more or less continuous manner to ultimately produce the observed across-arc variations in many arc systems (Kuriles, Izu-Bonin, New Britain, NE Japan, etc.). Our results support such a scenario in which small amounts of H_2O can leave their production site, probably facilitated by ductile deformation, and subsequently becoming collected in an anastomosing vein system (Widmer, 1996).

2.6 Conclusions

1. Eclogites from Trescolmen show petrographic evidence for fluid migration under high pressure conditions. Kyanite is partly replaced by paragonite, barroisitic amphibole overgrows older omphacite and high pressure (>2.0 GPa) talc veins infiltrate a Mg-rich eclogite body.
2. LAM-ICP-MS measurements on all high pressure mineral phases reveal that phengite is the dominant phase for Cs, Rb and Ba in eclogitic rocks, accommodating >90% of the whole rock budget in phengite-bearing samples. Other phases such as paragonite and amphibole have only a very limited capacity to incorporate these elements.
3. Comparison of whole rock and in-situ mineral data shows that secondary phases, even in the freshest rock samples, can severely alter the composition of whole rock samples for fluid-mobile elements such as Ba. This clearly demonstrates the advantage of in-situ geochemical methods over whole rock analysis in extracting petrogenetic information in complex metamorphic assemblages.
4. Cs/Rb and Ba/Rb ratios of eclogites and garnet micaschists retain the patterns of their likely protoliths, i.e. low-T altered basalt and upper continental crust, respectively. LILE pattern of amphibole in phengite-lacking samples plot outside any likely protolith, but are identical to patterns in amphiboles in phengite-bearing samples. The observed data can be explained by flow of fluid derived from metapelite through the eclogite bodies, leading to amphibole homogenisation. Nevertheless the amount was small enough to leave original phengite patterns intact.
5. Modelling of open system fluid-rock interaction give a range of possible W/R ratios of 0.01-0.1. This result is consistent with the observation of oxygen isotope heterogeneities in other alpine eclogite bodies, showing that in-situ LILE analysis are more suitable for regions of low W/R interaction.

2.7 Appendix to Chapter 2

First order estimates about $D^{\text{Min/Fluid}}$ can be made for the minerals of interest on the basis of very sparse experimental and our own data. A number of simplifications have to be made. Here, we do not differentiate between biotite and phlogopite, nor muscovite and phengite, pressure (0.02-2 GPa) and temperature (600-800°C) effects are not taken into account. Plank & Johnson (1997) measured bulk rock / fluid partition coefficients of Rb and Ba (1.5 and 0.7) in an experiment at 600°C/2.0 GPa with a red clay as starting material. Since typical red clays contains between 5-7% K_2O and muscovite and biotite were the only significant K-bearing phases we can estimate a modal abundance of about 30% of these two minerals. With this modal abundance and a similar partitioning behaviour of biotite and muscovite (Icenhower & London 1995), $D^{\text{Phe/Fluid}}$ can be calculated as 5 and 2.3 for Rb and Ba. It is encouraging to notice that Beswick (1973) and Melzer & Wunder (1999) derived similar $D^{\text{Phe/Fluid}}$ values for Rb (4.4 and 2, respectively). Volfinger (1976) determined a Rb-Cs K_D between muscovite and water. Using his experiments, a $(Rb/Cs)^{\text{Fluid}}/(Rb/Cs)^{\text{Phe}}$ value of 0.17 translates into a $D^{\text{Phe/Fluid}}$ for Cs of 0.8. From our natural $D^{\text{Amp/Phe}}$ ratios (0.0005, 0.004 and 0.001 for Cs, Rb and Ba respectively), $D^{\text{Amp/Fluid}}$ for Cs, Rb and Ba can then be estimated (0.0004, 0.02 and 0.003 respectively). Compared to $D^{\text{Amp/L}}$ values from experimental studies, our estimates are best matched by amphiboles with richteritic compositions ($D^{\text{Amp/L}}$ for Cs, Rb and Ba are 0.0008, 0.06 and 0.008; Brumm et al., 1998).

	$D^{\text{Phe / Fluid}}$	$D^{\text{Amp/Phe}}$	$D^{\text{Amp/Fluid}}$
Cs	0.8	0.0005	0.0004
Rb	5	0.004	0.02
Ba	2.3	0.001	0.003

Chapter 3. Trace element abundance in eclogitic rutile

3.1 Introduction

Rutile is a common phase in a wide range of lithologies (plutonic and metamorphic rocks, sediments, hydrothermal ore deposits). It has attracted considerable attention as the prime controller of Nb and Ta budgets in subduction zone processes (Saunders et al., 1980; McDonough, 1991; Brenan et al., 1994; Stalder et al., 1998). However, it has been known for a long time that rutile can accommodate a wide range of highly charged trace elements in addition to Nb and Ta (Fig. 9) up to the percent level, e.g. Cr, Fe, Al, V, Sn, Sb and W (Graham & Morris, 1973; Haggerty, 1991; Deer et al., 1992; Rice et al., 1998). Under experimental conditions, Mo has also been found to substitute readily into the rutile structure (Marinder et al., 1962). The relatively simple, incompatible behaviour of the chalcophile/siderophile elements Mo, Sn, Sb and W under magmatic conditions, in combination with their selective fluid mobility (depending on the nature of the fluid), makes them ideal tracers for various processes involving fluids, including seafloor alteration (for Sb and Sn see Jochum & Verma, 1996) and subduction zone systems (Noll et al., 1996). The link between the favourable crystal chemical structure of rutile for Mo, Sn, Sb and W on the one hand, and the behaviour of these elements in global chemical systems on the other, is not yet fully appreciated. Fitton (1995) observed a strong correlation between Nb and Mo in subduction related lavas, which he explained by rutile as a residual phase retaining both elements. McDonough (1999) reported high concentrations of Mo and W in rutiles from eclogitic xenoliths and pointed to rutile as an important reservoir for these elements in plate tectonic processes.

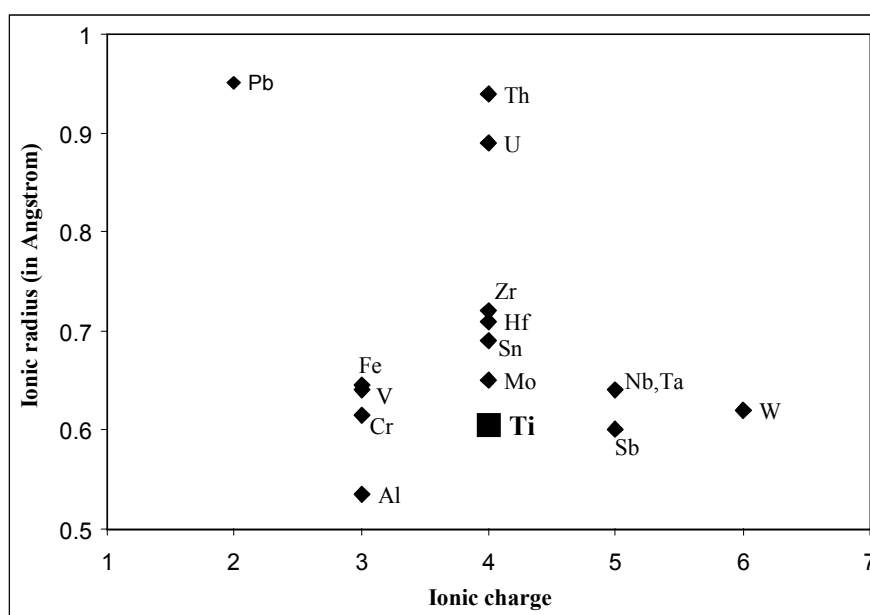


Fig. 9 Ionic charge against radius for elements investigated in this study. Charges reported in rutile structure were used, which closely corresponds to element charges in common geologic systems (Jochum & Hofmann, 1997), except for Mo (4+ instead of 5+; see Fitton, 1995). Ionic radii are from Shannon (1976).

The intention in this chapter is to evaluate the behaviour of a range of highly charged elements in hydrous eclogites and accompanying garnet mica schists, because both lithologies are potential sources for subduction zone-related fluids. Rutiles were analysed with electron microprobe (EMP) and laser ablation microprobe-ICP-MS (LAM). The EMP offers the advantage of higher spatial resolution whereas the LAM allows the study of the majority of naturally occurring trace elements. Of these elements, Mo, Sn, Sb and W are not routinely measured with LAM, making it necessary to pay special attention to potential analytical difficulties. Mass balance calculations of trace elements in a single whole rock are a powerful tool to evaluate the importance of different phases for different elements (Sorensen & Grossmann, 1989; Tribuzio et al., 1996). For one sample, all analysable phases with LAM have therefore been measured and their modal abundance as well as the whole rock trace element concentration has been determined.

This study provides strong evidence for the importance of rutile as a principal carrier for Cr, Nb, Ta, Mo, Sn, Sb and W in metamorphic rocks. The implications are far-reaching and are discussed for two different applications, sedimentary provenance studies and modelling of subduction zone processes.

3.2 Analytical procedures

3.2.1 Electron microprobe

Microprobe analyses of rutile were performed with a JEOL JXA 8900RL instrument in Göttingen. For high precision, low background measurements, 20 kV acceleration voltage, 80 nA beam current on the Faraday cup, 5 μm beam diameter and long counting times (between 60-180 sec on the peak for Si, Cr, Fe, Ca, Al and 360 sec for Nb, Sb and W) were chosen. An EDS detector was used for simultaneous Ti determination. Selected samples (Ad25, 50-13, 52-1, 77-5, Disentis, Laora) were analysed with 30 kV acceleration voltage to increase sensitivities, which was especially effective for W. Here, the measurement conditions were 80 nA beam current on the Faraday cup, 8 μm beam diameter and counting times on the peak were 16s for Ti, Fe, 120s for Mg, Al, Si, Ca, V, Cr, 300s for Mn, Zr, Nb and 600s for W. The matrix correction method for the raw counts is phi-rho-zet (Armstrong, 1991). We used an additional off-line correction especially designed for trace element analysis of rutile. The off-line correction was necessary since background corrected count rates on a pure synthetic rutile (Earth Jewelry Co. Japan) otherwise give negative values for certain elements (Al, Zr, Nb, W), with apparent negative concentrations of as large as 80 ppm (for W). Errors as large as this cannot be attributed to asymmetrically curved bremsstrahlung adjacent to element peaks (Fialin et al., 1999). It can be observed from Fig. 10 that bremsstrahlung adjacent to the Nb peak is highly linear inside the brackets given by spectrometer position where the backgrounds are measured. Similar linear relationships have also been obtained for W and Zr. We therefore interpret apparent negative concentrations as resulting from sample drift during the long counting times and high beam currents. Nevertheless, negative concentrations in the synthetic rutile are highly systematic and were corrected for by repeatedly measuring the synthetic rutile standards to obtain "true" zero-concentration count rates on the peaks. Each 5 analyses of rutiles from Trescolmen samples were followed by 2 analyses of the synthetic rutile standard. V $K\alpha$ overlap by Ti $K\beta$ was corrected online by the JEOL software after the method of Fialin et al. (1997). The analytical procedure allowed measurement of Nb concentrations at the 100 ppm level with a standard deviation of 5-10% (from counting

statistics). Calculated detection limits for measurements at 30 kV are 20-35 ppm for Mg, Al, Si, Ca, Cr, 40 ppm for Mn, Fe, 45 ppm for Nb, W and 80 ppm for Zr; calculated from repeated measurements ($n=26$, student's T-test) with a 95% confidence level which gives 2.05 times the standard deviation of peak count rates in the rutile standard. Mg and Mn concentrations are always, and Sb mostly, below detection limits, so that we do not include them in Table 4. However, for the most Sb-enriched rutile (sample 77-5), concentrations for Sb measured by electron microprobe are 75 ± 25 ppm and by LAM 81 ± 16 ppm), demonstrating an acceptable agreement between both methods for Sb measurements.

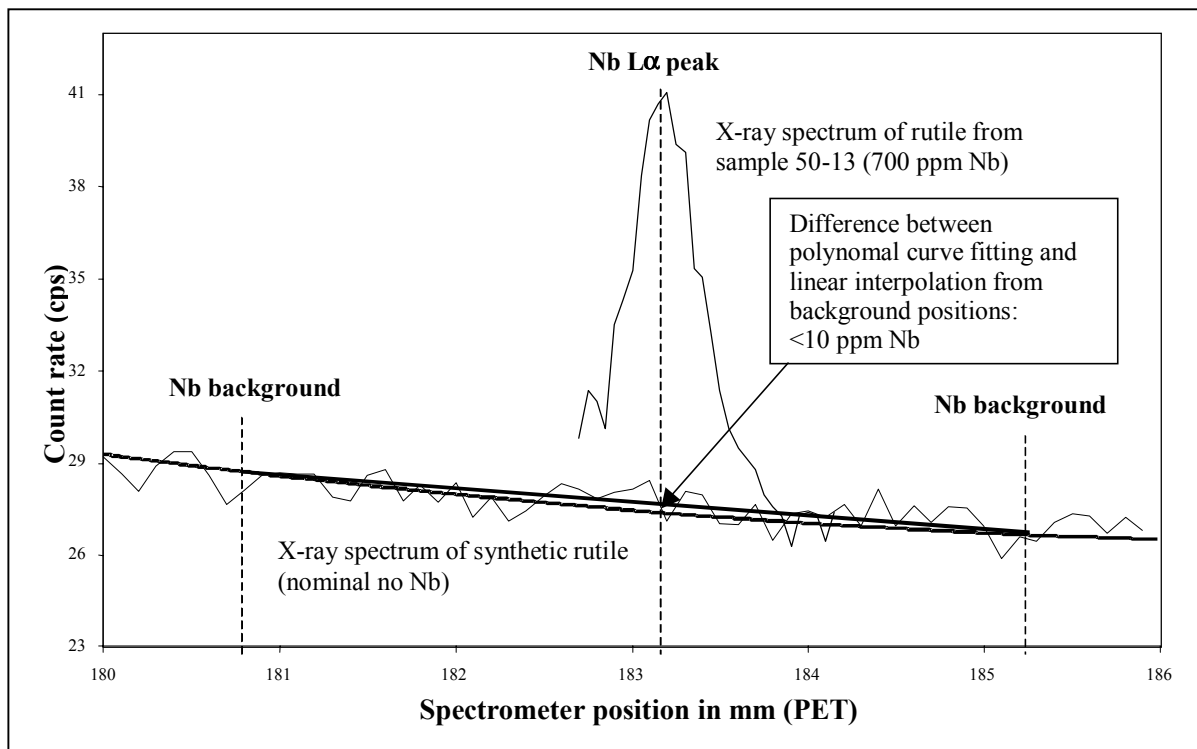


Fig. 10 X-ray spectrum of the area around the Nb $L\alpha$ peak are plotted from a synthetic rutile and a rutile from sample 50-13. The lack of an observable Nb peak in the spectra of the synthetic rutile validates the use of this sample as a "zero-concentration" standard. A significantly curved bremsstrahlung between the brackets of the Nb background positions can be ruled out as a source for error in the measurement of Nb trace element concentrations. Analytical conditions were 29 kV acceleration voltage, 80 nA beam current on the Faraday cup, 120 seconds per step and a step width of 50 μm of the PET spectrometer. Typical error is ± 10 cps per step.

In order to fully assess trace element mass balance in eclogite, element mapping of a whole thin section was performed on one sample (50-13). In this case, 288,000 single analyses (steps) were accumulated during a 6 hour experiment (70 ms per point, 50 microns step width, mapping area 3.6 x 2 cm) with Mg, Al, K, Ca, Fe by WDS, Na, Si, P and Ti on EDS and a simultaneous acquisition of the backscatter signal in composition mode. The data were processed with a graphical JEOL software package that assigns each data point to a particular phase (Fig. 11). This rapid technique offers a method to simultaneously determine the modal percentages of most phases (limited to those larger than about 5 μm diameter, so that zircon was not quantified) along with textural information.

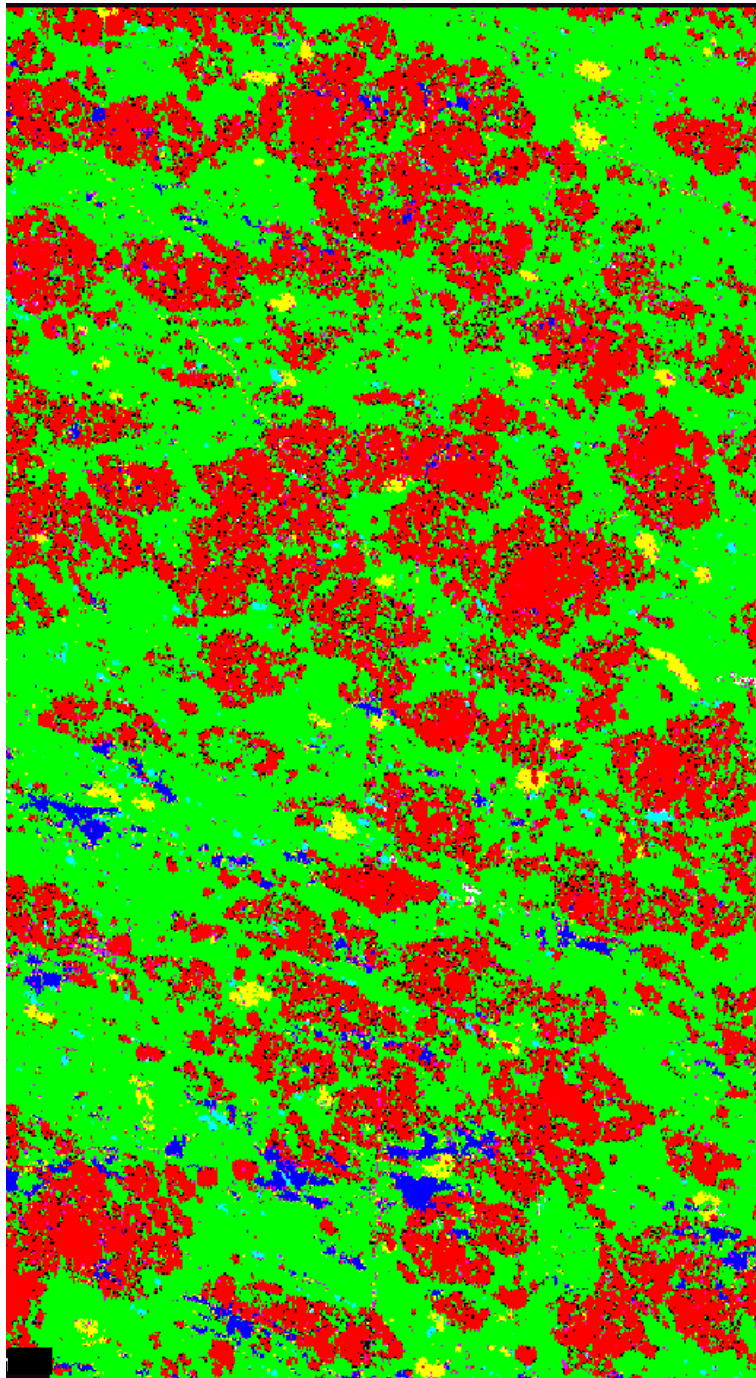


Fig. 11 Phase map of sample 50-13. Mineral phases are shown by different colours: green- clinopyroxene, red- garnet, yellow- amphibole, blue- phengite, turquoise- apatite, black- unspecified.

3.2.2 Laser ablation microprobe

Optimum laser tunings for the ablation of rutile in regular thin sections were reached with a defocused beam, with the focal point varying from 100 μm above the mineral surface at 0.05 mJ for smallest ablation pits (20 μm in diameter) to 300 μm above the surface at 0.4 mJ for largest ablation pits (100 μm in diameter). NIST glass standards SRM 610 and 612 were used for calibration, with recommended values taken from Pearce et al. (1997). Chalcophile and siderophile elements generally show different ablation behaviour compared to lithophile elements, leading to fractionation effects among the different element groups (Longerich et al., 1996). However, under the conditions described above, fractionation effects were minimised; even for antimony, the most difficult element, after one minute of rutile ablation Sb/Nb ratios deviated less than 20% from the starting value for both rutile and glass (Fig. 12). In some runs designed to achieve lower detection limits, Ti was taken out of the element menu to avoid tripping of the detector during rutile ablation. Here, Nb measured by electron microprobe was taken as the internal standard for both rutile and the glass standards. The use of Nb as an internal standard for rutile analyses is justified by the excellent agreement between Nb concentrations measured in several samples with both techniques (Fig. 13).

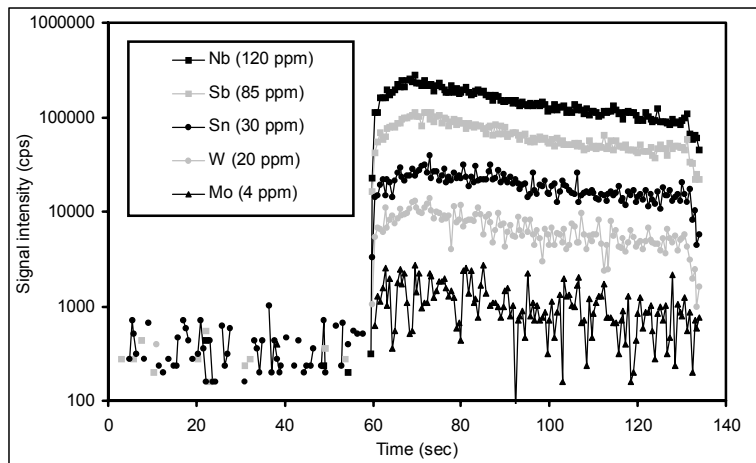


Fig. 12 Typical ablation signal of rutile in LAM analysis. In this example, Nb from EMP measurements has been taken as the internal standard.

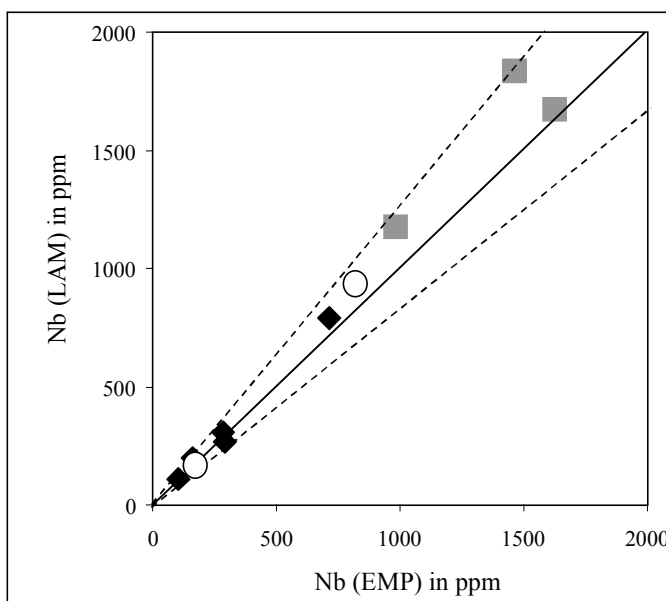


Fig. 13 Comparison of Nb concentrations in rutiles analyzed by electron microprobe (EMP) and LAM-ICP-MS (LAM). Black diamonds are rutiles from eclogites, grey squares represent rutiles from garnet micaschists and white circles rutiles from Disentis and Laora. Solid line represents a perfect 1:1 correlation, dotted lines are upper and lower range of a 20% deviation from the 1:1 line.

Given the combined uncertainties on Nb measurement of both techniques (15-20% for LAM, 1-10% for EMP) on Nb, all data are identical within error and no systematic offset can be detected for concentrations from 100 ppm to almost 2000 ppm. This statement can be extended to measurements of the elements Zr, V and W, where data have also been obtained by both methods in several samples. For W, concentrations down to 60 ppm measured by LAM (samples Ad25, 52-1) can be reproduced by EMP, whereas the extremely low concentration of 17 ppm (sample 77-5) was correctly predicted as being below the detection limit of the EMP (≤ 45 ppm). A comparison of EMP and LAM measurements for several trace elements stresses the validity of using completely different materials with contrasting ablation behaviour for LAM standardisation (oxide minerals vs. glass standard) and shows that all interferences relevant for the analysis of rutiles have been considered. On the other hand, it shows that trace element abundances down to 60 ppm can be *accurately* measured with the EMP if a "zero-concentration correction" can be applied.

For LAM analysis of Mn-rich phases, it was found that molybdenum has to be measured on the ^{98}Mo isotope. 0.5% MnO in garnet produces an overlap of $^{55}\text{Mn}^{40}\text{Ar}$ on ^{95}Mo that results in an apparent molybdenum concentration of about 1 ppm. For all other analysed phases this effect is not significant since Mn concentrations are always below 0.03%. $^{55}\text{Mn}^{40}\text{Ar}$ interferences have been reported previously (Becker et al., 1996) to form during plasma formation at a relative MnAr/Mn ratio of about $3.5 \cdot 10^{-5}$, which is about one order of magnitude less than measured during our runs. The formation of titanium argides may be significant for the analysis of Sr and Y in rutiles due to $^{48}\text{Ti}^{40}\text{Ar}$ and $^{49}\text{Ti}^{39}\text{Ar}$ producing an apparent Sr concentration of about 10 ppm and $^{49}\text{Ti}^{40}\text{Ar}$ an apparent Y concentration of about 1 ppm.

One other interference that might be significant in the analysis of elements measured in this study is $^{41}\text{K}_2\text{O}^+$ on ^{98}Mo (May & Wiedmeyer, 1998). We found the concentration of molybdenum in phengite (containing about 10% K_2O) to be 6 times higher if ^{98}Mo was analysed instead of ^{95}Mo , and therefore used ^{95}Mo for the analyses of phengites (less than 0.01% MnO) and ^{98}Mo for the remaining phases. A comparison of different isotopes of the same element (^{118}Sn and ^{120}Sn , ^{121}Sb and ^{123}Sb , ^{182}W and ^{184}W) gives excellent agreement in the phases rutile, clinopyroxene, garnet and phengite, therefore precluding any significant interferences for these elements. As a result of these considerations, the following isotopes were used in this study: ^{49}Ti , ^{51}V , ^{90}Zr , ^{93}Nb , ^{95}Mo , ^{98}Mo , ^{120}Sn , ^{121}Sb , ^{177}Hf , ^{181}Ta , ^{184}W , ^{208}Pb , ^{232}Th , ^{238}U . Zircon and sulphide grains (chalcopyrite and pyrite) were always too small ($< 20 \mu\text{m}$) for the acquisition of precise data. However, mixed analyses of these minerals with their surroundings were gathered, but only qualitatively processed to identify approximate abundances of investigated trace elements.

3.3 Evaluation of results

From the elements analysed in this study, most highly charged elements ($\geq 4+$) in rutile give good signal intensities with LAM-ICP-MS (Fig. 12). The only exception, where count rates were mostly below the detection limit, is Th, which is also the largest cation analysed (Fig. 9). Trace elements show different behaviour in terms of total variability (Table 4), with a large spread (more than a factor of 10) among all samples for Cr (140-16000 ppm), Nb (100-4400 ppm), Sb (4-80 ppm), W (17-235 ppm), Pb (< 0.1 -10 ppm), U (0.01-10 ppm) and a smaller spread for V

(1100-2000 ppm), Zr (80-250 ppm), Mo (2.3-7.0 ppm) and Sn (30-130 ppm). From this general observation one might suspect that the former elements will be potentially more interesting for characterising rutile populations.

Investigations of the homogeneity of Nb and Cr in rutiles showed that within an area of about 1 cm² in each sample, variations in measured Nb and Cr concentrations (both core to rim variations and variations between different grains) are generally less than statistical scattering of the EMP. The only exception is sample 55-3, a coarse grained Cr-rich metagabbro that did not thoroughly recrystallise under eclogite facies conditions (Chapter 4), where different rutile grains show wide compositional variations. Domains of former chromites contain Cr-enriched phases such as omphacite, phengite and rutile, with Cr concentrations in rutile up to 2.4% Cr₂O₃ (compared to 2500 ppm Cr outside the Cr-rich domains).

Table 4. Trace element compositions (in ppm) of rutiles from Trescolmen eclogites and garnet micaschists, measured by electron microprobe (EMP) and laser ablation microprobe-ICP-MS (LAM). Whole rock content of eclogites were determined by XRF, except for values marked with * which were analyzed by LAM on glass pellets (Reid 1998).

	Ad25	CHM30b	50-2	52-1	50-13	Eclogites		55-4	59-5	77-5
						50-14	55-3			
							low-Cr	high-Cr		
EMP										
Ca	880	366	459	70	434		272	1201		52
Al	293	79	116	143	221					216
Cr	1155	3157	142	682	1798	667	2532	16421	3965	670
Fe	2923	2513	2435	2489	2739	3222	5604	1671	1341	2088
Si	391	128		b.d.	147	112	388	318	125	b.d.
Nb	104	554	285	273	693	161	4446	1293	107	77
Zr	124			162	156					178
V	735			1495	1371					1160
W	65			61	290					b.d.
LAM										
V		1507		1927	1293				2008	
Zr	84	118	142	126	149	93			151	156
Nb			304	267	786	196			684	109
Mo	2.3	3.6	5.4	7.0	4.6	4.9				4.0
Sn	28	28	41	39	42	87				27
Sb	9.6	28	6.4	8.8	5.5	9.6				81
W	60	88	95	68	235	109				17
Pb	1.8	0.96	3.4	0.75	1.2	0.31			<0.12	3.4
Th	<0.03	0.017	<0.02	<0.01	<0.02	0.0043			<0.04	<0.01
U	0.11	0.23	2.6	0.90	0.92	1.4			0.22	4.1
Hf	3.0	6.1	5.7	5.2	5.5	3.7			6.7	6.5
Ta	7.57	34.8	21.6	15.3	48.2	11.8			41.0	6.57
Nb/Ta	13.6	15.9	14.1	17.4	16.3	16.6			16.7	16.6
Whole rock										
TiO ₂		0.9	2.34	2.95	1.19	2.42		0.67	1.13	0.84
Cr		1045	287	90	612	244		1030	664	803
Nb		8.4	11.2	12.8	12.9	4.04*		5.91*	7.98*	0.79*
Ta						0.24*		0.35*	0.51*	<0.1*
Nb/Ta						16.8		16.9	15.6	>7.9

Table 4 (continued).

	Garnet micaschists					Other rutiles	
	50-1	50-9	59-4	60-2	61-1	Disentis	Laora
EMP							
Ca	56	88	32	45	45	b.d.	b.d.
Al	134	200	139	275	108	100	76
Cr	703	352	473	267	408	1138	775
Fe	3323	5003	3800	10651	2347	3370	3671
Si		187	319		245	b.d.	b.d.
Nb	1215	1460	1626	1438	984	147	809
Zr						150	110
V						782	1569
W						b.d.	103
LAM							
V		1115	1102		1820		
Zr		97	105		167	141	84
Nb		1839	1672		1012	162	899
Mo		5.2	4.3		4.0	0.74	0.23
Sn		128	99		65	15	33
Sb		5.1	4.2		4.6	0.29	1.9
W		123	86.8		145	62	135
Pb		4.9	9.8		1.5		
Th		0.21	<0.03		<0.08		
U		7.4	9.7		7.2		
Hf		4.1	4.3		6.3	6.6	4.8
Ta		114	101		54	10	34
Nb/Ta		16.2	16.6		18.9		
Whole rock							
TiO ₂							
Cr							
Nb							
Ta							
Nb/Ta							

Large rutile grains from two other localities (Disentis, Switzerland, grown in post orogenic hydrothermal quartz veins; Laora, Minas Gerais, Brazil) were also analysed during the course of this study with the general aim of searching for homogeneous crystals suitable as standards for in-situ methods.

3.3.1 Mass balance calculation for eclogite sample 50-13

Mass balance calculations have been used in metamorphic rocks to evaluate the importance of each phase as a host for certain trace elements (Sorensen & Grossman, 1989; Tribuzio et al., 1996; Nagasaki & Enami, 1998; Chapter 2; Chapter 4). This approach requires knowledge of a number of parameters, the most important being the concentration of the trace elements of interest in *all* coexisting phases, the modal abundance of these phases and ideally the whole rock major and trace element concentrations as independent quality controls for the calculations.

We have performed a mass balance calculation on sample 50-13, since this eclogite is ideal for such an analysis in terms of freshness, coarse grain size and homogeneous mineral composition (Chapter 4). Additionally it can be seen

in Fig. 11 that the texture of this sample reveals a preferred orientation of omphacite, garnet, phengite and amphibole, indicating that these phases formed syntectonically under eclogite facies conditions. Microscopic observation confirms that rutile also recrystallized under these conditions, since rutile is commonly aligned as strings of grains parallel to the same foliation and shows no signs of corrosion or mineral overgrowth (e.g. by ilmenite).

The modal abundance estimates of omphacite, garnet and amphibole are entirely based on element mapping, whereas the modal abundance of accessory phases were estimated from XRF data (Ti for rutile, K for phengite and Zr for zircon; see Table 5 for details). These phase abundances cannot be precisely calculated by element mapping due to mixed analyses from small grain sizes of these accessory phases. Here, rutile abundance was adjusted from 2% given by element mapping to 1.1% calculated from TiO₂ content by XRF analysis, and phengite was adjusted from 1.8% to 5.8% as calculated from K₂O content. The lower value for phengite given by the element mapping is probably not only a result of its small grain size, but also a function of its platy shape inasmuch as a section perpendicular to the mica cleavage (as in this thin section, cut perpendicular to the main foliation) results in a minimum of areal coverage. However, the mass balance calculation is quite robust and small changes in modal abundances (e.g. for phengite) do not alter the following conclusions.

Table 5. Mass balance for eclogite sample 50-13. Numbers under mineral abbreviations give modal abundance measured by phase mapping, except numbers in bold that were calculated from XRF whole rock data. Trace element data for phases is measured by LAM, except K₂O content by EMP and Zr content in zircon given by stoichiometry.

	50-13						recon.	whole rock	mantle element ratios	MORB composition
	CPX	GRT	AMP	PHE	RUT	ZRC				
	55	36	2.0	5.8	1.1	0.018				
TiO ₂	0.074	0.045	0.26	0.35	100		*	1.2 ^a		0.7-3.2
K ₂ O			0.4	9.8			*	0.57 ^a		0.03-0.19
Nb	0.0095	0.046	0.093	0.58	786		9	13 ^a		0.7-21
W	0.029	0.006	0.018	1.7	235		2.7			0.007-0.17
Sb	<0.02	<0.02			5.5		0.061			0.03-0.05
Mo	0.12	0.11	0.08	0.12	4.6		0.20			0.18-0.69
Sn	0.79	0.17	1.2	2.0	42		1.1			0.6-2.6
Zr	2.0	3.6	5.9	0.3	149	491000	*	93 ^a		40-230
Cr	654	359	742		1883		522	612 ^a		70-410
Th								0.82 ^b		0.02-0.91
Ba								104 ^b		1.4-105
Pr								2.9 ^b		1.0-2.9
Sm								3.6 ^b		1.6-7.9
Sb/Pr								0.021		0.020 ^c
Sn/Sm								0.30		0.32 ^d
Mo/Pr								0.069		0.23 ^e
W/Th								3.3		0.20 ^f
W/Ba								0.026		0.0016 ^e

* - Reconstructed whole rock content for these elements is forced to coincide with XRF data. a- XRF data, b- Solution-ICP-MS data. c- Jochum & Hofmann (1997); d- Jochum et al. (1993); e- Newsom et al. (1986); f- Newsom et al. (1996). Additional MORB data (only from samples where Sb, Sn, Mo and W data exist): Peuchelt & Emmermann (1983), Melson et al. (1977).

The results for Nb, W, Sb, Sn, Mo and Zr are presented in Fig. 14, where distribution of the whole rock concentration among the phases is given by areal proportion. It can be observed that of all the analysed phases, rutile preferably accommodates elements with the highest ionic charges, so that with a modal abundance of only 1%, rutile takes up >80% of Nb, Ta, Sb (all 5+) and W (6+). In contrast, significant amounts of the 4+ ions Sn and Mo can be stored in the major phases clinopyroxene and garnet (from 5% whole rock budget of Sn stored in garnet up to 40% of Mo in clinopyroxene), although rutile is still the most important carrier for these elements (30 to 42%). Similarly, we note that zircon, with a modal abundance of only 0.018%, contributes >90% of the whole rock budget for Zr and Hf. In contrast, the element budget for chromium is mostly controlled by the major phases and even with a slight preference of Cr for rutile, this phase only contributes about 5% of the Cr whole rock budget.

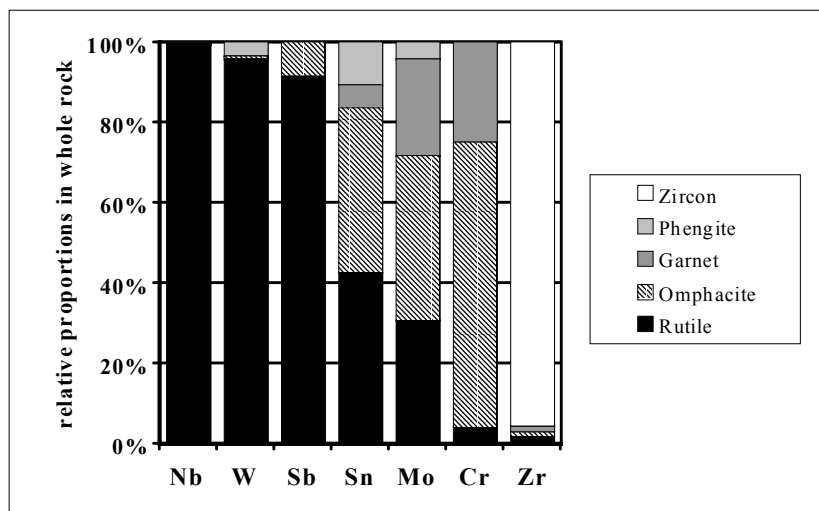


Fig. 14 Mass balance of selected elements in eclogite sample 50-13. Trace element compositions in mineral phases are measured by LAM, Zr of zircon by stoichiometry and mineral modes were estimated by phase mapping and XRF (see tables 5). Ta and Hf are not shown but follow closely Nb and Zr, respectively. Notice the decreasing preference in rutile for Nb > W > Sb > Sn > Mo > Zr.

A direct comparison of our mass balance calculation with sparse literature data from metamorphic environments is not possible since critical elements were either not analysed or were below detection limits in most phases. However, Sorensen & Grossman (1989) observed that the Ta/Ti ratios of garnet amphibolites are identical to Ta/Ti ratios of rutile from their samples and concluded that rutile is the likely carrier for Ta and also for Nb, a conclusion we can confirm after the analysis of coexisting major phases in this study. Sorensen & Grossman (1989) explained large deficits in their element budgets for Hf and Zr by the occurrence of small non-analyzable zircon. Our investigations support this interpretation, showing that large uncertainties in mass balancing may result from analysis of tiny zircon inclusions.

From our mass balance calculation, we conclude that rutile is by far the dominant carrier for Nb, Ta, W and Sb in eclogite. Mineral analyses of rutile will give the complete information about the host rock compositions of these elements if rutile thoroughly equilibrated with coexisting phases and if some estimates about the modal abundance of rutile can be made. This simplification cannot be made for Sn and Mo, where additional information is required concerning modal abundances of coexisting major phases.

3.3.2 Element ratios for eclogite 50-13

We have shown that whole rock compositions for a large range of HFS elements can be calculated by means of simple mass balance. Even though analytical problems with LAM and EMP data for these elements can be largely circumvented, it is essential to evaluate the data in a petrotextonic context. Elements with similar partition coefficients during melting and fractionation processes must have similar ratios from different suites of magmatic rocks, assuming that their mantle source is not heterogeneous (Hofmann & White 1983). Solely based on careful analysis of natural rocks, Sb-Pr, Sn-Sm, Mo-Pr and W-Th (or W-Ba) element pairs were found to show similar partitioning behaviour in most magmatic systems (Newsom et al., 1986, 1996; Jochum et al., 1993; Jochum & Hofmann, 1997).

We can therefore compare reconstructed whole rock concentrations of Sb, Sn, Mo and W with elements that can be analysed with conventional techniques. Pr, Sm, Th and Ba concentrations were measured by solution-ICP-MS on the whole rock sample 50-13 (Table 5). As can be seen, the Sb/Pr ratio of 0.021 and Sn/Sm ratio of 0.34 are in excellent agreement with ratios established for mantle-derived rocks (0.020 for Sb/Pr, Jochum & Hofmann 1997; 0.32 for Sn/Sm, Jochum et al. 1993). Our value of 0.056 for Mo/Pr is substantially lower than the ratio of 0.23 determined by Newsom et al. (1986). However, our value lies only slightly outside their range of measured Mo/Pr ratios (0.10-0.30).

For tungsten we see a discrepancy between values for 50-13 and mantle-derived samples that cannot be resolved with the available data set. The ratios W/Th and W/Ba are both higher, by a factor of 16, than our eclogite sample (0.026 and 3.3 instead of 0.0016 and 0.2; Newsom et al., 1986, 1996). Newsom et al. (1996) gave a range from 0.14 to 0.26 for W/Th ratios, significantly lower than our value of 3.3. Th and Ba have both been found to be mobile during alteration and high grade metamorphism, but this does not seem to explain the differences. In Chapter 4 it is shown that eclogites from Trescolmen have incompatible trace element patterns similar to MOR basalts. Comparing literature data for MORB with our reconstructed whole rock concentrations, it can be seen that all elements of interest fall in the same range, the only exception being tungsten (2.7 ppm instead of 0.002-0.16 ppm, Table 5). Therefore 50-13 seems to be unusually enriched in W and not depleted in Th or Ba. Analytical problems for the determination of the W content in rutiles from 50-13 can be ruled out. The common problem of contamination, e.g. through a tungsten carbide mill, can not arise since we use in-situ techniques and clean mineral surfaces are subject to considerable attention (Chapter 4). Additionally the high W content in the rutiles of 50-13 has been confirmed by *two* different techniques (see analytical section).

We can only speculate that if the eclogite protolith was a rift-related basalt as proposed in Chapter 4, the excess tungsten might have originated by contamination by continental crust during ascent of the source magma. Such a process is feasible given the enriched W/Th ratio of the continental crust and its high absolute abundance of W compared to mantle-derived magmas (Newsom et al., 1996). To our knowledge, W data for continental rift-related basalts have not been reported and a direct comparison is therefore not possible.

From our mass balance calculation and from element ratio considerations, we are confident that zircon and/or sulphides (chalcopyrite, pyrite), although identified in 50-13, cannot be important phases for the element budgets of

Nb, W, Sb, Mo and Sn. Reconstructed whole rock concentrations for these elements show that the estimated values are generally either in accordance with MORB data or are in excess (in the case of W). The only one of these elements for which we see a small deficit in the mass balance calculation is Mo, an element that could potentially be stored in sulphides due to its chalcophile character. We can estimate the Mo concentration in sulphides that is necessary to elevate our reconstructed whole rock data to the lower limit of observed Mo concentrations in MORB. Here we use the sulphur content in 50-13 (38 ppm, measured by XRF) to estimate the modal abundance of sulphides in the eclogite sample (0.007%). For an increase in reconstructed Mo content only from 0.16 ppm to 0.20 ppm, a concentration of 500 ppm Mo in the sulphides is needed. Although we could not perform quantitative measurements on sulphides due to their small grain size, we ablated sulphide grains along with their surrounding matrices. A concentration of 500 ppm would have shown a clear Mo signal. Since this was never observed, we can state that sulphides are not important carriers for Mo in our eclogite sample and hence likely also not for the other elements investigated.

3.3.3 Comparison of element ratios between rutile and whole rock

As shown, whole rock concentrations of TiO_2 , Nb, Ta, W and Sb in the eclogite sample 50-13 are almost completely controlled by rutile. This offers the prospect that ratios of this group of elements in rutile reflect rather precisely the ratios of their protolith source rock, in the same way that phengites record Cs/Rb and Ba/Rb ratios of their host rock (Chapter 2). A comparison of Nb/ TiO_2 (whole rock) versus the Nb concentrations of rutile from these samples shows a strong positive correlation (Fig. 15a), confirming the observation from 50-13 that rutile dominates the whole rock Nb and Ti budget. However, we notice an offset of some samples by as much as 30% between the Nb/ TiO_2 ratio of rutile and the whole rock. This could be caused by a phase highly enriched in Nb over TiO_2 , for which we find no evidence. Instead it is more likely that the offset is a function of the combined uncertainties of all four values. The fact that perfect agreement between rutile data and LAM measurement on whole rock glass pellet is reached (for 50-14, 55-4, 59-5; three points on the expected line in Fig. 15a) makes an analytical problem in the low concentration range of XRF analysis more likely than a missing Nb reservoir in some of the eclogite samples.

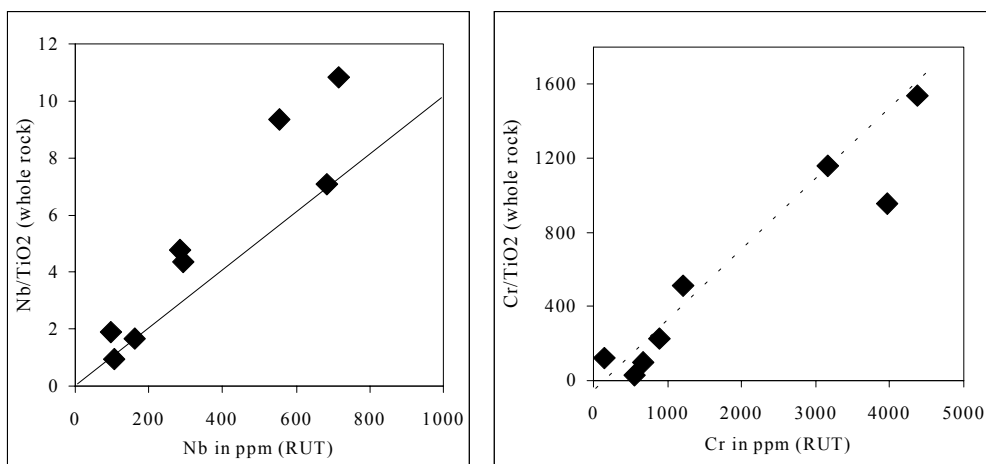


Fig. 15 a) Plot of Nb concentration in rutile vs. Nb/ TiO_2 ratio in corresponding host rock. Solid line marks expected Nb/ TiO_2 content in a whole rock at a given Nb concentration in the rutile. b) Cr concentration in rutile vs. Cr/ TiO_2 ratio in corresponding host rock, dotted line marks a good correlation between Cr content in rutile and Cr/ TiO_2 content in the whole rock.

Chromium is another geochemically important element for which we have collected both rutile and whole rock data. Although rutile is the phase with the highest Cr content, it enriches Cr only slightly in relation to coexisting phases (Table 5) and is therefore, as an accessory phase, not very significant for the whole rock budget for Cr. Nevertheless Cr contents in rutile are highly correlated with the Cr/TiO₂ ratio of corresponding whole rocks (Fig. 15b). This is surprising since the modal abundance and mineral parageneses in our investigated eclogite samples vary significantly (Chapter 4). Our preferred explanation is that Cr does not show a strong preference for any eclogite facies mineral (Table 5), so that the whole rock Cr budget is evenly distributed (although with a slight preference towards rutile) in the major phases and variations in Cr whole rock concentrations are reflected in the Cr content of rutile. This simple relationship will only occur as long as no other phase with a strong preference for Cr is part of a mineral paragenesis. One such phase is Cr-spinel, occurring as an inclusion in clinopyroxene in eclogite sample 55-3. Spinel is only a relict phase in 55-3 and is therefore not a stable eclogite facies phase (Chapter 4).

3.4 Applications

3.4.1 Provenance constraints by single grain analyses of detrital rutiles

We have shown that Nb and Cr contents in rutile enable close estimates of the Nb/TiO₂ and Cr/TiO₂ ratios of its host rock. Both trace elements are important tracers for magmatic processes, with low Nb contents corresponding to a large degree of melting and low Cr contents corresponding to large degrees of fractionation. Therefore it is not surprising that concentrations of Nb and Cr in rutile are clearly separated in our metapelitic and eclogitic samples (Fig. 16), both having experienced completely different petrogenetic histories. In the following this finding will be discussed in relation to its potential application to provenance studies.

The review by Force (1980) showed that rutile is an important accessory phase in medium- to high-grade metamorphic rocks, but rare to nonexistent in most volcanic and magmatic rocks. Exceptions are alkaline rocks (mostly kimberlites), mafic-ultramafic layered complexes and secondary rutile in porphyry copper and hydrothermal gold deposits. Where rutile growth is related to formation of mineral deposits, rutile can be expected to contain >1% of V, Nb, Sn, Sb and/or W as major components (see Rice et al. 1998). Rutiles from kimberlitic sources are also diagnostic, being highly enriched in Nb and/or Cr (always >1%, up to 21% Nb₂O₅ and 7% Cr₂O₃; Haggerty 1991). Hydrothermal quartz veins are a potential, though minor, source for trace element poor rutile. Brenan et al. (1994) measured one rutile from a high pressure quartz vein that contains only 50 ppm Nb and explained this low concentrations by a low capacity of fluids for transporting high field strength elements. Our investigated rutile from Disentis also originated in a hydrothermal quartz vein and supports the observation of Brenan et al. that rutiles from hydrothermal quartz veins are low in Nb (ca. 150 ppm).

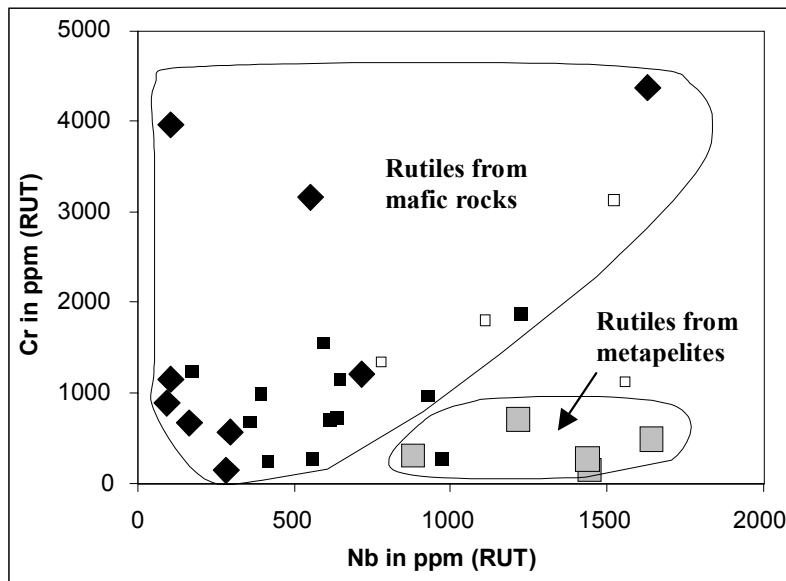
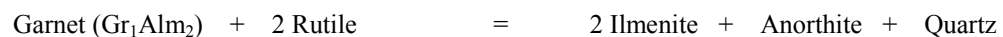


Fig. 16 Plot of Nb versus Cr concentrations in rutile from different high pressure environments: Trescolmen eclogites- black diamonds (this study); Trescolmen garnet micaschists- grey squares (this study); other eclogites (Norway, Venezuela, Bohemian Massif, various alpine localities)- black squares (Fett, 1995); mafic granulites- open squares (Fett, 1995).

The stability of rutile in metabasic rock types can be specified in terms of temperature / pressure conditions. The reaction



has been calibrated as a barometer for metabasic rocks by Bohlen & Liotta (1986), with rutile stabilized at the high pressure side. For a MORB composition this corresponds to a minimum pressure of 1.3 to 1.5 GPa (Ernst & Liu, 1998). However, this reaction is dependent on bulk composition, with rutile being stabilized towards lower pressure with high Mg and low Na bulk rock contents (as low as 0.6 GPa, Bohlen & Liotta, 1986).

High Mg and low Na contents are most commonly found in rocks with low degrees of fractionation, so that samples from fractionated basaltic protoliths should tend to stabilize rutile only under high pressure conditions (ca. >1 GPa). Since low Nb and Cr concentration are a proxy for this type of protolith, rutiles with low Nb and Cr content can only form under high pressure conditions (with the exception of rutiles from hydrothermal quartz veins (see above).

Rutile microprobe data from other high pressure environments are scarce. A comparison of our data with rutiles from other eclogite- and granulite-facies parageneses from metabasic bulk compositions is plotted in Fig. 16. Here rutiles of metabasic origin are restricted to Nb contents of <1000 ppm, confirming our observation made from a single eclogite locality. We note that rutiles from granulite-facies samples analysed by Fett (1995) tend to be higher in Zr content compared to eclogite samples (with >500 ppm, again only in metabasic samples). Since the Zr contents in our rutile are always buffered by excess zircon, the higher Zr content of granulite facies rutiles might be explained by breakdown of zircon and/or higher temperature facilitating Zr substitution in rutile.

Zircon, tourmaline and rutile are amongst the most stable heavy minerals during sedimentary and diagenetic processes. As a result, they still contain information on their source area even in mature sediments and after burial to significant depth. For this reason zircon and tourmaline have received considerable attention in provenance studies, e.g. zircon fission track dating (Hurford & Carter, 1991), zircon morphology (Lihou & Mange-Rajetzky, 1996), and

tourmaline chemistry (see Morton, 1991). Although it is well known that major and trace element compositions of single heavy minerals may contain crucial information on their former source rock (Morton, 1991), to our knowledge studies of chemical variations among detrital rutile grains have only been performed in one study by Preston et al. (1998). Here, detrital rutile fractions with high Nb content have been used to correlate oil-bearing sandstone layers in fossil-barren red-bed sequences.

We predict that trace element contents in detrital rutile will yield valuable provenance information since we have shown that chemical variations in rutile are large and can be highly diagnostic for its source rock. The chemical analysis of detrital rutile may offer several advantages. First, although rutile may be resistant during diagenesis and even during very low grade metamorphism, it has not been observed in low to medium grade metamorphic rocks, e.g. in pelites from the biotite zone up to the staurolite zone (Force, 1980). This distinguishes rutile from zircon, core compositions of which can survive several metamorphic cycles. Despite this, rutile chemistry always records its last metamorphic signature (closure temperature for the U/Pb system $\leq 400^\circ\text{C}$, Mezger et al., 1989). Second, several key elements in rutile are relatively easily and rapidly analysed with a modern electron microprobe. For example, to find populations of low Nb-Cr-rutile, 60 different grains can be measured per hour (to detect 1000 ppm of Nb, peak counting times of only 20 sec. are required at 20 kV). And finally, sufficient amounts of U in rutile allow single grain dating of representative samples from different populations with the SHRIMP technique (Sircombe, 1996), greatly enhancing the specifics in localizing source areas.

3.4.2 Role of rutile in subduction zones

Rutile may play a key role in subduction zone processes in retaining high field strength elements (HFSE) during dehydration reactions, thereby explaining the omnipresent negative Nb-anomalies in island arc volcanoes (Nicholls & Ringwood, 1973; Saunders et al., 1980). For this reason intensive studies have focussed on the partitioning behaviour of a number of trace elements (Nb, Ta, Zr, Hf, U, Th) between rutile and fluid (Brenan et al., 1994; Stalder et al., 1998) as well as between rutile and melt (Jenner et al., 1993). These experimental results are essentially consistent with earlier models showing that Nb and Ta behave as highly compatible elements in the presence of rutile.

Zr and Hf are not considered in the following discussion since they are expected to be controlled by zircon and not by rutile (Fig. 14). However, we point out that subduction zone dehydration models for Zr and Hf based on rutile/fluid partition coefficients must, therefore, yield erroneous results. The incorporation of zircon in dehydration models might lead to an explanation of why island arc magmas almost always show negative Nb-Ta anomalies, but sometimes lack negative Zr-Hf anomalies (Briqueu et al., 1984).

Nb/Ta ratios have recently received considerable attention following the finding that these elements may be significantly fractionated from each other by Ti-rich phases (Green & Pearson, 1987; Brenan et al., 1994). Subduction-related rocks have Nb/Ta ratios spanning a range from subchondritic to superchondritic (8-33; Stolz et al., 1996; Münker, 1998) and seem to follow at least two different trends (Münker, 1998). The interpretation, however, is controversial. Green (1995) and Münker (1998) referred to the difference of $D_{\text{Nb}}/D_{\text{Ta}}$ partition

coefficients between rutile/fluid and rutile/melt, where the presence of rutile produced melts with elevated Nb/Ta and fluids with lowered Nb/Ta ratios. Stolz et al. (1996) also favoured the argument that elevated Nb/Ta ratios in high-K lavas were produced by a melt component from the subducted slab, and in addition they questioned the capacity of fluids to change significantly the Nb/Ta ratio in the source area of more common low-K and calc-alkaline lavas. Low Nb/Ta ratios can be explained by re-melting of already depleted mantle (Eggins et al., 1997), where a difference in $D_{\text{Nb}}/D_{\text{Ta}}$ between clinopyroxene and melt (Jenner et al., 1993) causes a lowering of the Nb/Ta ratio in the residuum. The key difference between the two models is that fluid loss from subducting oceanic crust will either produce a superchondritic Nb/Ta ratio in the eclogitic residuum in the former case, but will leave no impact in the latter case. Our data seem to support the latter model. Starting from a low-temperature hydrothermally altered basalt (Chapter 2), we infer that eclogites from Trescolmen have lost between 2-4% H₂O by dehydration (Schmidt & Poli, 1998), similar to subducted oceanic crust underneath volcanic arcs. Rutilites from this locality have largely chondritic or slightly subchondritic Nb/Ta ratios, with an average of 17.4 (Table 4). One sample (77-5) has a significantly higher Nb/Ta ratio of 31.7 and excluding this sample we obtain an average value of only 15.9, with a range of 9 eclogitic rutilites from 13.6 to 17.4. This value is identical to Nb/Ta ratios from rutilites in similar continental settings (16.0; Rudnick, 1998). However, superchondritic rutilites (with a median Nb/Ta ratio of 33) supporting the first model have been found in eclogitic xenoliths (Rudnick, 1998) so the debate remains open.

As pointed out by Fitton (1995) and McDonough (1999), Nb and Ta systematics tell only part of the rutile story since rutile can also be important for other HFSE. We have shown that besides Nb and Ta, rutile is an important phase for Sb, W, Mo and Sn in metabasitic and -pelitic systems at conditions relevant for subducting slabs underneath volcanic arcs (Schmidt & Poli 1998). From the elastic strain model of Blundy & Wood (1994) and Beattie (1994), it should be expected that in terms of rutile-fluid partitioning, Nb, Ta, Sb (and W?) behave as one group and Mo and Sn as another group in subduction zone environments, taking into consideration ionic radius and charge (Fig. 9). This would be consistent with the trace element systematics of sample 50-13, as described earlier (Fig. 14). Nevertheless, this applies only as long as the crystal structure dominates the trace element partitioning e.g. in rock samples with several solid phases.

We can now investigate the behaviour of the extended HFSE group in subduction zones with respect to the role of rutile. Fitton (1995) showed that subduction-related lavas from the western US are strongly depleted in Nb and Mo compared to similarly incompatible elements (La, Nd), as well as being highly correlated with each other, and concluded that rutile retains both Nb and Mo in the downgoing slab during dehydration. No clear trend can be found for Sn and W in subduction-related lavas, showing neither pronounced enrichment nor depletion in terms of Sn/Sm and W/Th ratios (Jochum et al., 1993; Noll et al., 1996). Instead Sb is one of the most enriched elements in volcanic arc rocks in terms of its ratio with Pr and follows similar enrichment trends to B, As, Tl and Pb (Ryan et al., 1995; Noll et al., 1996; Jochum & Hofmann, 1997).

Trace elements enriched in volcanic arc rocks are inferred to be carried by a fluid from the dehydrating slab. Assuming that light REE (LREE, La-Sm) as well as Th are moderately mobilized in these fluids (Brenan et al., 1995; Stalder et al., 1998), it can be said that Nb, Ta and Mo are less enriched in the fluid, Sn and W similarly, and Sb highly enriched compared to corresponding LREE (and Th). Sb is highly enriched in pelagic sediment and altered oceanic crust (Jochum & Verma, 1996), both likely source rocks for fluids in dehydrating slabs. Nevertheless high Sb concentration in the fluid caused only by an anomalously enriched source can be ruled out for the following

reason. If Sb were as mobile or even less mobile than LREE in dehydrating fluids, Sb/LREE ratios would be expected to be higher than in MORB, but should stay constant (or slightly increase) in across-arc traverses, as normally observed for Nb/La ratios. However, the contrary is observed in across-arc studies, where Ryan et al. (1995) and Noll et al. (1996) showed for the Japan and Kurile arc transects that Sb/Ce ratios continuously decrease in volcanic arc rocks with increasing depths to the subducting slab.

Combining the observations of subduction zone studies with our own results, we can conclude that neither an enriched source area nor the mineral assemblage of the downgoing slab (dominated by rutile) can be solely responsible for the extreme enrichments of Sb in subduction-related magmas. An alternative might be found in the behaviour of the aqueous fluid itself, with the ability to fractionate Sb from Nb, which otherwise show similar partitioning behaviour in eclogite assemblages and are not fractionated from each other in magmatic systems.

Experimental studies on rutile/fluid partitioning of the extended HFSE group are required to test such a statement and should give some highly desired insight on fluid behaviour under upper mantle conditions. Rutile/fluid experiments would have the advantage of forming a relatively simple system stable under a wide range of PT-conditions. One of the most challenging questions concerns whether complexing systematics in low pressure environments can be applied to upper mantle conditions. Noll et al. (1996) discussed the complexing properties of Mo, Sn, W and Sb, and concluded that subduction zone systematics could be explained by preferentially transporting Sb in a H₂S-rich and Cl-poor, reducing and acidic hydrothermal fluid. This is problematic with respect to the observation of Cl-enrichment in island arc volcanics in relation to MORB (Ito et al., 1983) and calculations of Manning (1998) that showed that high pressure fluids in equilibrium with blueschists/eclogites have rather basic properties. Nevertheless, this discussion shows the prospect of characterizing fluid properties coming from dehydrating oceanic crust and better evaluating the role of rutile in fractionating element ratios on a global scale.

Chapter 4. Evaluating hydrous eclogites from Trescolmen for their use of deriving trace element partitioning values for subduction zone modelling

4.1 Introduction

Experimentally determined trace element partition coefficients between mineral and fluid ($D^{\text{Min/Fluid}}$) have been used extensively to characterize the trace element composition of fluids emanating from subducting oceanic crust undergoing prograde dehydration reactions (e.g. Brenan et al., 1995a, 1998; Ayers et al., 1997; Stalder et al., 1998). Although estimates of $D^{\text{Min/Fluid}}$ for a range of minerals and trace elements exist, there are no data for phases relevant for subducting oceanic crust other than clinopyroxene, garnet, amphibole, apatite and rutile (Ayers & Watson, 1993; Brenan et al., 1994, 1995a, b, 1998; Ayers et al., 1997; Stalder et al. 1998; Melzer et al., 1998; Najorka et al., 1999). Additionally, experimental data for phengite/fluid partitioning for Cs and Rb have also been obtained (Beswick, 1973; Volfinger, 1976; Melzer & Wunder, 1999).

However, phase relations in metabasaltic assemblages (only *one* component of the oceanic crust) are considerably more complex. In a review of their experimental results, Schmidt & Poli (1998) listed, in addition to amphibole and phengite, also chlorite, lawsonite, zoisite, paragonite, chloritoid and talc as relevant hydrous phases in mafic systems undergoing subduction. For the latter phases, there are currently no estimates for mineral/fluid partitioning behaviour and neglecting these phases in subduction zone models can severely affect any calculation regarding the fluid composition from dehydrating slabs.

A potentially powerful tool to overcome the lack of experimental mineral/fluid values is to combine experimentally determined $D^{\text{Min1/Fluid}}$ (e.g. clinopyroxene as Min1) with measured $D^{\text{Min1/Min2}}$ (Min2 being a phase for which no partitioning data are currently available) in natural systems that are appropriate for subduction zone environments, such as blueschist- and eclogite-facies assemblages (Zack & Foley, 1997; Brenan et al., 1998). Although time scales in natural metamorphic systems are several orders of magnitude longer than in any experiment, the major drawbacks to deriving meaningful partition coefficients between different phases are nevertheless sluggish reaction rates. For instance, convincing examples of disequilibrium processes were found in trace element zoning studies of garnet (Hickmott & Shimizu, 1990). They inferred that trace-element-enriched surface layers were trapped in the crystal structure in certain metamorphic environments, leading to a disequilibrium pattern (see also Watson, 1996). Additionally, Getty & Selverstone (1994) used trace element partition coefficients calculated from coexisting phases to argue against attainment of equilibrium in Tauern eclogites. However, an increasing number of studies have demonstrated that a close approach to equilibrium was reached in other cases for a range of trace elements in different assemblages (Messiga et al., 1995; Yang et al., 1999; Kretz et al., 1999).

In this chapter, data is presented from a suite of eclogite-facies samples where strong evidence exists for a close approach to equilibrium at the trace element level. The eclogite locality at Trescolmen was chosen because of its extensive record of previous investigation (Heinrich 1982, 1986; Santini, 1992; Meyre & Puschig, 1993; Meyre et al., 1997, 1999; Meyre & Frey, 1998; Chapter 2) and because of the widespread occurrence of well crystallized hydrous high pressure phases such as amphibole, phengite, paragonite, zoisite, talc and apatite.

The aim is to present a reliable set of Min/clinopyroxene values (where Min= amphibole, phengite, zoisite, paragonite and apatite) that can be combined with experimental $D^{\text{Clinopyroxene/Fluid}}$ values for application to subduction zone modelling, since clinopyroxene is the phase most intensively studied in terms of mineral/fluid partition coefficients (Brenan et al., 1995a, b, 1998; Ayers et al., 1997; Stalder et al. 1998). LAM analyses are therefore limited to trace elements that have attracted most attention in subduction zone studies and for which $D^{\text{Clinopyroxene/Fluid}}$ values are already available (i.e. Li, Be, B, Sr, Y, Zr, Nb, Ba, Ce, Nd, Sm, Pb, Th, U). A discussion of other subduction-relevant trace elements from the same sample suite has been presented in Chapter 2 concerning phengite systematics (Cs, Rb; Chapter 2) and in Chapter 3 concerning rutile systematics (Sb, W, Sn, Mo; Chapter 3).

A wide range of techniques was applied including careful petrographic observation, high resolution back scattered imaging, thin section mapping, whole rock XRF and solution-ICP-MS analysis, and quantitative electron microprobe and laser ablation microprobe-ICP-MS (LAM) analysis of major and trace element composition of selected phases. This integrated approach allows it to develop textural and chemical criteria for the recognition of equilibrium in metamorphic samples. Finally attention is drawn to the fact that once the equilibrium partition coefficients are known, partitioning data can yield information about the crystallization history of assemblages that have not attained full trace element equilibration.

4.2 Analytical methods

Major and minor elements in the different phases were measured with a Cameca SX51 electron microprobe in Heidelberg and a JEOL JXA 8900 RL electron microprobe in Göttingen, both equipped with five WDS spectrometers and synthetic mineral standards. Specific details about measurement conditions for amphibole and phengite can be found in Chapter 2. For routine analysis and small scale variation measurements, operating conditions were 15 kV acceleration voltage, 12 nA beam current on the Faraday cup, 1-5 μm beam diameter and 15-30 seconds counting time on the peak of all measured elements. A PAP correction for the Heidelberg microprobe and a phi-rho-zeta correction for the Göttingen microprobe was applied to process the raw counts. For a subset of clinopyroxene and garnet analyses, operating conditions were optimized for minor elements (Mn, Cr, Ti). Acceleration voltage was increased to 20 kV, beam current to 80 nA, beam diameter to 10 μm and counting times on the peak were 15 s for Na, Ca, K, Fe, 30 s for Al, Si, Mg, Mn and 60 s for Cr, Ti. Even at these high energies, no loss of Na in clinopyroxene was observed compared to normal operating conditions. Under the conditions described, Ti in clinopyroxene and garnet were measured with a precision of better than 5% for concentrations above 300 ppm.

Trace element analysis on the different phases was conducted with the laser ablation system at Memorial University of Newfoundland (MUN). Horn et al. (1997) were able to operate under ideal conditions, which include the use of standards with an almost identical matrix to the samples, constant measurement conditions and unlimited, homogeneous sample material. For their results, both accuracy and precision of better than 10% were obtained for a range of trace elements. However, analyses of natural phases in thin section with variable grain sizes and a different matrix to the available glass standards obviously decrease the precision, but a comparison of electron microprobe and laser ablation microprobe analyses of Ba in phengite (Chapter 2) as well as selected trace elements in rutile (Chapter 3) has shown that the accuracy of laser ablation measurements is in the range of 15-20%. The laser was focused 100-500 μm above the mineral surface to reduce fractionation effects (Chapter 2). Application of a defocused beam in this study was found to be most important for Pb measurements. Here, Pb fractionation (compared to the Ca signal) during a 1 minute ablation was reduced from 50% for a beam focused at the sample surface to 20% for a beam focused 500 μm above the surface (2 mJ pulse energy in both cases). Fractionation effects of e.g. 20% for the most extreme element ratio (Pb/Ca) are not a serious problem since fractionation during ablation is similar in both the glass standard and the minerals of interest and can be corrected for when using similar ablation procedures in all analyses (pit sizes, integrated time intervals).

The determination of trace element concentrations in low-T eclogites represents a challenge for any analytical technique, because their abundances in clinopyroxene and amphibole are exceptionally low due to the coexistence of accessory phases in which the trace elements are concentrated (Messiga et al., 1995). With trace element concentrations commonly in the low ppb range, contamination from various sources has to be taken into account and instrument sensitivity must be optimized. This was achieved in the following ways.

- 1) A rigorous cleaning procedure was applied to avoid surface contamination. Test runs have shown that elements such as Zr, Ce, Ba and Pb can be anomalously enriched on grease-contaminated surfaces (e.g. apparent Ba concentration in clinopyroxene can vary from 5 ppm down to 0.05 ppm depending on cleaning procedure). Thin sections were therefore polished with 0.3 μm aluminum oxide powder, washed in an ultrasonic bath for 2 minutes and then cleaned with pure alcohol before each LAM analysis. Thin sections were carefully inspected with a high magnification reflected light microscope. If grease droplets (down to 1 μm) were detected on mineral surfaces, cleaning with alcohol was repeated until grease droplets were completely removed.

- 2) Even though eclogites from Trescolmen are characterized by their unusual freshness, solid and fluid inclusions as well as alteration along microcracks can alter trace element compositions by several orders of magnitude. Therefore inclusion-free areas were selected with the petrographic microscope, which in the MUN system is an integral part of the LAM instrumental set-up (Jackson et al., 1992). Submicroscopic inclusions were detected by inspecting each block of data acquisition in time-resolved mode and only elements with a regular ablation behaviour were treated as elements belonging in the crystal structure, with "spiky" signals being excluded from data reduction under the assumption that they are due to inclusions (see Figs. 4 and 5 of Fryer et al., 1995). Even under perfect conditions, regular ablation behaviour can only be proven for concentrations down to ca. 100 ppb by inspecting the ablation signal of the trace element in relation to the element signal used for normalization (e.g. Ca). Below this range, although counted signals are often significantly above the background, they arrive too irregularly to demonstrate homogeneous distribution in the ablated mineral. Therefore measured concentrations below 100 ppb can only be taken as maximum values.

3) To reach the lower ppb range for the elements of interest, element menus were split and the largest practical laser pulse energies, depending on the size of optically inclusion- and alteration-free areas, were applied (for clinopyroxene between 1.5 to 2.7 mJ at 10 Hz with a beam focused 300 to 500 μm above the sample surface). For these reduced element menus (between 6 and 12 elements), the ICP-MS was tuned to have the highest sensitivity in the chosen mass range. Helium was used as a carrier gas for the ablated material when light elements were analyzed. This increases sensitivity for Li, Be and B by a factor of >20 when compared with Ar as a carrier gas. With He as a carrier gas, calculated detection limits (2σ above background signals) on 60 μm wide ablation pits are 0.04, 0.3 and 0.7 ppm for Li, Be and B respectively. Optimized sensitivity for the heavier elements in combination with a reduced element menu and high laser pulse energies leads to detection limits on U in clinopyroxene of between 0.6 to 10 ppb in different samples, depending on crystal size and inclusion density. For most trace elements, Ar was used as the carrier gas since it was found that sensitivity is similar for both carrier gases so that the cheaper option can be used.

4.3 Whole rock geochemistry

Eclogites from Trescolmen span a large range of chemical composition, even though the sample region is limited to less than 1 km^2 in a single continuous metapelite layer, which might imply a cogenetic origin for all or most of the investigated samples. Eclogite protoliths can be subdivided into gabbroic and basaltic groups by means of their Al_2O_3 and TiO_2 content (Fig. 17), as demonstrated for Koralpe and Saualpe eclogites by Miller et al. (1988) and for Ötztal eclogites by Miller & Thöni (1995). Here, three of our samples fall in the field of gabbros (CHM30, 59-1, 55-3), the remaining in the field of basalts and FeTi basalts. This is in accordance with textural observations, where all of our very coarse-grained, unfoliated eclogites belong to the metagabbroic group and three out of four foliated, medium- to fine-grained eclogites belong to the metabasaltic group (compare Tables 1 and 6). In addition to their low TiO_2 and variable Al_2O_3 contents, our metagabbroic samples also have the highest MgO (9.7-12.1 %) and Cr contents (810-1020 ppm) of all investigated samples.

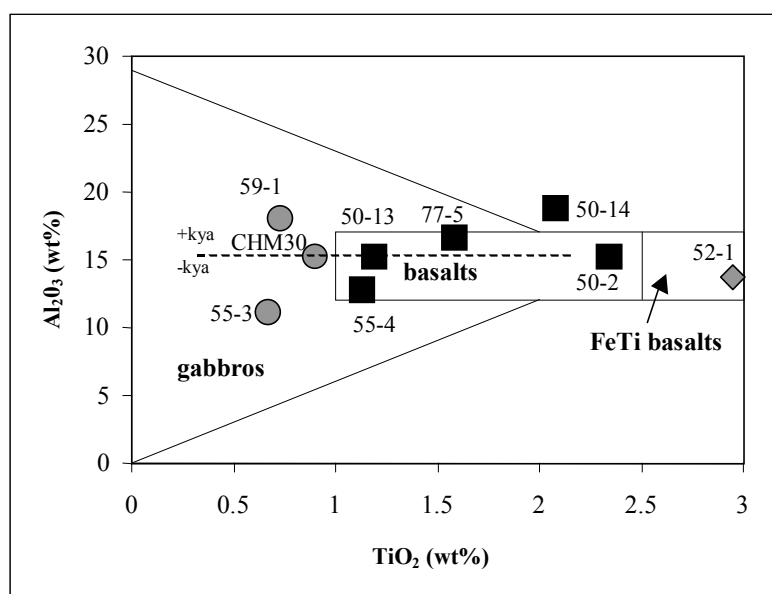


Fig. 17 Al_2O_3 - TiO_2 discrimination diagram for mafic rocks, modified after Miller et al. (1988). Plotted are whole rock analyses (with sample number) of selected eclogites from Trescolmen. The following symbols are used to signify probable protoliths of the samples: grey circles- gabbros; black squares- basalts; grey diamond- FeTi basalt. Dashed line marks approximate limit for kyanite stability in Trescolmen eclogites (≥ 15 wt% Al_2O_3).

Table 6. Whole rock geochemical data of selected eclogite samples. Samples are ordered by increasing TiO₂ content, for the classification see Fig. 17.

	metagabbros			metabasalts					FeTi metabasalt
	55-3	59-1	CHM30	55-4	50-13	77-5	50-14	50-2	52-1
SiO ₂ (XRF)	53.15	47.75	49.22	52.20	48.87	46.42	46.20	47.92	48.86
TiO ₂	0.67	0.73	0.90	1.13	1.19	1.58	2.08	2.34	2.95
Al ₂ O ₃	11.15	18.14	15.29	12.88	15.25	16.64	18.85	15.26	13.66
FeO(total)	7.70	8.11	7.86	8.74	7.72	9.59	11.56	12.38	14.18
MnO	0.20	0.15	0.15	0.24	0.14	0.16	0.20	0.21	0.27
MgO	12.09	11.31	9.69	9.51	8.63	6.77	5.40	7.33	5.68
CaO	9.31	10.31	12.22	12.33	10.61	13.63	9.00	7.98	10.20
Na ₂ O	3.35	2.64	2.66	2.34	4.00	2.64	4.50	3.70	2.25
K ₂ O	0.43	0.01	0.02	0.05	0.57	0.16	0.04	0.04	0.01
P ₂ O ₅	0.11	0.075	0.1	0.13	0.18	0.08	1.27	0.19	0.23
Zr	71	34	53	55	93	93	111	182	403
Cr	1021	813	815	664	460	276	244	221	109
Li (ICP)	41.0	13.4	13.2	16.9	18.7	18.2	21.4	16.5	7.1
Sr	68	71	383	99	111	243	267	136	279
Y	15.9	16.0	14.6	17.3	19.2	28.4	41.0	41.2	51.6
Ba	47.5	2.13	1.61	3.92	65.1	15.9	3.59	7.30	0.25
Ce	30.0	6.40	12.1	11.9	21.8	10.1	17.6	16.5	4.95
Nd	15.8	5.68	7.87	6.97	13.4	10.4	17.4	13.0	5.02
Sm	3.44	1.74	2.05	1.77	3.60	3.81	7.03	4.27	2.77
Pb	3.05	3.08	15.7	4.45	3.98	2.57	3.81	4.28	6.39
Th	3.45	0.16	0.46	0.60	0.82	0.18	0.67	0.65	0.25
U	0.86	0.34	0.17	0.070	0.39	0.61	0.34	0.29	0.044
CaO/Na ₂ O				5.3	2.7	5.2	2.0	2.2	4.5
Ti/Zr				122	76	102	112	77	44

In the following, the close chemical similarity between Trescolmen metabasaltic eclogites and mid ocean ridge (MOR)-type basalts is demonstrated. Note that we use the term "mid ocean ridge" to describe the tectonic setting (e.g., as opposed to continental rifting) and the term "MOR-type basalts" in a chemical classification sense (e.g., as opposed to OIB). To classify eclogites on a chemical basis, the assumption is made that all metamorphic processes occurred largely isochemically, at least for major and immobile trace elements. On the basis of Na₂O-CaO relationships, our basaltic samples may have been affected by weak spilitization, with two samples (50-2 and 50-14) having CaO/Na₂O ratios below 2.5 (see Table 6), an arbitrary limit set for spilites by Graham (1976). Ti, Zr, Y and Sr are most widely used to discriminate the tectonomagmatic setting of basaltic rocks and their metamorphic equivalents (Pearce & Cann, 1973). According to Pearce & Cann (1973), only basalts with 12% < MgO + CaO < 20% should be used. However, two of our samples (77-5 and 55-4) have slightly higher concentrations (20.4 and 21.8% respectively). These samples are marked separately in the following figures to demonstrate consistency of chemical behaviour with the other samples. To screen highly fractionated basalts from more primitive ones, Winchester & Floyd (1977) used Ti-Zr relationships, with a Ti/Zr cut-off ratio below 50. Only one of our metabasalts (sample 52-1), has a lower Ti/Zr ratio (43), with all other samples having ratios between 76 and 122.

The anomalous sample is also highly enriched in TiO_2 (2.95%), FeO total (14.2%) and depleted in Cr (109 ppm). It resembles highly fractionated basalts from the Galapagos spreading ridge and is accordingly termed FeTi basalt (Clague et al., 1981). The remaining samples (50-2, 50-13, 50-14) are plotted together with 55-4 and 77-5 in Ti-Zr-Y and Ti-Zr-Sr discrimination diagrams of Pearce & Cann (1973; Fig. 18a and 18b). In both diagrams all five samples fall into the field defined for MOR-type basalts.

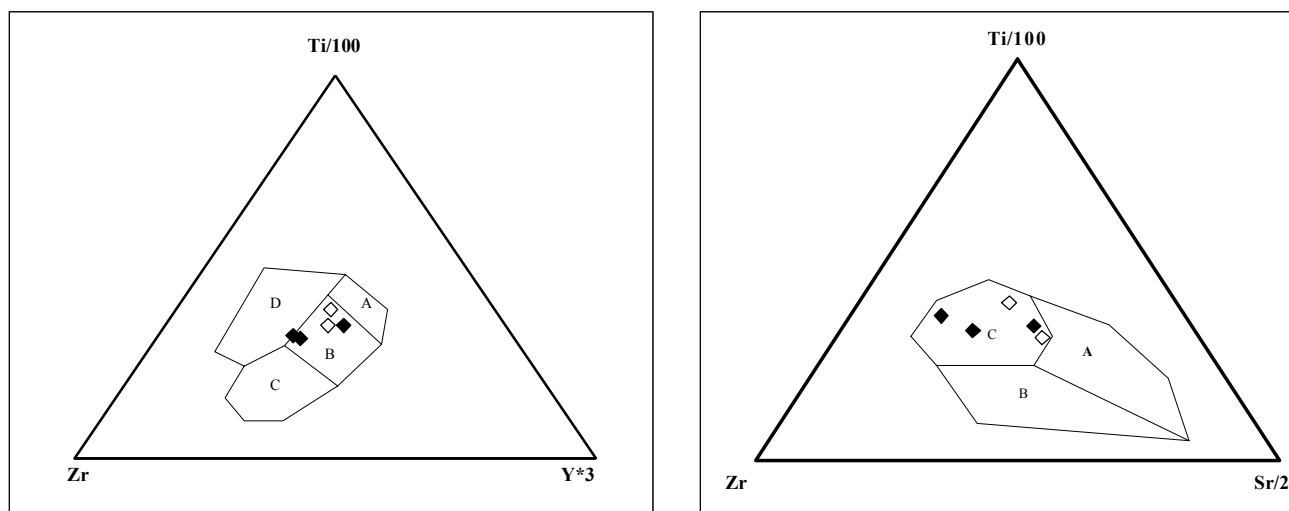


Fig. 18 Discrimination diagrams for basalts after Pearce & Cann (1973). Basaltic samples that passed the screening procedure of Pearce & Cann are marked by black diamonds; basaltic samples that do not pass are marked by open diamonds. See text for further information. a) Ti-Zr-Y diagram: A- island-arc tholeiites; B- ocean floor basalt (MORB), island-arc tholeiites, calc-alkali basalts; C- calc-alkali basalts; D- within-plate basalts. b) Ti-Zr-Sr diagram: A- island-arc tholeiites; B- calc-alkali basalts; C- ocean floor basalts (MORB).

However, these characteristics do not have to imply an origin of such rocks at a mid ocean ridge. As summarized by Miller et al. (1988), continental tholeiites with a similar chemical fingerprint to MORB are known, and an initial rifting environment with MORB-type magmas injecting into and/or extruded onto thinned continental crust is a plausible scenario (similar to Triassic volcanic sequences on the passive margin of the northeastern USA). In such a setting, small magma chambers, dikes injected into sedimentary sequences, lava flows and tuffs (subaeric and/or submarine, in the latter case commonly accompanied by hydrothermal alteration) are expected features. An origin of the metabasalts of the Adula nappe in a transitional continental/oceanic rifting environment is attractive as it explains a number of observations, as summarized below. A rifting environment avoids the requirement for a foreign origin for the eclogite protoliths in relation to the surrounding metapelites, which was suggested by Santini (1992). In a rifting environment, metapelites and metabasalts are juxtaposed before collision, which is in accord with the observation that Trescolmen metapelites experienced the same high pressure conditions as the eclogites they enclose (Meyre et al., 1999). As opposed to true oceanic floor environments, this geotectonic setting also explains the almost complete lack of ultramafic rocks in the Northern and Middle Adula nappe (Heinrich, 1983). Another argument in favour of an early rifting scenario is the occurrence of FeTi metabasalt (sample 52-1). According to Clague et al. (1981), FeTi basalts are highly fractionated constituents of the oceanic crust that are restricted to propagating rift settings and off-axis fracture zones. Clague et al. discussed the conditions that must exist to form FeTi basalts. They argued that at the tip of a propagating rift, single batches of magma can inject into

old, cool crust where extreme fractionation is possible due to faster cooling and less magma replenishment than in normal MOR environments. Single magma batches injected into cool surroundings are the exception in normal oceanic crust, but common in continental rift systems. The Adula nappe is interpreted to be derived from the former outermost passive margin of the European continent prior to the Alpine orogeny (Froitzheim et al., 1996), with magmatism possibly having occurred at the same time as the Triassic volcanic sequences in the Tauern Window, situated in an identical geotectonic setting (Kurz et al., 1998b).

A thorough testing of the early rifting environment hypothesis for the eclogite protoliths can only be achieved by demonstrating crustal contamination during magmatism that was not obliterated by later low-T hydrothermal alteration (Chapter 2). Extreme W/Th ratios reported in rutiles from Trescolmen eclogites might be such an indicator as tungsten is immobile during hydrothermal alteration, but highly incompatible during magmatic conditions and enriched in continental crust in relation to mantle-derived magmas (Chapter 3).

Despite our preferred origin for the Trescolmen eclogites in a rifting environment, the most significant feature of our samples is a close chemical similarity to true MOR basalts, so that Trescolmen eclogites can be taken as direct analogues for modelling subducting oceanic crust. This can be further illustrated by comparing fractionation sequences of MOR basalts with the chemical compositions of our samples. Using TiO_2 as a fractionation index, Trescolmen eclogites span the whole range of MORB compositions and follow almost perfectly the same fractionation trend as MORB, best illustrated by Cr- TiO_2 (Fig. 19a), MgO- TiO_2 (Fig. 19b), SiO_2 - TiO_2 (Fig. 19d) and FeO- TiO_2 (Fig. 19e) relationships. Only CaO and especially Na_2O contents seem to be disturbed (Fig. 19c and 19f), which may be explained by spilitization.

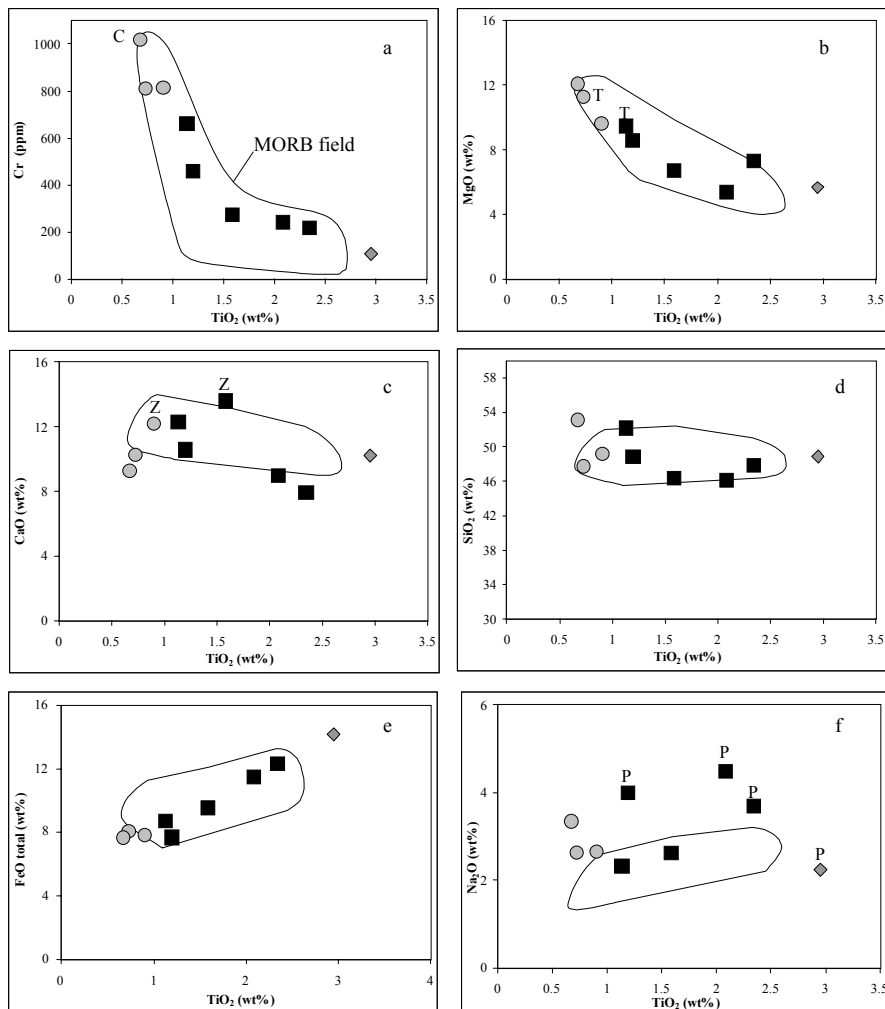


Fig. 19 Element- TiO_2 variation diagrams after Widmer (1996). Field for MOR basalts is based on data from Schilling et al. (1985). For description of symbols see Fig. 17. Letters next to samples are for stable (or relict) phases dependent on corresponding element concentration in the whole rock: a) Cr- TiO_2 diagram, C- chromite (relicts); b) MgO- TiO_2 diagram, T- talc; c) CaO- TiO_2 diagram, Z- zoisite; d) SiO_2 - TiO_2 diagram; e) FeO total- TiO_2 diagram; f) Na_2O - TiO_2 diagram, P- paragonite.

The close chemical relationship with MORB makes Trescolmen eclogites ideal for evaluating the importance of several hydrous phases in subducting oceanic crust, at least under the PT conditions reached at Trescolmen (ca. 650°C, 2.0 GPa; Meyre et al. 1997). This can aid in the determination of the relative importance of different OH-bearing phases in various mafic assemblages (gabbros vs. basalts, hydrothermally altered vs. unaltered, etc.). For our suite of samples, there are good correlations between major element compositions and occurrences of corresponding phases. For instance, zoisite occurs in eclogites with ≥ 12 wt% CaO (Fig. 19c), talc in two of the three MgO-rich eclogites (Fig. 19b) and three out of four paragonite-bearing eclogites are the most Na₂O-enriched samples (≥ 3.7 wt% Na₂O, Fig. 19f). Amphibole occurs in all investigated eclogites and there is a weak positive correlation between the modal abundance of amphibole and the Mg#. 50-14 has the lowest modal amount of amphibole (<1%; see Table 1) with a low Mg# (45.4; see Table 2) whereas 59-5 has the highest amount of amphibole (21%) with a high Mg# (71.3). The modal abundance of the hydrous phases phengite and apatite is directly proportional to the K₂O and P₂O₅ contents in the whole rocks since they are the only significant potassium- and phosphorous-bearing phases in Trescolmen eclogites (for potassium see Chapter 2). In addition to the hydrous phases, the existence of kyanite and chromite relics can also be correlated with the whole rock composition. The occurrence of kyanite is restricted in Trescolmen eclogites to samples with ≥ 15 wt% Al₂O₃ (indicated in Fig. 17) and the only chromite relics (see below) were found in the most Cr-rich sample (Fig. 19a). Since parageneses are closely linked to whole rock chemistry in each sample, and all samples in turn lie directly on the fractionation line of MOR basalts, it can be concluded that abundances of hydrous phases were not controlled by H₂O availability or other elemental mass transfer processes during metamorphism.

All correlations between whole rock chemistry and phase abundances in Trescolmen eclogites can only be first order approximations. Phase relationships are inevitably more complex and depend on many variables. A more precise knowledge of the occurrence of phases in complex systems involves the application of rigorous thermodynamic methods, such as the Gibbs free energy minimization (Meyre et al., 1997) or solution of simultaneous non-linear equations (THERMOCALC; Powell et al., 1998).

4.4 Mineral chemistry

Mineral chemical heterogeneities and zonations have been studied qualitatively by high resolution back scattered electron imaging and quantitatively by spot analyses with the electron microprobe in order to define areas in each phase that are part of the Trescolmen stage equilibrium parageneses. These areas were then analyzed by LAM for trace element contents. All relevant phases are described below and selected electron microprobe data for clinopyroxene, garnet, zoisite and clinozoisite are given in Tables 7 to 9.

Table 7 Electron microprobe data for clinopyroxene (in wt%). Average compositions are marked by *, remaining data are representative analyses.

	Ad25	CHM30a *	CHM30b *	50-2 *	50-13 *	50-14	52-1 *	55-3
SiO ₂	55.84	55.57	55.63	56.72	56.47	56.95	56.39	55.60
TiO ₂	0.086	0.061	0.062	0.080	0.075	0.098	0.079	0.068
Al ₂ O ₃	10.36	8.36	9.01	12.78	12.03	13.15	11.61	9.60
Cr ₂ O ₃	0.025	0.119	0.148	0.026	0.095	0.052	0.045	1.91
FeO	2.30	3.33	3.21	3.50	2.52	3.33	3.82	3.07
MnO	0.020	0.047	0.019	0.022	0.019	0.038	0.024	0.024
MgO	10.22	10.97	10.69	7.56	8.68	7.05	8.18	9.18
CaO	15.34	16.29	15.72	11.21	13.08	11.11	12.50	13.59
Na ₂ O	5.70	4.98	5.24	7.91	6.83	8.27	7.16	6.79
K ₂ O	0.004	0.014		0.003	0.009	0.003	0.001	0.002
Total	99.89	99.74	99.73	99.81	99.80	100.05	99.80	99.83

	55-4 *	59-1	77-5 *
SiO ₂	55.36	56.64	55.80
TiO ₂	0.066	0.065	0.086
Al ₂ O ₃	7.04	9.85	11.16
Cr ₂ O ₃	0.17	0.2	0.046
FeO	4.53	1.53	4.45
MnO	0.029	0.016	0.020
MgO	11.26	10.89	8.49
CaO	16.9	16.03	13.25
Na ₂ O	4.65	5.58	6.73
K ₂ O	0.008	0.005	
Total	100.01	100.81	100.02

Table 8 Electron microprobe data for garnet (in wt%). Rim compositions in contact with clinopyroxene.

	50-13	50-2	52-1	CHM30b	77-5
SiO ₂	39.34	38.52	39.12	40.41	39.70
TiO ₂	0.036	0.065	0.024	0.016	0.091
Al ₂ O ₃	22.53	21.83	21.46	23.21	22.39
Cr ₂ O ₃	0.042	0.010	0.051	0.079	0.096
FeO	21.21	24.92	25.01	17.74	22.85
MnO	0.41	0.55	0.56	0.39	0.67
MgO	10.61	8.43	7.50	12.03	7.61
CaO	6.27	5.64	6.72	7.38	8.36
Na ₂ O	0.011	0.008	0.026		0.016
Total	100.45	99.97	100.47	101.26	101.78

Table 9 Electron microprobe data for amphibole, paragonite, apatite, zoisite, clinozoisite and talc (in wt%).

Only microprobe data for amphibole from sample 77-5 are included here, other data are given in Chapter 2.

	AMP	PAR			APA		ZOI			CZO	TLC
	77-5	50-13	50-14	52-1	50-13	50-14	Ad25	CHM30b	77-5	77-5	55-4
SiO ₂	47.58	45.99	45.75	46.31			39.21	39.09	39.38	38.90	62.90
TiO ₂	0.36	0.16	0.093	0.20			0.03	0.03	0.05	0.12	0.02
Al ₂ O ₃	14.12	38.26	38.94	38.09		0.01	32.13	31.55	31.84	28.92	0.45
Cr ₂ O ₃	0.062	0.12	0.046	0.059					0.02	0.13	0.02
FeO	8.96	0.35	0.34	0.63	0.04		1.15	1.72	2.49	5.85	2.67
MnO	0.05	0.01	0.01	0.01	0.01	0.03	0.02	0.03	0.01	0.01	0.05
MgO	13.74	0.31	0.21	0.31	0.01		0.07	0.07	0.07	0.29	29.86
CaO	7.91	0.41	0.23	0.32	54.5	54.03	24.67	24.08	24.05	23.46	0.03
Na ₂ O	4.59	6.92	7.43	6.92							0.14
K ₂ O	0.56	1.24	0.46	1.44	0.01	0.01					
P ₂ O ₅					41.73	40.78					
F					4.25	5.37					
Cl					0.02	0.05					
Total	97.94	93.78	93.51	94.27	100.97	100.68	97.28	96.57	97.91	97.68	96.14

4.4.1 Clinopyroxene

Clinopyroxene shows a wide spread in jadeite content (from 27-57 mol%) and Mg# (from 76-95, see Figs. 20a and 20b). Most clinopyroxenes are omphacites having Jd contents exceeding 30%, but some analyses from three samples have lower Jd-contents and are thus not true omphacites (Morimoto et al., 1988). Clinopyroxenes from most individual samples form distinct clusters in a Mg# vs Jd plot (samples 50-2, 50-13, 55-4, CHM30a and CHM30b, see Fig. 20a). Large heterogeneities in clinopyroxene composition are confined to a few samples (Fig. 20b) and can be correlated with textural features and/or whole rock geochemistry. For instance, 55-3 and 59-1 are

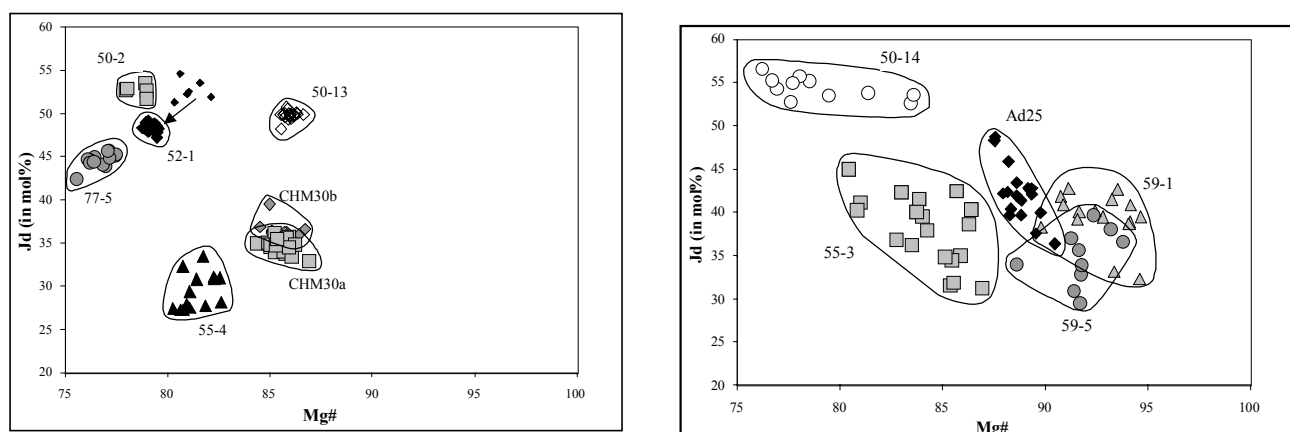
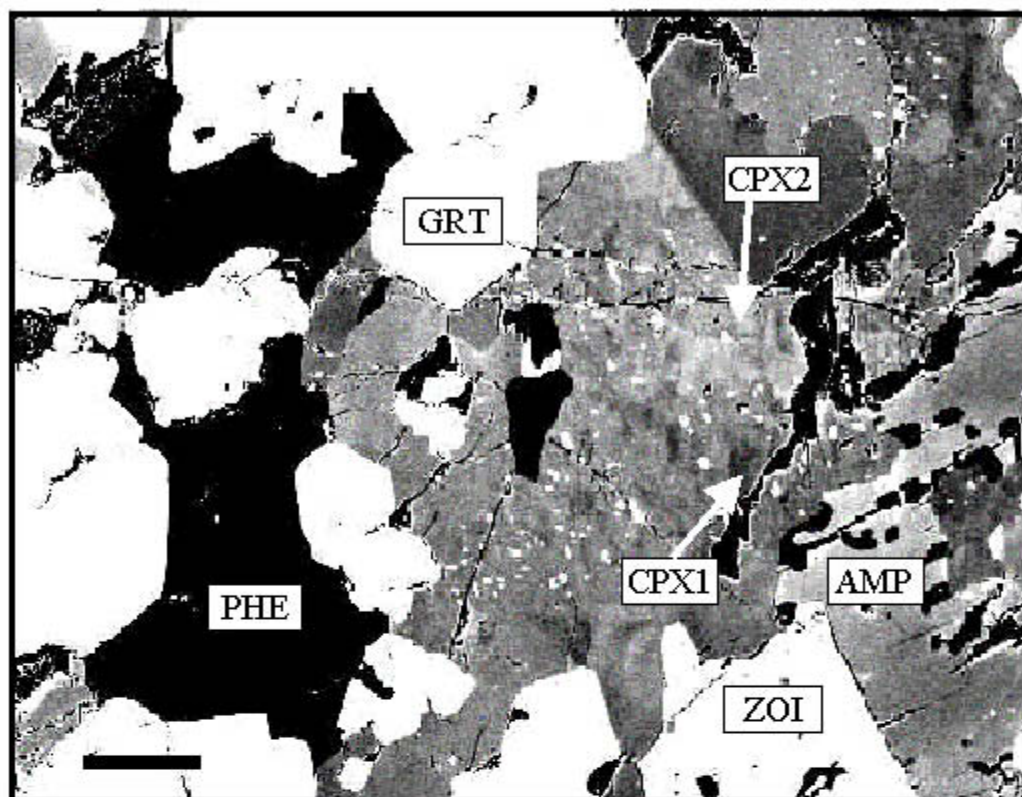
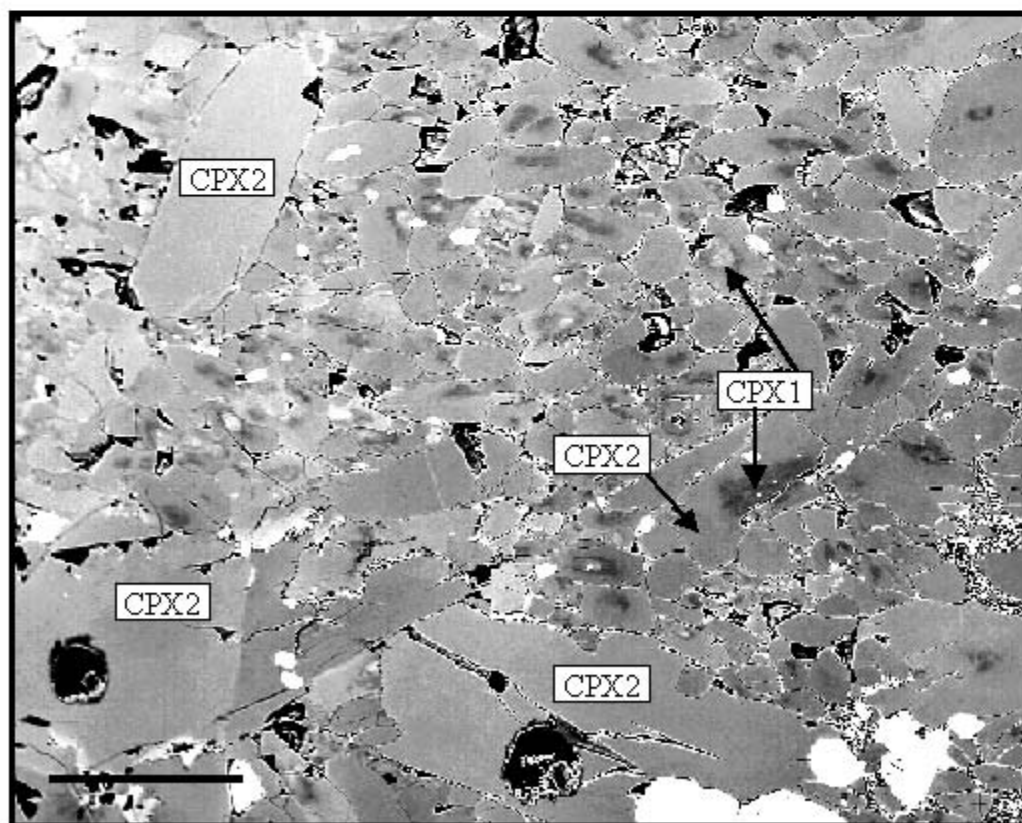
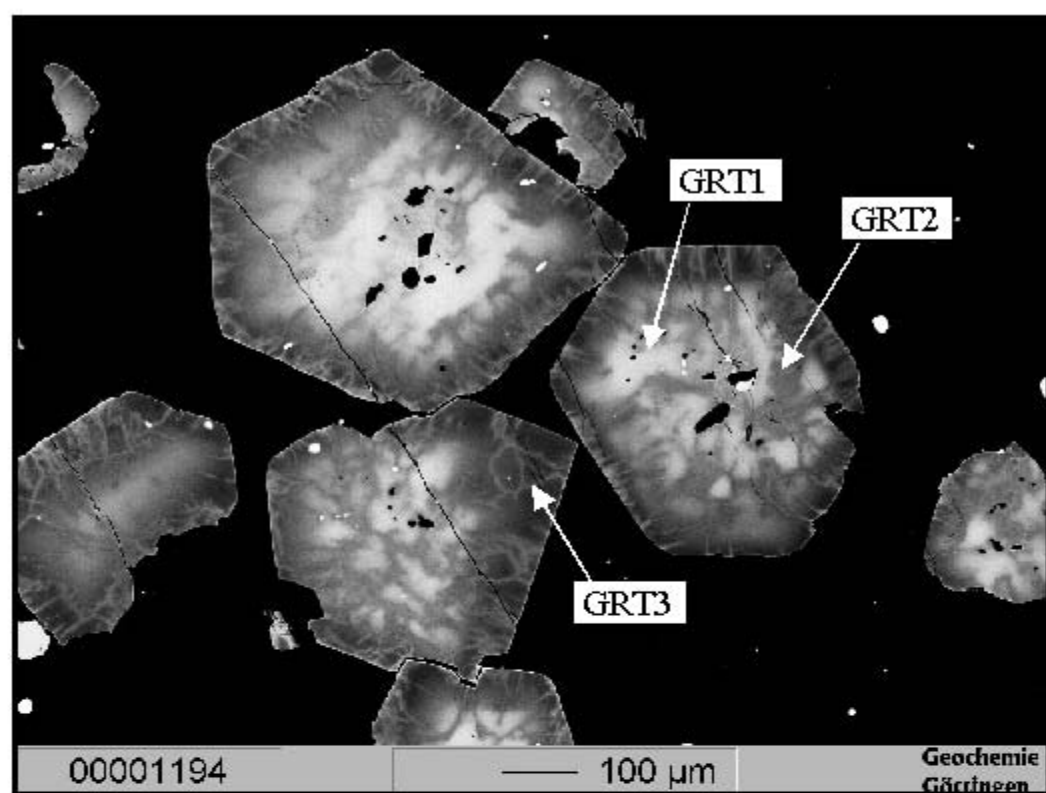
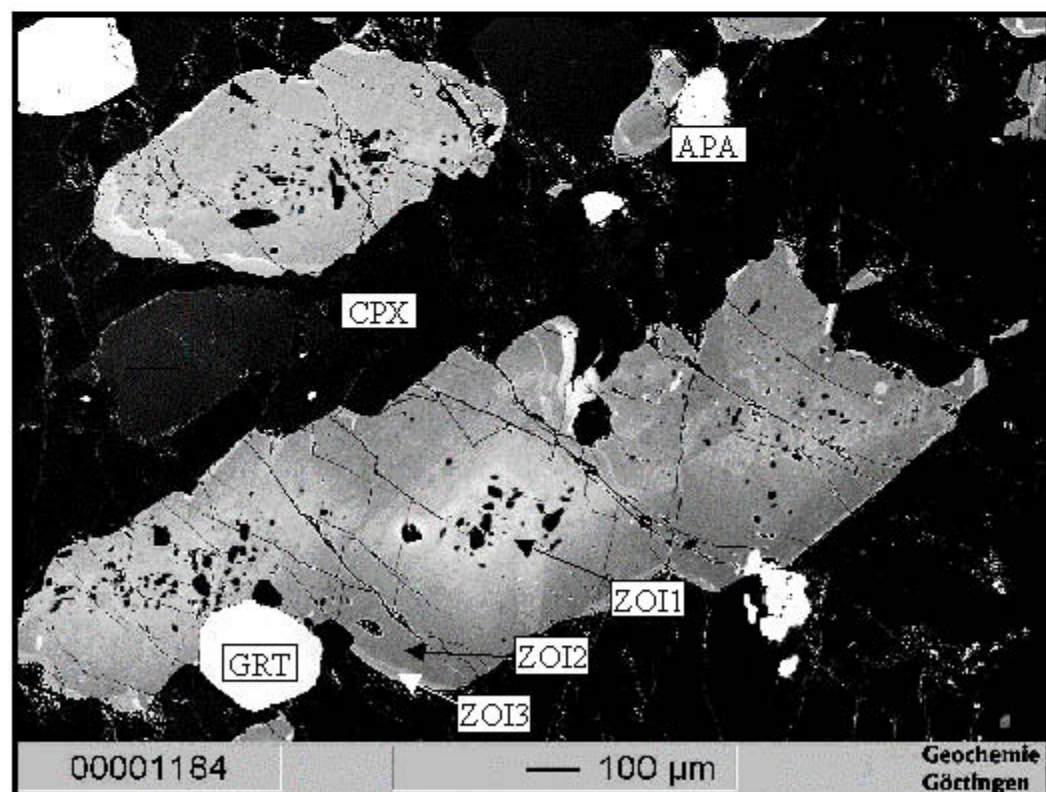


Fig. 20 Jd-Mg# diagram for clinopyroxene compositions. a) Samples with relatively homogeneous clinopyroxenes. Small diamonds are core compositions of small clinopyroxenes from sample 52-1, arrow marks zoning trend in these clinopyroxenes. b) Samples with strongly heterogeneous clinopyroxenes.

metagabbroic samples, characterized by very coarse grain sizes and a lack of penetrative foliation. 55-3 provides a spectacular example of disequilibrium at a thin section scale. In addition to pronounced variation in Jd content and Mg#, this sample contains millimetre wide mineral aggregates, with a striking green colour in thin section, consisting of phases with high Cr-contents (e.g. clinopyroxene with up to 1.9% Cr₂O₃, phengite with up to 2% Cr₂O₃, compared to concentrations of 0.2% Cr₂O₃ outside the aggregates). Chromite inclusions that occur in such Cr-rich clinopyroxenes are interpreted as relict magmatic grains (see Messiga et al., 1999). Cr mobility during eclogite facies metamorphism was therefore limited in this sample to the size of the Cr-rich clusters (about 1 mm). Back scattered imaging of clinopyroxenes from Ad25 reveals light and dark domains (Fig. 21a) that are chemically distinct in terms of jadeite content. However, quantitative electron microprobe analyses do not result in distinct clusters in a Mg# vs Jd plot (Fig. 20b) and the spread might be explained by mixing of analyses of two different clinopyroxene compositions, which could imply a miscibility gap between jadeite-rich (Jd₅₀) and jadeite-poor (Jd₃₅) clinopyroxenes in this sample. Unfortunately, this cannot be assessed with current thermodynamic models since different models give widely varying results for clinopyroxene solutions at 600°C/2.0 GPa, ranging from a miscibility gap between Jd₀₈-Jd₄₃ in one model to complete miscibility in another model (Meyre et al., 1997).

Large, idiomorphic and inclusion-poor clinopyroxenes (commonly aligned in the foliation) were found to be the most homogeneous type of clinopyroxene in our samples. It can be seen in Fig. 21b that fine-grained clinopyroxenes, as in 52-1, are mostly zoned (with a core to rim decrease in Jd-content from 54 to 47 and in Mg# from 83 to 79; see Fig. 20a), whereas large clinopyroxenes are unzoned and have a Jd-content and Mg# identical to rim compositions of fine-grained clinopyroxenes. We therefore infer that the large clinopyroxenes are younger than cores of small clinopyroxenes and suggest that this may be an indication of annealing and Ostwald ripening of suitably oriented grains. Overgrowth of strained fine-grained clinopyroxenes, as observed in Trescolmen eclogites, can be explained by a dominance of mass transfer processes over dislocation creep (Godard & van Roermund 1995). We correlate the influx of fluids under the eclogite facies conditions during the Trescolmen stage (Chapter 2) with the net transfer hydration reactions in the Trescolmen area. Fluids as a mass transfer medium have also been advocated by Philippot & van Roermund (1992) to explain local annealing of clinopyroxene in a former mylonitic fabric. The trend of decreasing Jd-content and Mg# in sample 52-1 can be correlated with concomitant growth of paragonite (as a sink for sodium) and amphibole (which has a higher Mg# than clinopyroxene) during fluid influx. The sequence of clinopyroxene compositions in 52-1 is opposite to that in Tauern eclogites, where small clinopyroxenes (Jd₄₉) formed by dynamic recrystallization from large clinopyroxenes (Jd₃₅) in which subgrain boundaries and undulose extinction are common (Kurz et al., 1998a). The latter type of grain-size reduction has been attributed to an increase in finite strain, with rotation of subgrains in large porphyroclastic clinopyroxenes producing polycrystalline aggregates (Lardeaux et al. 1986, Buatier et al. 1991). We correlate such dynamically recrystallized clinopyroxenes with the early fine-grained clinopyroxenes in Trescolmen eclogites.

*Fig. 21a**Fig. 21b*

*Fig. 21c**Fig. 21d*

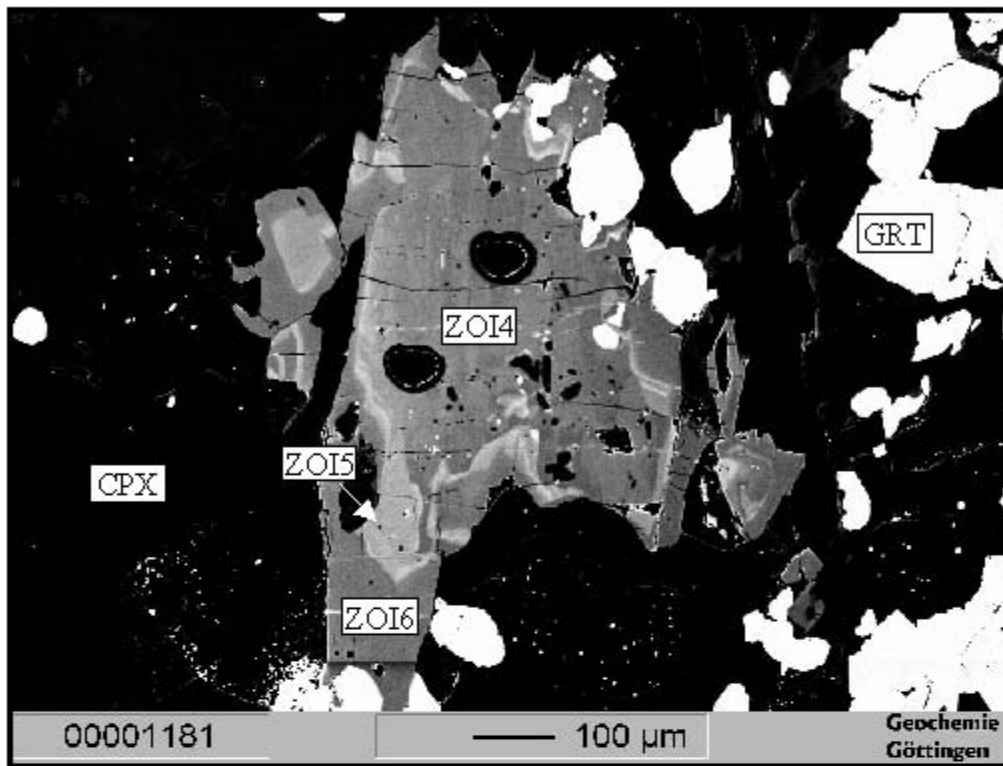


Fig. 21e

Fig. 21 High contrast back scattered images of selected microtextured relationships in Trescolmen eclogites. For abbreviation of phases see Table 6. a) Small scale heterogeneities in clinopyroxene from sample Ad25. CPX1- jadeite-rich domains, CPX2- jadeite-poor domains, small white grains in clinopyroxene crystal are rutiles. Scale bar is 100 μ m. b) Two different generations of clinopyroxene in sample 52-1. Cores of small clinopyroxenes (CPX1, darker in back scattered image) are jadeite richer and have higher Mg# than rims of small clinopyroxenes and large clinopyroxenes (CPX2; see Fig. 9a). In the lower part of the figure are two LAM craters in large clinopyroxenes, the spot in the middle was not used for quantification. Scale bar is 300 μ m. c) Annealed cracks in garnets from sample 55-3. GRT1- undisturbed garnet core, GRT2- annealed cracks in garnet cores with compositions similar to garnet rims (Trescolmen stage) indicating eclogite-facies conditions, GRT3- late annealed cracks mostly in garnet rims of probable amphibolite-facies conditions. d) Zonation pattern of zoisites from sample CHM30b. Different colours in zoisite are primarily caused by different Sr content. ZOI1- zoisite core with high Sr concentrations (up to 12000 ppm), ZOI2- inner rim composition of zoisite, assumed to be part of the Trescolmen stage (ca. 3500 ppm Sr), ZOI3- resorbed rim of zoisite with extremely high Sr compositions (up to 21000 ppm). Inclusions in zoisite cores are omphacites. e) Zonation pattern in zoisite from sample Ad25. Different colours in zoisite are primarily caused by different Sr content. ZOI4- zoisite core with small scale Sr heterogeneities, ZOI5- complex resorption pattern in zoisite with at least two different high-Sr rims, ZOI6- low-Sr overgrowth. Inclusions in zoisite are omphacites. In the center of the large zoisite are two test laser pits (data not used because of apparent zonation).

4.4.2 Garnet

In general, all samples show garnet zonation typical for growth under prograde conditions, characterized by increasing Mg# and decreasing MnO contents. There is also a decrease of CaO content from core to rim (Fig. 22). The cores of some garnets still preserve pre-eclogitic inclusions consisting of epidote, tschermakitic amphibole and rare plagioclase (Heinrich 1986). Towards their rims, garnets are clear and are virtually free of inclusions, except for minor quartz and omphacite (59-5). The rim compositions are interpreted as being part of the eclogite facies assemblage, as indicated by omphacite inclusions and direct grain contact with unaltered matrix omphacite. A common feature in Trescolmen eclogites, observable in back scattered images, is a patchy zoning in garnet cores, where old core areas (light grey in Fig. 21c) are replaced along irregular annealed cracks and fractures by recrystallized garnet (darker grey). A second type of annealed fracture is visible in the most altered samples (55-3, 77-5) and clearly postdates eclogite facies garnet rims. In backscattered electron images, straight and anastomosing bright fractures can be seen to penetrate garnet rims, propagating from the rim radially into the garnet interior (Fig. 21c). Spot analyses reveal that the older generation of cracks approach the compositions of rims and can therefore be related to the eclogite-facies stage. Erambert & Austrheim (1993) described similar annealed cracks, formed under eclogite-facies conditions, and interpreted them as fluid pathways, indicating that volume diffusion was insignificant in comparison to the role of fluids in controlling the element mobility and degree of re-equilibration in garnet. Likewise we infer that fluid infiltration during the Trescolmen stage was the source for the patchy zoning of the garnet cores. Atoll garnets in some samples (50-2, 52-1, 55-3) formed by a partial or complete replacement of the garnet cores by quartz, phengite, small euhedral garnets (5-10 μm , identical in composition with rims of atoll garnets) and rare euhedral omphacite, indicating eclogite facies conditions. The formation of atoll garnets probably also occurred during fluid influx, but, in contrast to the formation of the annealed garnet cracks, may represent a more evolved stage of reaction under open system conditions. The second generation fractures can be chemically distinguished from eclogite-facies fractures as they are displaced from the normal garnet zoning trend (mostly Ca-Mg exchange, Fig. 22) towards higher Fe and Mn contents at a given Ca content. A similar trend can also be seen at

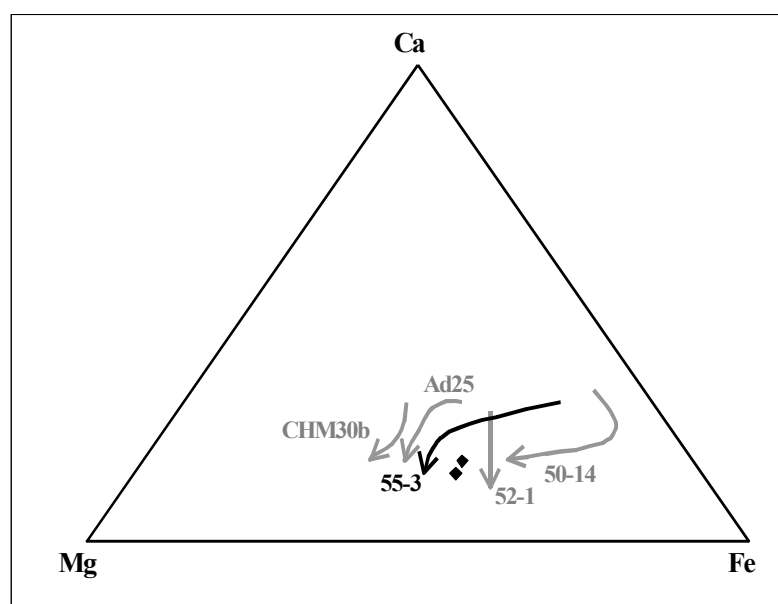


Fig. 22 Ca-Mg-Fe triangle for garnet compositions. Schematic zonation patterns of large garnets from selected samples are indicated by arrows. Black diamonds are compositions of late annealed cracks in garnets from sample 55-3 (GRT3 in Fig. 21c).

the outermost rim of some garnets from Trescolmen (e.g. sample 50-12 in Meyre et al., 1999). Both the late annealed fractures and the outermost rim zonation can be ascribed to amphibolite facies overprinting and may be similar to the annealed garnet fractures described by Kurz et al. (1998a). The small scale relationships of several generations of garnet in a single grain can in principle be resolved with the LAM technique if highly enriched trace elements are analyzed and the diameter of the laser beam is reduced ($\leq 20 \mu\text{m}$ scale). However, a major obstacle to applying this set-up in our study is that concentrations of most trace elements of interest are below 100 ppb in garnet, so that the beam size was always chosen to be at least $60 \mu\text{m}$. Therefore, we do not present trace element ratios of coexisting garnet/mineral pairs, since the measured garnet concentrations are always mixed analyses of different garnet compositions. The data set for garnet trace elements is however used in the section on mass balance calculations.

4.4.3 Zoisite, clinozoisite and allanite

Zoisite was only found in three of our investigated samples (Ad25, CHM30b, 77-5) and coexists with clinozoisite in only one sample (77-5). In this sample, distinct crystals of zoisite and clinozoisite in mutual grain contact, show limited variations within one sample (X_{Fe} from 0.037-0.058 in zoisite and 0.098-0.132 in clinozoisite). In backscattered electron images, we did not observe systematic zonation patterns. An inferred miscibility gap between zoisite and clinozoisite (Franz & Selverstone, 1992), can only be compared with other eclogite localities in the absence of experimentally calibrated relationships as a function of P and T. Paragonite eclogites from Dabie Shan, which are inferred to have equilibrated under similar PT conditions to the Trescolmen eclogites (ca. 1.9 GPa, 700°C; Okay, 1995), have zoisite-clinozoisite assemblages that have almost identical chemical compositions to those in sample 77-5 (average compositions are $X_{\text{Fe}} = 0.049$ for zoisite and 0.135 for clinozoisite; Okay, 1995).

Zoisites from Ad25 and CHM30b also show some variation in terms of the Fe^{3+} content, X_{Fe} ranging from 0.021 to 0.042 in Ad25 and from 0.037 to 0.055 in CHM30b. The X_{Fe} composition of these zoisites is lower than those from 77-5, which might reflect a lower Fe^{3+} bulk rock concentration of the former samples and is consistent with the observation that no clinozoisite has been observed in these samples. Zoisites in both samples show pronounced zonation patterns in backscattered images (Fig. 21d and 21e). Brightness differences are not a function of variation in major element composition, as X_{Fe} variations are limited, but can be correlated with changes in Sr concentration. Bright areas of zoisites in CHM30b (Fig. 21d) have Sr enrichments of up to 21000 ppm (ZOI3), whereas dark areas are distinctively lower in Sr concentration (3500 ppm; ZOI2).

Zonation patterns in zoisite in CHM30b (ZOI1 to ZOI3 in Fig. 21d) can be best explained by growth zoning and late resorption processes. Zoisite cores with high Sr concentrations (ZOI1) formed under eclogite-facies conditions, indicated by numerous omphacite inclusions (Fig. 21d). Due to the strong preference of Sr for zoisite, Sr is concentrated in the zoisite cores and depleted in the surrounding matrix. Subsequent zoisite growth (ZOI2) is characterised by lower Sr concentrations, similar to more common garnet growth zoning patterns. ZOI2 growth still continued under eclogite-facies conditions, as documented by rare omphacite inclusions and common mutual grain boundaries with matrix omphacite. Extreme enrichments of Sr, of up to 21000 ppm, occur only in the outermost rim of zoisites (ZOI3). These zones are unevenly distributed around zoisite and mostly less than $30 \mu\text{m}$ thick. This

pattern, combined with the high Sr concentrations, points to zoisite resorption which released Sr that was redistributed in the surface layers of the remaining zoisite. Since amphibolite-facies overprinting occurs on grain boundaries, we correlate the origin of the high Sr rims with beginning of zoisite breakdown under amphibolite-facies conditions.

Zonation patterns of zoisite from eclogite sample Ad25 (Fig. 21e) are very complex. Cores (ZOI4) are low in Sr (ca. 2800 ppm) and show small-scale heterogeneities in back scattered electron images. They are surrounded by at least two narrow zones of Sr enrichment (up to 10000 ppm; ZOI5). At the margins of zoisite grains, Sr concentrations drops to about 1000 ppm (ZOI6). The origin of the two or more zones of high Sr content might point to episodic fluid infiltration into the eclogite bodies, with Sr transported by the fluid. The growth of zoisite in AD25 with respect to the P-T path cannot be worked out and choices of areas in zoisite suitable for equilibrium considerations with coexisting phases are subject to uncertainty. However, all zoisite areas grew under eclogite-facies conditions, indicated by omphacite inclusions in ZOI4 and ZOI6.

Allanite occurs as an accessory phase in several samples (50-2, 50-13, 52-1, 55-3), mostly as irregular grains less than 40 μm in length. An exception are allanites in 50-13, where several large grains are up to 400 μm and numerous omphacite inclusions show a preferred orientation parallel to the eclogite-facies foliation. This strongly suggests that allanite, at least in sample 50-13, is part of the eclogite-facies assemblage.

4.4.4 Other hydrous phases (*amphibole, phengite, paragonite, talc, apatite*)

Chemical compositions of amphibole and phengite, as well as textural relationships of all hydrous phases, are presented in Chapter 2 and a summary of the most important chemical characteristics is given below. *Amphibole* occurs in varying amounts in every sample and shows a wide range of composition, ranging from tremolitic to tschermakitic with a significant glaucophane component. Following the classification scheme of Leake et al. (1997), amphiboles from most samples can be termed barroisites. A strong correlation between Na on the M4 site of amphibole cores and the jadeite content of associated omphacite is evidence for the growth of amphibole under eclogite-facies conditions, as already observed by Heinrich (1986). An increase of Na(M4) is coupled with an increase of Na+K(A-site), as long as amphibole core compositions are considered. However, core-rim zonation trends are characterised by the opposite trend, with a decrease of Na(M4) and increase of Na+K(A-site) towards the rim. Amphibole rim compositions are not correlated with associated omphacites and we therefore treat amphibole cores as belonging to the eclogite-facies parageneses (Trescolmen stage), whereas amphibole rims must have grown after the Trescolmen stage, either during uplift under waning eclogite-facies conditions or during the amphibolite-facies overprint.

Phengites have high celadonite contents (37-47 mol%) and low paragonite contents (Na/Na+K ratio 0.05-0.20), with a negative correlation between these two parameters from sample to sample. Zonation trends of paragonite and celadonite components inside phengite grains can be explained by late diffusion processes, which are limited to grain boundaries and cleavage planes (Chapter 2). Laser ablation measurements have therefore been limited to the cores of fresh phengites with no observable cleavage planes.

Other hydrous phases do not have pronounced chemical variations. *Paragonites* show limited celadonite and muscovite substitution (up to 1.4 wt% K₂O; Table 9). *Talc* also occurs as an almost pure end member, with 0.45 wt% Al₂O₃ and 2.7 wt% FeO as minor components (Table 9). *Apatites* from Trescolmen can be classified as F-apatites (4.3 to 5.4 wt% F), characterised by low Cl concentrations (200-500 ppm Cl).

4.5 Mass balance calculations

Following the method of Sorensen & Grossman (1989), bulk rock data and modal abundances of high pressure phases have been combined with results from LAM data of *in-situ* mineral analyses to perform mass balance calculations for the investigated trace elements. The purpose of these calculations is twofold. On the one hand, differences between measured and calculated whole rock concentrations allow an evaluation of the importance of possible non-analyzed accessory phases. On the other hand, the combination of trace element concentration and modal abundance of each phase gives a clear impression of the dominant carriers for each trace element in eclogites. Calculations are reported for two samples, chosen to represent phengite-rich eclogites (50-13) and zoisite-rich eclogites (CHM30). For these two samples, the most complete data set is available, but similar results are also obtained for the other investigated eclogites.

The results for sample 50-13 are plotted in Fig. 23a. The trace element budget of sample 50-13 has been modelled for Cs, Rb, Ba (Chapter 2) and for Nb, Zr, Sb, Sn, Mo, W (Chapter 3). It has been demonstrated that phengite dominates the Ba budget of the whole rock, rutile dominates Nb and zircon dominates Zr. Therefore Ba, Nb and Zr are not plotted in Figs. 23a and 23b, but the conclusions of the former studies are generally confirmed by the larger data set of this study. For the remaining elements, the differences between calculated and measured whole rock concentrations of Li, Sr, Pb and Y are generally less than 20% (slightly >20% in the case of Li). These are treated as balanced calculations (Sorensen & Grossman, 1989). For Be and B, no whole rock data exist and the calculated whole rock is normalized to 100%. The difference from the 100% level of the calculated whole rock in Fig. 23a is due to not plotting amphibole, which makes up 3% of the Be and 6% of the B budget. For all other elements, the contribution of amphibole is less than 1% in eclogite sample 50-13. Large deficits between calculated and measured whole rock concentrations exist for Ce, Nd, Sm, Th and U. The deficits for REE are most likely explained by the existence of non-analyzed allanite in 50-13 (confirmed by qualitative EDS analyses). Allanite is characterized by extreme LREE (light REE, here Ce) enrichments and a strong decrease towards HREE (heavy REE, here Y is treated as a HREE). In the absence of quantitative data, it is possible to balance measured and calculated whole rock REE concentrations using the average composition of allanites from garnet amphibolites (38200 ppm Ce, 17150 ppm Nd; Sorensen & Grossman, 1989) and assuming a modal abundance of allanite of 0.04%. With these assumptions, concentrations of 1400 ppm Th and 600 ppm U in allanite are necessary in order to balance the deficit of these trace elements entirely from allanite. Th and U can also be highly enriched in zircon. Since the modal abundance of zircon can be calculated by the Zr content in the whole rock (0.018%; Chapter 2), a concentration of 4300 ppm Th and 2000 ppm U in zircon are required to balance the deficit in the Th and U budget entirely by zircon.

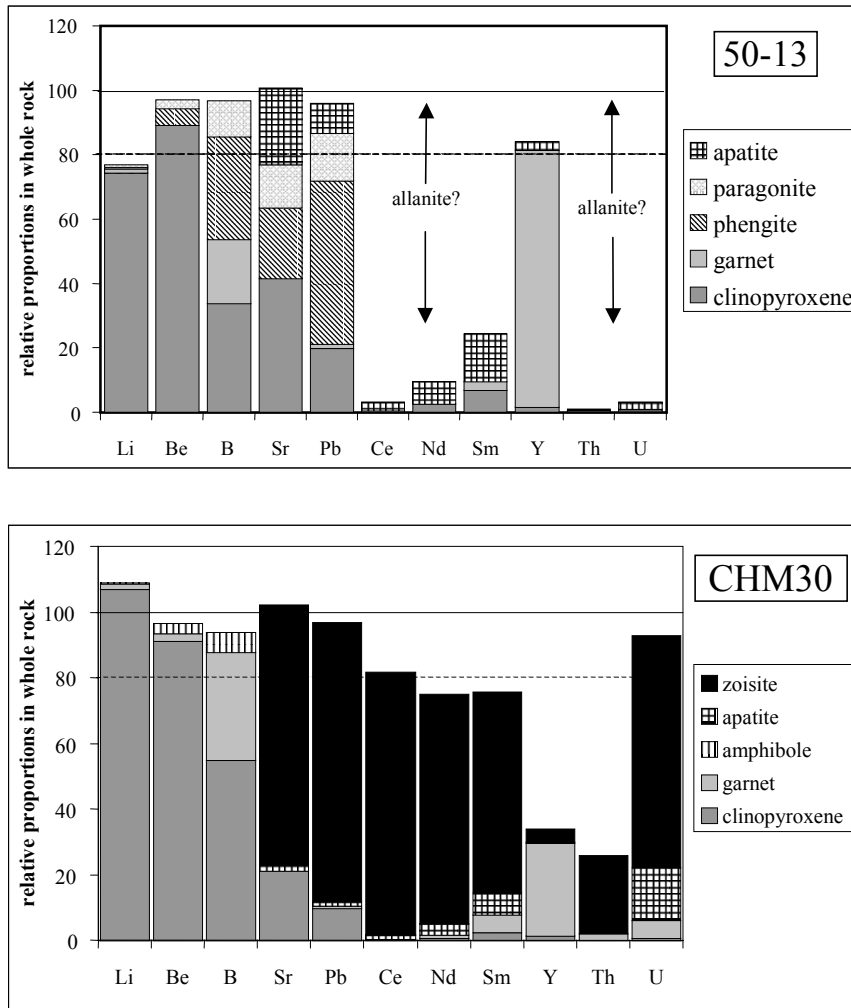


Fig. 23 Mass balance calculation for a) a phengite-rich eclogite (sample 50-13) and b) a zoisite-rich eclogite (sample CHM30). Bar length corresponds to percentage of trace element in each phase relative to whole rock concentration. The result for each trace element is considered to be well balanced if the concentration calculated from modal proportion and LAM analyses is between 80-120% (stippled line) of measured whole rock concentrations (solid line). In other cases, the presence of the element in an unanalyzed phase (e.g., allanite) is suspected.

A mass balance for sample CHM30 is adequately achieved for all trace elements except Y and Th (Fig. 23b). The deficit in Y may be explained by the neglect of garnet cores in the mass balance (due to a high inclusion density in garnet cores), since garnets of Trescolmen are always zoned in Y, a feature commonly observed in prograde growth zoning of garnets (e.g. Hickmott & Shimizu, 1990). The deficit in Th cannot be explained satisfactorily. Zircon is unlikely to contain the missing Th, since no zircons have been reported with extreme enrichments in Th over U. Given the large compositional differences in a single zoisite (Fig. 21d), with Th/U ratios between 0.4 and 5.1, the data from one grain probably fail to represent the average composition of zoisites in the whole rock. Nevertheless, this illustrates the complexities of trace element distribution in natural eclogite-facies rocks, especially for Th and U systematics. In the following, results from the mass balance calculations are summarized element by element and compared with findings from other studies.

Li, Be, B. Mass balances in both samples reveal the dominant role of clinopyroxene for the Li and Be budgets. All other phases incorporate <10% of the whole rock content. B is more evenly distributed among different phases, so that in sample 50-13 paragonite, phengite, garnet and clinopyroxene all contribute >10% of B to the whole rock budget. Although phengite is the most important residence site for B in this sample, phengite is neither a dominant

phase nor is it the phase with the highest B concentration, since paragonite contains four times as much B as phengite. These findings are in accord with data from the eclogite-facies rocks analyzed by Domanik et al. (1993), who reported high B concentrations in phengite (60-100 ppm) and significant amounts in omphacite (ca. 5 ppm). In contrast, Be concentrations are similar in both phengite and clinopyroxene in our samples. However, taking mass balance calculations into consideration, the conclusion of Domanik et al. that phengite is the primary host of B and Be cannot be confirmed, at least not for our metabasaltic samples where clinopyroxene is a major phase. To our knowledge, no other Li data for minerals in eclogite-facies rocks exist. Although the occurrence of Li-rich micas in pegmatites might imply that micas are likely to be important carriers for Li, the review by Guidotti & Sassi (1998) has shown that Li is commonly present in regional metamorphic metapelitic micas only at trace element levels (<100 ppm), a conclusion which we can extend for eclogite-facies phengites in our study.

Sr and Pb. The elements Sr and Pb can be discussed together since they show some similar partitioning behaviour in both samples. In CHM30b, zoisite dominates the Sr and Pb budget by incorporating >80% of the whole rock content. The only other significant phase for the Sr budget in CHM30b is clinopyroxene. In sample 50-13, which lacks zoisite, important phases for Sr and Pb are apatite, paragonite, phengite and clinopyroxene. In detail, clinopyroxene is the most important carrier for Sr (40%; 20% for Pb), whereas phengite is most important for the Pb budget (50%; 20% for Sr). Interestingly, allanite does not seem to be a significant carrier for Sr and Pb, which show almost perfect agreement between calculated and measured whole rock concentrations. However, this does not exclude high total concentrations of these elements in allanite. Due to the calculated low modal abundances in sample 50-13, concentrations of as high as 5000 ppm Sr and 200 ppm Pb in allanite would incorporate less than 3% of the measured whole rock content. The importance of zoisite (or the epidote-group in general) as a carrier for Sr and Pb has been stressed in several previous studies, both in terms of absolute concentrations (Hickmott et al., 1992; Domanik et al., 1993) and dominance in mass balance calculations (Sorensen & Grossman, 1989; Nagasaki & Enami, 1998). It has been proposed from these findings that upon dehydration of zoisite, large quantities of Sr and Pb are released into the fluid (Hickmott et al., 1992; Nagasaki & Enami, 1998). However, this study shows that in the absence of zoisite, Sr and Pb can also be incorporated in significant quantities in clinopyroxene, which is stable well beyond the upper stability of zoisite (Schmidt & Poli, 1998). A strong zoisite signature in the released fluid will therefore not inevitably develop upon zoisite breakdown, but instead this depends on a more complex interplay of partition coefficients between zoisite, clinopyroxene and fluid.

REE and Y. Even though REE concentrations and modal abundance of allanite (in 50-13) and zoisite (in CHM30) are very different, combining these two factors shows that the importance of both phases for the REE inventory is remarkably similar. LREE (Ce) are almost completely (>90%) accommodated in allanite and zoisite, whereas the dominance of these two minerals decreases steadily towards the HREE, with the relative proportions in allanite and zoisite Ce>Nd>Sm>Y. For the HREE (here proxied by Y), zoisite and allanite are not significant carriers and instead garnet dominates the element budget (in 50-13 >80%). No other phase is a major carrier for REE in the investigated samples, even though absolute concentrations in the case of apatite can be significant. However, apatite has lower absolute concentrations of REE in relation to zoisite as well as allanite and occurs in lower modal proportions than zoisite in zoisite-bearing eclogites. Again, these results are in good agreement with previous studies where mass balance calculations have been performed. In eclogites from Liguria (Tribuzio et al., 1996), allanite is the dominant phase for LREE, whereas garnet dominates the HREE budget. In the case of zoisite-bearing rocks,

Sorensen & Grossman (1989) described garnet amphibolites where the LREE budget is dominated by zoisite and the HREE budget by garnet.

Th and U. Due to the lack of data for allanite and zircon in this study, large uncertainties remain concerning the element budgets for Th and U. Calculations for CHM30 indicate that zoisite seems to control the element budget for U and probably also for Th, given the large variation in Th (and U) in a single zoisite grain. As a result, zoisite with higher than measured Th concentration is a more likely phase to balance the Th budget than zircon. The whole rock Th/U ratio of 2.7 in sample CHM30 can also be better explained with zoisite as the dominant carrier, since measured Th/U ratios in zoisite (from 0.4 to 5.1) enclose this value, whereas zircons in eclogites have ratios that are too low (<0.02; Creaser et al., 1997) to match the whole rock ratio in sample CHM30. Considering the similar trace element contents of allanite and zoisite, as well as the ability of allanite to store large Th concentrations (up to 6000 ppm; Sorensen & Grossman, 1989), allanite is the likely carrier for Th and U in sample 50-13, which lacks zoisite. However, the role of zircon and allanite for Th and U budgets in eclogites requires further study, especially in systems that are not dominated by zoisite. In any case, this study clearly demonstrates that the major phases garnet and clinopyroxene are insignificant for the Th and U budget in eclogites (both phases together incorporate always <5% of the measured whole rock content of Th and U).

4.6 Mineral/mineral partitioning systematics

4.6.1 Evaluating samples for trace element equilibration studies

The mineral chemistry and textural information gained from high resolution back scattered images has allowed us to confidently isolate appropriate assemblages which thoroughly equilibrated under eclogite facies conditions and can therefore be used for trace element partitioning studies of eclogite-facies processes in other areas. In general, the inner rim areas of zoisite and garnet, the core areas of amphibole, phengite (Chapter 2), paragonite and apatite as well as the large clinopyroxene grains are all part of the re-equilibrated eclogite stage (Trescolmen stage; Fig. 3).

However, the approach towards equilibrium proceeded to different degrees in the investigated samples. We use the variability of clinopyroxene chemistry within individual samples as one criterion for evaluating equilibrium. Clinopyroxenes from samples Ad25, 50-14, 55-3 and 59-1 show the greatest scatter and are clearly heterogeneous (Fig. 19b). In the case of Ad25, the variation occurs on a ca. 20 μm scale (Fig. 20a) and cannot be resolved with the LAM set-up used in this study. For 50-14, 55-3 and 59-1, we were unable to correlate the chemical variation with textural observations and detailed element mapping is required. All other samples have restricted clinopyroxene compositions on an electron microprobe scale (<5 μm , Fig. 19a) and are therefore well suited for trace element analysis with LAM (>40 μm).

We obtained another criterion for equilibrium from the textural relationships between the different phases. From all samples with restricted clinopyroxene composition, only 50-2, 50-13, 52-1 and 77-5 are well foliated eclogites

(Table 1). In these samples, hydrous phases define the main foliation with clinopyroxene, implying that they dynamically recrystallized together. Deformation significantly enhances material transport (Messiga et al., 1995), whereas solid state diffusion must have been too slow during the short-lived high temperature history of the Trescolmen eclogites to produce equilibrium compositions among different phases (Watson, 1996). Eclogite facies phases in CHM30b, CHM30a and 55-4 are also in apparent major element equilibrium, but we cannot judge the likelihood of trace element equilibration in the absence of signs of dynamic recrystallization.

In summary, we can order our samples in terms of the probability of showing equilibrium trace element partitioning behaviour. The most ideal samples are 50-2, 50-13, 52-1 and 77-5, which were therefore also the most thoroughly analyzed. They are taken as reference samples in the following discussion and are marked separately in the following figures. CHM30a, CHM30b and 55-4 comprise the second group, which have homogeneous clinopyroxene compositions, but the lack of dynamic recrystallization textures suggests the need to apply caution. The samples Ad25, 50-14, 55-3 and 59-1 belong to the third group in which major element inhomogeneities were observed in clinopyroxene and can therefore also be expected for trace elements.

For low-T undeformed eclogites from Liguria, Messiga et al. (1995) have shown that chemical equilibrium of the REE commonly occurs in microdomains. We have therefore limited our trace element analyses to only one sub-area per thin section. The smallest possible sub-area was about 1 cm², which was necessary in order to find enough large inclusion-free grains of each mineral for trace element analysis. This size is larger than the sub-areas analyzed by Messiga et al. (1995), but the higher temperatures (650°C instead of 450°C) in combination with dynamic recrystallization in some of the Trescolmen eclogites make larger equilibrium domains more likely.

Different chemical properties (diffusion rates, affinities to different phases, etc.) of many trace elements make it likely that the approach towards equilibrium is a function of both trace element and phase in question. Therefore it would be ideal if a homogeneity test as applied to major components in clinopyroxene could be performed for every trace element distribution in each analyzed phase. However, at this stage we can only give some estimates of the degree of homogeneity in our samples. Despite the large number of LAM analyses (>400 single spot analyses) accumulated for this study, many data points (i.e., for the concentration of one trace element in one phase in a particular sample) are based on only one or two analyses. Where three or more data points exist, we can use the standard deviation as a homogeneity test (Kretz et al., 1999). We use a threshold of 25% standard deviation as an upper limit for analytical scattering and a lower limit of 35% standard deviation as a strong indication for trace element heterogeneity on a 40-100 µm scale. Data points with an average concentration below 0.1 ppm were not evaluated for heterogeneity due to possible undetectable contamination and can therefore only be treated as maximum values (see analytical section). The results of this homogeneity test are shown in Tables 10 to 13, where homogeneous data points are marked in bold and inhomogeneous data points are marked by italics. Other data points are either below 0.1 ppm or based on less than 3 analyses. The threshold value of 25% is larger than the estimated precision of 10% for regular LAM analyses of standard glasses under constant conditions (Horn et al., 1997) and was chosen to compare data from different analytical set-ups and from different spot sizes. It should be noted that, in detail, we do not follow the procedure described by Kretz et al. (1999), in which threshold values were solely based on precision that was calculated from repeated analyses of standard glasses under constant conditions.

Table 10. Average trace element data for clinopyroxene by laser ablation microprobe in ppm. Numbers in bold are considered to represent homogeneous concentration of specified trace element in sample ($\leq 2.5\%$ std. deviation of ≥ 3 analyses); numbers in italics are averages of heterogeneous compositions ($\geq 3.5\%$ std. deviation of ≥ 3 analyses).

	50-2	50-13	52-1	CHM30b	CHM30a	Ad25	77-5	50-14	55-3	55-4	59-1
Li	28	25	16	30	-	42	64	40	-	-	-
Be	2.60	2.53	1.88	2.71	2.39	1.10	1.15	4.07	1.79	-	-
B	4.18	2.72	3.63	3.15	3.80	4.88	5.05	4.78	-	-	-
Sr	168	82	187	183	172	82	8.2	56	75	71	149
Y	1.21	0.59	1.24	<i>0.37</i>	<i>0.34</i>	0.65	0.23	0.87	0.74	0.72	0.94
Zr	2.44	2.00	2.54	2.19	2.35	2.13	4.05	1.85	1.92	2.74	2.10
Nb	0.0046	0.0095	<0.02	<0.01	<0.01	<0.02	0.0070	0.0063	0.015	0.017	0.014
Ba	0.043	0.0036	0.023	0.031	0.0063	0.076	0.0074	<0.05	0.072	<0.02	0.054
Ce	0.82	0.28	0.46	0.046	0.055	0.015	0.017	0.10	<0.03	0.16	0.20
Nd	1.69	0.62	1.29	<i>0.10</i>	<i>0.15</i>	0.11	0.0035	0.31	<0.3	0.44	0.84
Sm	1.15	0.44	1.20	0.10	<i>0.18</i>	<0.03	0.0084	0.34	<0.3	0.36	0.67
Pb	3.13	1.40	2.96	3.36	2.48	1.49	0.040	<i>1.30</i>	2.37	<i>1.66</i>	5.04
Th	<0.01	0.010	0.0098	0.0007	0.0015	0.0020	0.0035	0.0021	0.020	0.00070	<0.01
U	0.0068	0.0055	0.0038	0.0030	0.0012	0.0070	0.0006	0.0059	0.044	0.016	0.016

Table 11. Average trace element data for amphibole by laser ablation microprobe in ppm. For explanation of bold and italic numbers see Table 10.

	50-2	50-13	52-1	CHM30b	CHM30a	Ad25	77-5	55-3	55-4	59-1
Li	2.47	0.98	1.50	1.14		6.7	1.40	<i>18</i>		
Be	5.83	3.18	3.48	2.22	1.26	1.05	1.57	2.22		
B	11.8	9.32	9.02	8.02	5.58	10.3	11.6	4.30		
Sr	171	99	180	31	38	<i>12.2</i>	14.4	46	74	82
Y	4.2	2.32	4.03	1.30	<i>1.23</i>	1.96	0.92	5.43	0.80	2.35
Zr	6.03	5.51	6.10	2.96	2.69	3.45	7.63	2.82	1.77	3.29
Nb	0.048	0.11	0.058	0.026	0.031	<0.02	0.03	0.032	0.017	0.015
Ba	4.80	3.67	5.25	5.74	4.09	<i>1.66</i>	5.58	1.02	2.07	4.41
Ce	0.23	0.14	0.18	0.0082	0.037	0.028	0.32	0.79	0.27	0.14
Nd	1.14	0.26	0.78	<0.04	<i>0.10</i>	<0.03	0.022	2.25	0.56	0.85
Sm	1.77	0.51	1.60	0.019	0.18	0.017	0.0054	1.27	0.38	1.03
Pb	6.94	5.63	9.02	1.01	2.44	<i>0.66</i>	0.13	2.28	3.49	7.38
Th	0.0028	<0.02	<0.01	<0.01	0.0006	<0.01	0.0008	0.0026	0.0029	0.0025
U	<0.01	0.0067	0.0067	0.0021	0.0094	0.0037	0.0015	0.0065	0.0013	<0.01

Table 12. Average trace element data for phengites and selected trace element data for garnets by laser ablation microprobe in ppm. For explanation of bold numbers see Table 10.

	PHE							GRT				
	50-2	50-13	52-1	CHM30a	Ad25	77-5	55-3	CHM30b	50-2	50-13	52-1	77-5
Li	1.11	2.20	0.65	4.20	39	2.06		0.68	<0.6	0.10		2.41
Be	2.15	1.39	1.34	1.17	0.48	0.27	2.47	<0.13				
B	22	25	18	14.5	30	10.5	7.5	2.7				
Sr	597	417	409	601	285	49	413	0.056	0.27	0.050	0.25	
Y	0.055	0.049	0.063	0.037	<0.04		0.076	12.2	156	42	76	
Zr	0.37	0.21	0.27	0.22	0.43	0.33	0.32	2.62	5.96	3.60	1.98	
Nb	0.19	0.51	0.21	0.32	0.096	0.055	0.62	<0.01	<0.09	0.046	0.017	<0.01
Ba	2044	1313	2280	2419	1173		1666		0.077	0.072	<0.18	
Ce	<0.01	0.078	0.073	0.002			0.0076	0.10	0.047	0.019	0.052	<0.01
Nd	<0.03	0.023	<0.19	<0.03	<0.05		<0.02	0.30	<0.07	0.030	0.097	0.046
Sm	<0.04	0.011	0.20	<0.01	<0.06		0.0031	0.35	0.69	0.28	1.32	0.45
Pb	38	35	21	29	31	0.51	24	0.35	1.50	0.15	1.05	0.012
Th	<0.01	0.0029	<0.01	0.0006	<0.01	<0.01	0.0036	<0.03	<0.08	<0.02	<0.04	<0.01
U	0.030	0.0056	0.0047	0.050	0.0021	<0.01	0.014	<0.03	<0.05	0.026	0.0011	<0.19

Table 13. Average trace element data for paragonite, apatite, zoisite, clinozoisite and talc by laser ablation microprobe in ppm. For explanation of bold numbers see Table 10.

	PAR				APA				ZOI			CZO	TLC
	50-2	50-13	52-1	50-14	50-2	50-13	52-1	50-14	CHM30b	Ad25	77-5		
Li		25	2.4	7.1					<0.15				
Be		9.0	7.0	9.7					<1.0				
B		98	83	14					<5				
Sr	6428	2971	2807	2584	6938	2826	7643	2623	3316	2833	1517	1138	0.026
Y	0.057			0.021	106	63	96	88	5.8	29	21	21	<0.01
Zr	0.34	3.89	1.03	0.078									<0.01
Nb	0.052	0.10	0.10	0.016									0.0055
Ba	231			46				0.067					<0.03
Ce	0.008			0.011	187	65	189	98	40	56	30	43	0.0032
Nd	<0.2			<0.01	364	106	353	188	25	49	30	45	<0.03
Sm	0.072			0.0084	190	64	183	108	6	16	10	17	<0.03
Pb	74	119	136	17	47	45	40	11	135	148	15	7.6	0.082
Th	<0.03	<0.07	<0.06	0.00030	0.37	0.18	0.17	0.12	0.78	0.71	0.35	1.10	0.0035
U	<0.04	<0.01	<0.04	0.0041	2.25	1.09	0.47	0.75	<0.29	0.69	0.12	0.22	<0.01

4.6.2 Trace elements buffered by single phases

The most convincing case for trace element equilibrium behaviour between different phases exists if Henry's law behaviour can be demonstrated, as regularly considered in experimental trace element partitioning studies (e.g. Beattie, 1993). Here, trace element partition coefficients between two phases are independent of concentration, and different mineral pairs with different trace element enrichment levels plot on a straight line passing through the origin on a trace element distribution diagram. However, different enrichment levels in phases will not occur for a trace element that is buffered by an accessory phase in which this trace element is a major component. In all investigated Trescolmen eclogites, Ti and Zr are buffered by the accessory phases rutile and zircon. As can be seen for all phases except amphibole (Tables 10 to 13), Ti and Zr concentrations are fairly constant in each phase. The variation of Ti and Zr concentrations in amphibole can be correlated with the Al content of the tetrahedral site (Fig. 24). According to Skulski et al. (1994), both Zr and Ti can be substituted as a Tschermarks component, $\text{Ca}(\text{Zr}, \text{Ti})\text{Al}_2\text{O}_6$, in clinopyroxene. Therefore an increase in Al on the tetrahedral site in amphibole probably also facilitates the incorporation of both trace elements in the crystal structure. However, constant concentration is expected for buffered trace elements like Ti and Zr in phases where crystal chemistry does not vary with respect to relevant substitution mechanisms (i.e., no measurable Tschermarks component in eclogitic clinopyroxene), as long as PT conditions are constant and equilibrium is reached. Therefore, we have to stress that the absence of a linear trend in a distribution diagram for Ti from coexisting mineral pairs in rutile-buffered systems is not an indication of trace element disequilibrium. (for a contrary conclusion see Getty & Selverstone, 1994).

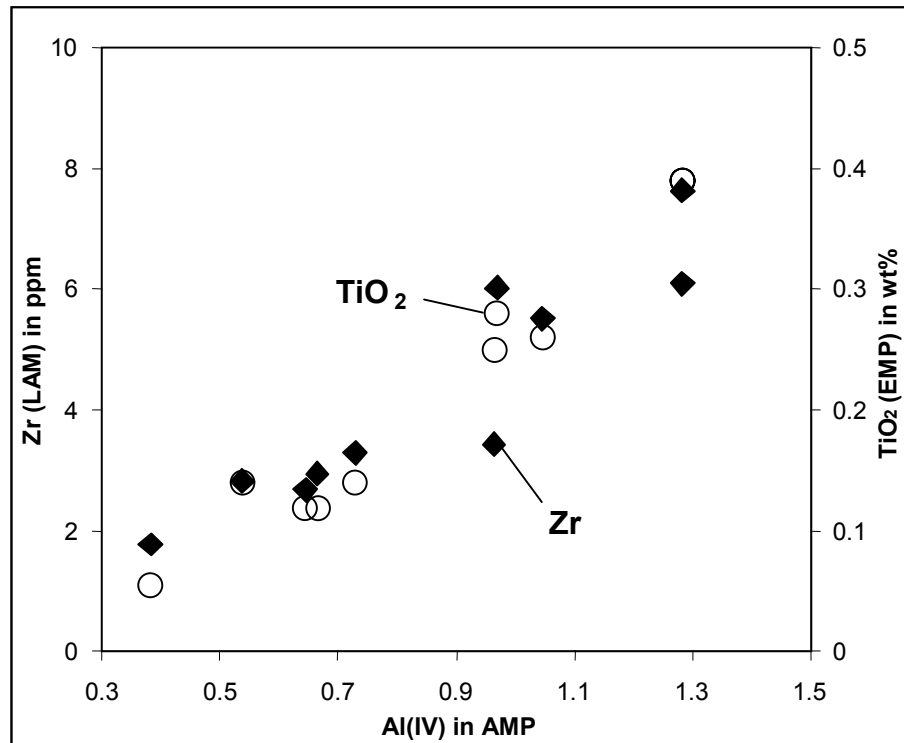


Fig. 24 Correlation of the Al(IV) component on the Zr and TiO_2 concentrations in amphibole.

4.6.3 Amphibole/clinopyroxene partitioning

Among the analyzed elements, REE (Ce, Nd, Sm), Y, Sr and Pb show the largest variation in clinopyroxenes and in amphiboles from different samples (Tables 10 and 11). Since for many analyzed samples there are sufficient good data (standard deviation <25%) for both phases, amphibole/clinopyroxene ratios for these elements are ideal to evaluate the approach towards equilibrium in our samples. We observe an excellent correlation for Sm concentrations between coexisting mineral pairs, plotted against each other in Fig. 25a. Over a concentration range of three orders of magnitude, different samples lie on a straight line passing through the origin, demonstrating similar $D^{\text{AMP/CPX}}$ partition coefficients (of ~ 1) for Sm in all samples. A characteristic of all zoisite-bearing samples (Ad25, CHM30b, 77-5) is their low Sm contents. As shown in a previous section, zoisite has a strong preference for

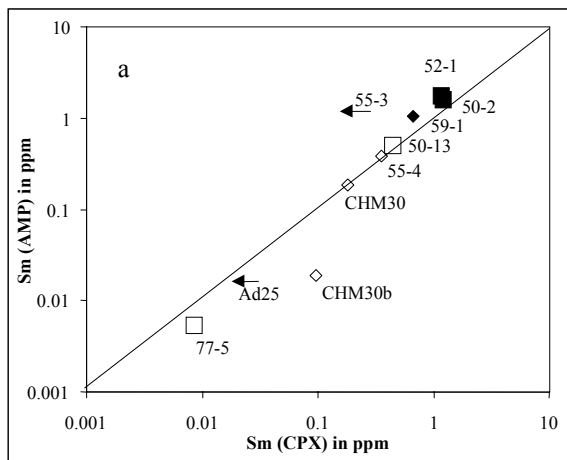
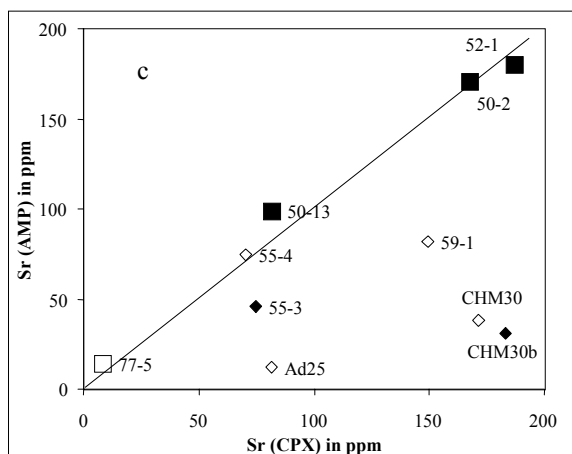
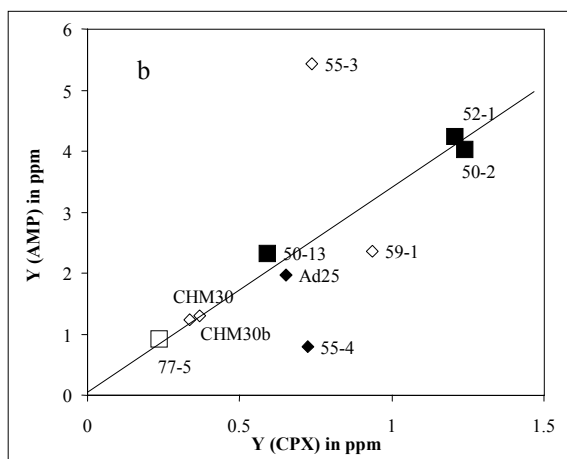


Fig. 25 Distribution diagrams for trace elements partitioned between clinopyroxene and amphibole. Quality of mineral pairs is indicated as follows: large black squares- preferred samples (foliated eclogites, homogeneous clinopyroxene major element composition), open small diamonds- remaining samples; black symbols- possible homogeneous composition of both clinopyroxene and amphibole for the trace element under consideration, open symbols- probable heterogeneous composition of at least one phase or uncertain quality of analysis. Solid lines mark average $D^{\text{Amphibole/Clinopyroxene}}$ values of our preferred samples, extrapolation of the lines to the origin demonstrate Henry's Law behaviour. Arrow in Sm(AMP) versus Sm(CPX) diagram indicates that concentration of Sm in clinopyroxene is below detection limit.



this element, so that under equilibrium conditions, samples with similar bulk trace element concentrations will have coexisting phases with different Sm concentrations depending on modal zoisite abundance. Sample 77-5 with the highest zoisite and clinozoisite abundance (together 15 modal %, Table 1), has lower Sm concentrations in both clinopyroxene and amphibole than Ad25 and CHM30b (both between 6-8 modal % zoisite). These two samples in turn have much lower Sm concentrations in clinopyroxene and amphibole than zoisite-absent samples. Since all samples have a variation in Sm whole rock concentration of only a factor of about two (1.8-4.3 ppm), we can conclude that zoisite controls the Sm concentration of both clinopyroxene and amphibole, which independently supports the observation that all three phases crystallized under eclogite-facies conditions. However, in detail CHM30b and Ad25 have disturbed partitioning behaviour for Nd and Sm. While other phases have D -values for Nd of about 0.8 and for Sm of about 1.1, both samples have $D^{\text{AMP/CPX}}$ values for Nd <0.4 and CHM30b has a D -value for Sm of 0.2 (Table 14).

With two exceptions, $D^{\text{AMP/CPX}}$ partition coefficients for yttrium are also very uniform, with a factor of ~ 4 (Fig. 25b). Only mineral pairs from 55-3 and 55-4 do not plot on the line defined by the average of the remaining partition coefficients. Although yttrium compositions of 55-4 in both clinopyroxene and amphibole passed our homogeneity test, $D^{\text{AMP/CPX}}$ is a factor of 3 lower than the average value. In contrast, Sm values for both phases in 55-4 are probably inhomogeneous (Fig. 25a), but element ratios are indistinguishable in comparison to the remaining samples. We therefore conclude that the low standard deviation of repeated measurements on a 40-100 μm scale is not a good indicator of an approach towards equilibrium, and that textural considerations and electron microprobe data on a 5 μm scale are better criteria.

$D^{\text{AMP/CPX}}$ partitioning systematics for Sr show evidence for disequilibrium processes in some of the investigated samples. Again, our preferred samples (50-2, 50-13, 52-1, 77-5) plot close to a straight line ($D \sim 1$) passing through the origin, implying a good approach towards equilibrium. All other samples, except 55-4, have lower $D^{\text{AMP/CPX}}$ ratios. Here, the zoisite-bearing samples Ad25 and CHM30b are most extreme. The partitioning behaviour of Pb follows closely that of Sr, as shown in Fig. 26. As Sr is one of the most reliable elements in LAM analyses, this correlation independently confirms the reliability of Pb data, which are prone to fractionation effects during ablation

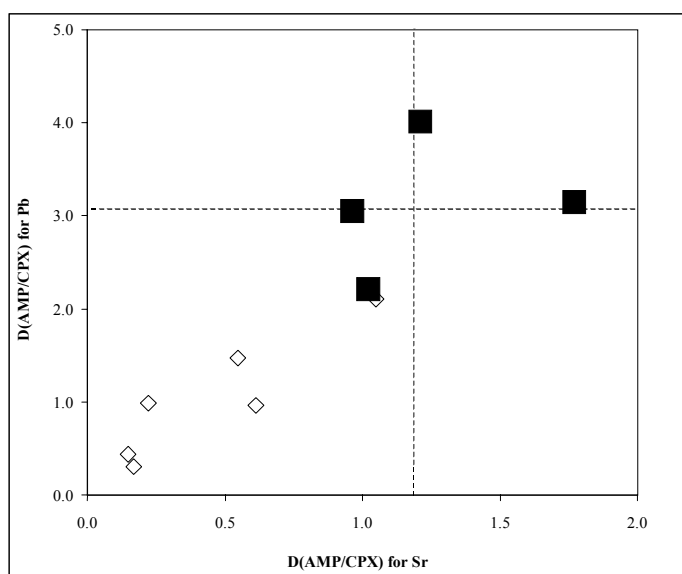


Fig. 26 Illustration of similar partitioning behaviour of Sr and Pb between coexisting amphibole/clinopyroxene pairs. Black squares- preferred samples; open diamonds- remaining samples; stippled lines- preferred $D^{\text{Amphibole/Clinopyroxene}}$ values (1.2 for Sr, 3.1 for Pb).

(Longerich et al., 1996). For the disequilibrium distributions for $D^{\text{AMP/CPX}}$ of Sr, Pb, Nd and Sm, we envisage a process whereby zoisite crystallizes with amphibole, but clinopyroxene fails to re-equilibrate with these phases. This is explored in a later section.

Crystal chemical variations can have a profound influence in trace element partitioning behaviour. We have previously shown for Trescolmen eclogites that changes in the A-site occupancy of amphibole have a strong influence on $D^{\text{PHE/AMP}}$ for Ba (Chapter 2). However, the large spread in $D^{\text{AMP/CPX}}$ for Sr cannot be explained by crystal chemical variations. Since Sr has a similar ionic radius to Ca, it is generally assumed to be accommodated in the M2 site of clinopyroxene (Blundy & Wood, 1994) and the M4 site of amphibole (LaTourrette et al., 1994). Although there is a weak positive correlation of $D^{\text{AMP/CPX}}$ for Ca and Sr, this is statistically insignificant and a wide range of amphibole/clinopyroxene ratios for Ca can be found in our preferred samples (0.53-0.66), which otherwise have almost identical $D^{\text{AMP/CPX}}$ for Sr. A possible explanation for the reduced role of crystal chemical variation in trace element partitioning behaviour between amphibole and clinopyroxene in this study is the strong correlation of the major element chemistry of both phases, as shown by correlations among jadeite *versus* edenite content and Mg# (Heinrich, 1986).

An interesting feature in the $D^{\text{AMP/CPX}}$ data is the similar trace element partitioning behaviour in samples CHM30a and CHM30b (Table 10 and 11, Fig. 25b and 25c). They comprise phengite- and zoisite-rich domains, respectively, from the same block <40 cm apart. Even if we assume strong Sr disequilibrium behaviour related to zoisite formation, the process must have been similar on a dm scale, which is additional evidence for the presence of an interconnecting fluid phase during eclogite facies re-equilibration. Nevertheless, in detail amphibole is more strongly depleted in Ce, Sm and Nd in the zoisite-rich domain (CHM30b).

Other trace elements show only a limited variation between different samples in a given phase, so that constant partition coefficients cannot be demonstrated by concomitant increases in trace element concentrations in mineral pairs from different samples. However, consistency in partition coefficients of the remaining analyzed trace elements can be evaluated from Table 14. Of the 14 trace elements chosen for this study, 9 elements have standard errors for average $D^{\text{AMP/CPX}}$ values between 9 and 23%. A high degree of confidence exists for the partition coefficients for Li, Be, B, Y, Nd and Sm, which are always based on at least 5 mineral pairs. It is encouraging to note that partition coefficients derived from the whole data set (total average) are very similar to the values derived from the subset of our preferred samples (preferred average). The range of partition coefficients for Zr, Sr and Pb has already been discussed, so that the spread of $D^{\text{AMP/CPX}}$ for Zr is mostly a function of the crystal chemistry of amphibole (tetrahedral Al varies strongly in amphibole, but is almost non-existent in all clinopyroxenes), whereas for Sr and Pb the bias between total average values and preferred values is attributed to the incorporation of disequilibrium samples in the former value.

Partition coefficients for Nb, Ba, Ce, Th and U are more uncertain since concentrations are extremely low (mostly <100 ppb) in either one (e.g. Ba in clinopyroxene) or both phases. In these cases standard deviations for single analyses are very high and contamination cannot be totally excluded. Our preferred samples are subject to the same problems, so we recommend the use of the total averages of the partition coefficients since they represent a larger data set with better absolute counting statistics. These values are the best estimate until future studies can incorporate data with standard deviations <25% at the 1-100 ppb concentration level.

Table 14 Amphibole/clinopyroxene partitioning coefficients.

	Li	Be	B	Sr	Y	Zr	Nb	Ba	Ce	Nd	Sm	Pb	Th	U
50-2	0.090	2.2	2.8	1.02	3.5	2.5	10.5	112	0.27	0.68	1.5	2.2		
50-13	0.039	1.3	3.4	1.21	3.9	2.7	11.4	1022	0.50	0.43	1.2	4.0		1.2
52-1	0.092	1.9	2.5	0.96	3.3	2.4		228	0.39	0.61	1.3	3.0		1.8
77-5	0.022	1.4	2.3	1.77	3.9	1.9	3.6	753			0.6	3.2	0.22	2.7
CHM30b	0.038	0.8	2.5	0.17	3.6	1.4		187	0.18		0.2	0.3		0.71
CHM30	0.046	0.5	1.5	0.22	3.7	1.1		649	0.67	0.67	1.0	1.0	0.39	7.7
55-4				1.05	1.1	0.6	1.0		1.6	1.2	1.1	2.1	4.1	0.08
Ad25		1.0	2.1	0.15	3.0	1.6		22	1.9			0.4		0.53
55-3		1.2		0.61	7.4	1.5	2.1	14				1.0	0.13	0.15
59-1				0.55	2.5	1.6	1.1	81	0.68	1.0	1.5	1.5		
average	0.055	1.3	2.5	0.77	3.6	1.7	5.0	341	0.78	0.78	1.1	1.9	1.2	1.9
std. error	22	15	9	22	14	12	39	36	29	16	15	21	80	48
pref. ave.	0.061	1.7	2.8	1.2	3.7	2.4	8.5	529	0.39	0.57	1.2	3.1	0.22	1.9

Average- average based on all samples; std. error- standard error (standard deviation divided by number of analyses); pref. ave.- preferred average, based on samples 50-2, 50-13, 52-1 and 77-5.

4.6.4 Zoisite/clinopyroxene partitioning

$D^{\text{ZOI/CPX}}$ values in the three zoisite-eclogites scatter widely from sample to sample (Table 15), with differences for most elements of more than one order of magnitude. This clearly shows that trace element equilibration between zoisite and clinopyroxene was approached to different degrees in the analyzed samples. $D^{\text{ZOI/CPX}}$ values derived from sample 77-5 are considered to most likely represent equilibrium conditions, since strong disequilibrium for the other two zoisite-bearing samples (Ad25, CHM30b) have been demonstrated in the amphibole/clinopyroxene section. However, zoisite/clinopyroxene ratios from 77-5 are subject to a significant degree of uncertainty, since, because of its equilibration with zoisite, trace element concentrations in clinopyroxene are extremely low. This seems to affect especially $D^{\text{ZOI/CPX}}$ values for Ce, whereas in the other two samples partition coefficients decrease steadily in the order Ce>Nd>Sm>Y. Contamination affecting the Ce value of the clinopyroxenes from 77-5 cannot be excluded, so that the $D^{\text{ZOI/CPX}}$ value for Ce in 77-5 must be considered as a minimum value and it is expected that the real value is higher than that for Nd.

With the partition data from 77-5 taken as reference values, the zoning pattern of zoisites from CHM30b can be examined. The $D^{\text{ZOI/CPX}}$ values of Table 15 are all based on zoisite inner rim compositions, for reasons outlined above. However, if Sr core compositions are used (12200 instead of 3300 ppm, see Fig. 20d), $D_{\text{Sr}}^{\text{ZOI/CPX}}$ values for CHM30b increase from 18 to 66, which is significantly closer to the value of 186 derived from 77-5. Nevertheless, zoisites in equilibrium with clinopyroxenes from CHM30b should have Sr concentrations of 34000 ppm. This is probably outside the concentration level for Henry's law behaviour, so that constant D-values can no longer be applied (Beattie, 1993).

The coexistence of zoisite and clinozoisite in 77-5 makes it possible to also derive trace element partition coefficients for clinozoisite. In general, concentrations in both phases are very similar (Table 13). For most trace elements, zoisite/clinozoisite ratios range by less than a factor of 2. Only Th and U are significantly more enriched in clinozoisite in relation to zoisite ($D^{ZOI/CZO}$ of 0.32 and 0.5 respectively). As a first order approximation, clinozoisite partitioning behaviour can therefore be modelled together with zoisite.

Table 15 Zoisite/clinopyroxene partition coefficients.

	Sr	Y	Ce	Nd	Sm	Pb	Th	U
77-5	186	88	1746	8510	1234	369	102	214
CHM30b	18	16	870	242	65	40	1111	
Ad25	35	45	3797	448		99	363	99

Bold numbers represent our preferred values, except for Ce which is probably too low. See text for discussion.

4.6.5 Mineral/clinopyroxene partitioning of other hydrous phases

4.6.5.1 Phengite

Extensive trace element data were also collected for phengite. For most trace elements, $D^{PHE/CPX}$ values are based on 6 or 7 mineral pairs. As can be seen in Table 16, average $D^{PHE/CPX}$ values tend to give the same results as the subset from our preferred samples. For U however, along with Nb, Ba, REE and Th, large uncertainties exist due to extremely low concentrations either in clinopyroxene (Nb, Ba), phengite (REE) or both phases (Th, U). With the exception of Li, the remaining elements give consistent results, with standard errors between 5 and 21%. An interesting finding is the similarity of $D^{PHE/CPX}$ values for Sr and Pb in the zoisite-bearing samples Ad25 and

Table 16 Phengite/clinopyroxene partition coefficients.

	Li	Be	B	Sr	Y	Zr	Nb	Ba	Ce	Nd	Sm	Pb	Th	U
50-2	0.040	0.83	5.4	3.6	0.046	0.15	42	48000				12		4.5
50-13	0.088	0.55	9.4	5.1	0.083	0.11	53	370000	0.28	0.038	0.026	25	0.28	1.0
52-1	0.040	0.71	4.9	2.2	0.051	0.11		99000	0.16		0.16	7.1		1.2
77-5	0.032	0.24	2.1	6.0		0.08	7.9					13		
CHM30	0.14	0.49	3.8	3.5	0.11	0.10		380000	0.036			12	0.36	41
Ad25	0.94	0.44	6.1	3.5		0.20		15000				21		0.31
55-3		1.4		5.5	0.10	0.17	41	23000				10	0.18	0.32
average	0.21	0.66	5.3	4.2	0.079	0.13	36	160000	0.16	0.038	0.10	14	0.27	8
std. error	69	21	19	12	17	13	27	45	44		73	17	19	82
pref. ave.	0.050	0.58	5.4	4.2	0.060	0.11	34	170000	0.22	0.038	0.10	14	0.28	2.3

For abbreviations see Table 14.

CHM30a compared with the values from our preferred samples. For Ad25 and CHM30a, this implies a close approach towards equilibrium between phengite and clinopyroxene, which in turn has the consequence that phengite cannot be in equilibrium with zoisite and amphibole, as these phases have been shown to be in disequilibrium with clinopyroxene.

4.6.5.2 Paragonite and apatite

LAM measurements of paragonite and apatite were performed in four samples for a limited range of trace elements (Tables 17 and 18). In our preferred samples (50-2, 50-13, 52-1), trace element partitioning between paragonite and clinopyroxene as well as between apatite and clinopyroxene suggests a close approach to equilibrium, as indicated by similar paragonite/clinopyroxene and apatite/clinopyroxene values, respectively, between the different samples. Large discrepancies occur only for Li partitioning between paragonite and clinopyroxene. However, partition coefficients in the second choice sample, 50-14, are significantly different for $D^{\text{PAR/CPX}}$ for B and $D^{\text{APA/CPX}}$ for REE (Ce, Sm, Nd) with respect to our preferred samples. Nonetheless, trends in REE partitioning behaviour can be observed in all samples, with a systematic decrease in $D^{\text{APA/CPX}}$ in the order Ce>Nd>Sm>Y. At this stage we cannot evaluate if discrepancies in sample 50-14 compared to our preferred values are caused by disequilibrium processes or by the unusually high jadeite content in clinopyroxene. The latter could militate against the incorporation of REE on the M2 site and therefore increase $D^{\text{APA/CPX}}$ for REE, whereas disequilibrium is indicated by the presence of kyanite relics in paragonite, which indicate that the paragonite grew after the main eclogite-facies mineralogy (Chapter 2).

Table 17 Paragonite/clinopyroxene partition coefficients.

	Li	Be	B	Sr	Y	Zr	Nb	Ba	Ce	Sm	Pb	Th	U
50-2				38	0.047	0.14	11	5419	0.010	0.063	24		
50-13	1.0	3.6	36	36		1.9	10				85		
52-1	0.15	3.7	23	15		0.41					46		
50-14	0.18	2.4	2.8	46	0.024	0.042	2.5		0.12	0.024	26	0.14	0.69
average	0.44	3.2	21	34	0.036	0.63	8.1	5419	0.064	0.044	45	0.14	0.69
std. error	63	13	47	20	33	70	35		85	44	32		

For abbreviations see Table 14.

Table 18 Apatite/clinopyroxene partition coefficients.

	Sr	Y	Ce	Nd	Sm	Pb	Th	U
50-2	41	88	227	215	164	15		332
50-13	35	107	230	173	145	32	17	200
52-1	41	77	412	274	152	13	18	125
50-14	47	101	1031	608	313	16	57	127
average	41	93	475	318	194	19	31	196
std. error	6	7	40	31	21	23	43	25

For abbreviations see Table 14.

4.6.5.3 Talc

Trace element concentrations of talc have been analyzed in one sample (55-4, Table 13). For all measured elements, concentrations were extremely low (<100 ppb) and commonly below the calculated detection limits. Partition coefficients between talc and clinopyroxene have not been tabulated since partition coefficients between amphibole and clinopyroxene in 55-4 commonly deviate from our preferred values (see above). However, $D^{\text{TLC/CPX}}$ values from sample 55-4 suggest talc cannot incorporate a large range of incompatible elements.

4.7 Mechanisms of trace element equilibration

4.7.1 Equilibration processes

A subset of our sample suite (50-2, 50-13, 52-1 and 77-5), carefully chosen through a combination of textural criteria, high resolution backscattered observation and electron microprobe major element measurements, gives consistent trace element partitioning values for a range of elements at different concentration levels that we interpret as a strong argument for close attainment of equilibrium. The most important characteristic of these samples is a preferred orientation of all eclogite-facies phases. We can therefore support the observation of Messiga et al. (1995) that synmetamorphic plastic deformation enhances trace element equilibration processes. Messiga et al. favoured a process of higher surface reaction exchange rates due to the continuous production of crystal defects and dislocations during plastic deformation.

The presence of a free fluid phase along grain boundaries is expected to be a prerequisite for attaining equilibration (Jamtveit et al., 1990; Dipple & Ferry, 1992), but from our studies we can infer that it does not enhance equilibration processes as efficiently as plastic deformation. We have shown in a companion study that Cs-Rb-Ba systematics in phengite and amphibole from Trescolmen eclogites indicate at least metre-scale fluid mobility during eclogite-facies conditions (Chapter 2). These patterns are observed in both deformed and undeformed eclogites, e.g. also in 59-1. Since a free fluid phase was present in both foliated and unfoliated eclogites, but attainment of equilibrium was more pronounced in the deformed ones, the controlling process was more likely the deformation rate rather than the presence of a free fluid. However, the interaction between deformation and fluid infiltration is very complex and examples of both fluid induced deformation (Boundy et al., 1992; Erambert & Austrheim, 1993; Pennacchioni, 1996) as well as deformation enhancing fluid infiltration (Holness & Graham, 1995; Holness, 1997) have been reported.

4.7.2 Reasons for lack of trace element equilibration

The gabbroic samples CHM30a and CHM30b afford insight into processes operating under eclogite facies conditions that lead to disequilibrium features. In both samples, Sr has partition coefficients between some phases significantly different to those in well equilibrated eclogites, specifically for amphibole/clinopyroxene partitioning

(0.17 instead of 1.2) and of zoisite rim/clinopyroxene partitioning (18 instead of 190). In contrast, Sr partitioning for phengite/clinopyroxene (in CHM30a) and zoisite rim/amphibole pairs (in CHM30b) gives surprisingly similar ratios compared to our preferred samples (3.5 instead of 4.2 and 107 instead of 108, respectively). One explanation might be found in the crystallization sequence in CHM30a and CHM30b. In this scenario, phengite and clinopyroxene crystallized concurrently, followed later by crystallization of zoisite and amphibole. This is in accord with the PT path for Trescolmen (Fig. 3), where at the peak pressure condition (2.4 GPa) phengite can still be a stable phase together with clinopyroxene (Schmidt & Poli, 1998). Zoisite and amphibole crystallized later during fluid infiltration at the Trescolmen phase, still at high pressure conditions (2.0 GPa). If an origin of all chemical components for zoisite and amphibole from an outside fluid is excluded, this process requires chemical exchange with the other high pressure phases such as clinopyroxene and garnet. Clinopyroxenes in equilibrium with zoisite rims and amphibole in CHM30a and CHM30b would have only 30-40 ppm Sr. However, such low-Sr clinopyroxenes might well exist since we have only analyzed the largest clinopyroxenes (>40 μm). In this example, major element homogeneity in clinopyroxene (both small and large clinopyroxenes have been analyzed) might not exclude heterogeneity for certain trace elements.

Trace element heterogeneities were not obliterated by deformation in the metagabbroic samples, in contrast to the situation in foliated metabasaltic eclogites where continued element exchange and recrystallization apparently operated. In general, a close approach to equilibrium for the investigated trace elements was often not reached in metagabbroic samples (CHM30a, CHM30b, Ad25, 59-1). This is correlated with the lack of penetrative deformation in these samples. The only exception is a gabbroic sample with a pronounced foliation defined by clinopyroxene and amphibole (Ad25), which nonetheless displays a strong heterogeneity both at major and trace element levels. In this respect, it is of particular interest that studies concerning fluid mobility in eclogite facies rocks have commonly been conducted on metagabbroic and undeformed metabasaltic samples. The small scale inhomogeneities, as observed for fluid inclusion and oxygen systematics in metagabbroic eclogites from west Alpine ophiolites (Philipot & Selverstone, 1991; Barnicoat & Cartwright, 1997), point to fluid immobility, as suggested by the authors. Therefore, studies aiming at understanding fluid processes in deformed sections of the basaltic layer of the subducting oceanic crust, the site of the highest enrichment of fluids and mobile trace elements due to hydrothermal alteration (Staudigel et al., 1996), must be performed. Only few studies have focused on fluid processes in metabasaltic eclogites (Barnicoat & Cartwright, 1995; Cartwright & Barnicoat, 1999), mostly where little deformation occurred under high pressure conditions in the investigated rocks (pillow structures were still preserved), so it is not surprising that no evidence of fluid mobility has yet been documented in metabasaltic eclogites. Considerable shear stresses might exist at the slab-mantle interface in subducting slabs (Yuen et al., 1977), so that plastic deformation in the basaltic layer of the subducting oceanic crust can be expected. Natural examples of deformed metabasaltic eclogites, such as samples 50-2, 50-13, 52-1 and 77-5 from Trescolmen, therefore permit a better insight into the scale of fluid mobility in subducting crust and this study suggests that they provide evidence for a close approach to trace element equilibrium under these conditions.

4.8 Concluding remarks

The partition coefficients from this study between eclogite facies hydrous phases (amphibole, zoisite/ clinozoisite, phengite, paragonite, apatite) and clinopyroxene for a large suite of trace elements are intended to form a framework for further modelling of the trace element composition of fluids liberated from dehydrating slabs. Despite the problems that arise in the trace element analysis of metamorphic phases, we have demonstrated that reliable data can be extracted with a careful selection of assemblages (dynamically recrystallized metabasalts) and detailed pre-investigation with the electron microprobe (back scattered electron imaging, quantitative major element analysis). The results of our study imply a dominant role of penetrative plastic deformation for the attainment of trace element equilibration between the eclogite facies phases, reinforcing the suggestion that dynamic recrystallization enhances reaction rates, both at the surface and within crystals. Deformation is either facilitated by fluid infiltration or has promoted fluid mobility; in both cases a free fluid phase is required as an agent to transfer the trace element between the phases. Back scattered electron imaging has revealed a rich microtextural inventory in the investigated samples, e.g. several generations of clinopyroxene, annealed cracks in garnet, complex zoning pattern in zoisite. These examples clearly show that attempts to derive partition coefficients between coexisting phases by measuring rim-rim compositions adjacent to apparently fresh grain boundaries cannot be considered reliable data unless microtextural information is included.

Mass balance calculations reveal that zoisite, allanite, phengite and paragonite are important carriers for trace elements in eclogite facies systems. From these phases, zoisite and phengite are of special importance since they are probably widespread minor phases in subducting oceanic crust underneath volcanic arcs (Schmidt & Poli, 1998). In the presence of zoisite, the element budget of Sr, Pb, LREE, Th and U is dominated by this phase, whereas phengite is the most important carrier for Ba (and Rb, Cs; Chapter 2) and an important carrier for B, Sr and Pb. Therefore it is essential to include $D^{\text{Zoisite/Fluid}}$ and $D^{\text{Phengite/Fluid}}$ values for modelling concentrations of these trace elements in fluids liberated from dehydrating oceanic crust. Caution regarding the lack of partition coefficients for many hydrous phases has already been raised by Brenan et al. (1995a) in their models including only clinopyroxene, garnet and amphibole partition coefficients. Our mass balance calculations have shown that amphibole, clinopyroxene and garnet are insignificant carriers for LREE, Ba, Th and U in eclogite-facies metabasalts (<5% of the trace element mass budget). In contrast, dehydration modelling based only on $D^{\text{Clinopyroxene/Fluid}}$ and $D^{\text{Garnet/Fluid}}$ values (Brenan et al., 1998) for the elements Li and Be correctly incorporate the most important phases in our eclogite samples (>80% of the trace element mass budget) and are also a good approximation for B.

A major obstacle in combining our $D^{\text{Min/Clinopyroxene}}$ values with experimental $D^{\text{Clinopyroxene/Fluid}}$ values are the different chemical compositions of clinopyroxenes and PT conditions from the different data sets. Our samples are jadeite-rich (25-55 mol% Jd) and have re-equilibrated at ca. 650°C/2.0 GPa whereas experimental clinopyroxenes are diopside-rich (<10 mol% Jd) and crystallized at $\geq 900^\circ\text{C}/\geq 2.0$ GPa (Brenan et al., 1995a, 1995b, 1998; Stalder et al., 1998). We can expect that extrapolation from experiments (diopsidic clinopyroxene, 900°C/2.0 GPa) to our Trescolmen samples (omphacitic clinopyroxenes, 650°C/2.0 GPa) will require adjustment of experimentally determined $D^{\text{Clinopyroxene/Fluid}}$ values by applying correction factors of up to more than several orders of magnitude (for variations in D-values due to T effects, e.g. see Brenan et al., 1994)

Conditions as experienced by Trescolmen eclogites are similar, but not identical to typical subducting oceanic crust underneath volcanic arcs. The largest difference to subducting slabs underneath the volcanic front are lower P at about the same T conditions that result in some important differences in mineral parageneses. While phengite, clinopyroxene and garnet are still stable phases under increased pressure conditions, paragonite and amphibole are no longer stable and zoisite is replaced by lawsonite (Schmidt & Poli, 1998). Trace element partitioning data from lawsonite-bearing assemblages are almost completely missing. In order to complement the partition coefficient data set from this study and to enable calculation of complete dehydration models of subducting oceanic crust, further studies on the trace element incorporation of allanite, zircon and lawsonite in eclogite and blueschist facies rocks are highly desirable.

Chapter 5. References

- Armstrong, J. T., 1991. Quantitative elemental analysis of individual microparticles with electron beam instruments. In: Heinrich, K. F. J., Newbury, D. E. (Eds.), *Electron probe quantification*. Plenum Press, New York, pp. 261-315.
- Ayers, J. C., Watson, E. B., 1993. Apatite/fluid partitioning of rare-earth elements and strontium: Experimental results at 1.0 GPa and 1000°C and application to models of fluid-rock interaction. *Chem. Geol.* 110, 299-314.
- Ayers, J. C., Dittmer, S. K., Layne, G. D., 1997. Partitioning of elements between peridotite and H₂O at 2.0-3.0 GPa and 900-1100°C, and application to models of subduction zone processes. *Earth Planet. Sci. Lett.* 150, 381-398.
- Banner, J. L., Hanson G. N. (1990) Calculation of simultaneous isotopic and trace element variations during water-rock interaction with applications to carbonate diagenesis. *Geochim. Cosmochim. Acta* 54, 3123-3137.
- Barnicoat, A. C., Cartwright, I., 1995. Focused fluid flow during subduction: Oxygen isotope data from high-pressure ophiolites of the Western Alps. *Earth Planet. Sci. Lett.* 132, 53-61.
- Barnicoat, A. C., Cartwright, I., 1997. The gabbro-eclogite transformation: An oxygen isotope and petrographic study of west Alpine ophiolites. *J. Metamorphic Geol.* 15, 93-104.
- Baumgartner, L. P., Rumble, D. (1988) Transport of stable isotopes. I. Development of a kinetic continuum theory for stable isotope transport. *Contrib. Mineral. Petrol.* 98, 417-430.
- Beattie, P., 1993. On the occurrence of apparent non-Henry's Law behaviour in experimental partitioning studies. *Geochim. Cosmochim. Acta* 57, 47-55.
- Beattie, P., 1994. Systematics and energetics of trace-element partitioning between olivine and silicate melts: Implications for the nature of mineral/melt partitioning. *Chem. Geol.* 117, 57-71.
- Bebout, G. E. (1991) Field-based evidence for devolatilization in subduction zones: Implications for arc magmatism. *Science* 251, 413-416.
- Bebout, G. E., Barton, M. D. (1989) Fluid flow and metasomatism in a subduction zone hydrothermal system: Catalina Schist terrane, California. *Geology* 17, 976-980.
- Becker, J. S., Seifert, G., Saprykin, A., Dietze, H.-J., 1996. Mass spectrometric and theoretical investigations into the formation of argon molecular ions in plasma mass spectrometry. *J. Anal. Atom. Spectrom.* 11, 643-648.
- Ben Othman, D., White, W. M., Patchett J. (1989) The geochemistry of marine sediments, island arc magma genesis, and crust-mantle recycling. *Earth Planet. Sci. Lett.* 94, 1-21.
- Berger, G., Schott, J., Guy, C. (1988) Behaviour of Li, Rb and Cs during basalt glass and olivine dissolution and chlorite, smectite and zeolite precipitation from seawater: Experimental investigations and modelization between 50° and 300°. *Chem. Geol.* 71, 297-312.
- Berman, R. G. (1990) Mixing properties of Ca-Mg-Fe garnets. *Am. Mineral.* 75, 328-344.
- Beswick, A. E., 1973. An experimental study of alkali metal distributions in feldspars and micas. *Geochim. Cosmochim. Acta* 37, 183-208.
- Bickle, M. J., McKenzie, D. (1987) The transport of heat and matter by fluids during metamorphism. *Contrib. Mineral. Petrol.* 95, 384-392.
- Blundy, J., Wood, B., 1994. Prediction of crystal-melt partition coefficients from elastic moduli. *Nature* 372, 452-454.

- Bohlen, S. R., Liotta, J. J., 1986. A barometer for garnet amphibolites and garnet granulites. *J. Petrol.* 27, 1025-1034.
- Boundy, T. M., Fountain, D. M., Austrheim, H., 1992. Structural development and petrofabrics of eclogite facies shear zones, Bergen Arcs, western Norway: Implications for deep crustal deformational processes. *J. Metamorphic Geol.* 10, 127-146.
- Brenan, J. M., Ryerson, F. J., Shaw, H. F., 1998. The role of aqueous fluids in the slab-to-mantle transfer of boron, beryllium, and lithium during subduction: Experiments and models. *Geochim. Cosmochim. Acta* 62, 3337-3347.
- Brenan, J. M., Shaw, H. F., Phinney, D. L., Ryerson, F. J., 1994. Rutile-aqueous fluid partitioning of Nb, Ta, H, Zr, U and Th: Implications for high field strength element depletions in island-arc basalts. *Earth Planet. Sci. Lett.* 128, 327-339.
- Brenan, J. M., Shaw, H. F., Ryerson, F. J., Phinney, D. L., 1995a. Mineral-aqueous fluid partitioning of trace elements at 900°C and 2.0 GPa: Constraints on the trace element chemistry of mantle and deep crustal fluids. *Geochim. Cosmochim. Acta* 59, 3331-3350.
- Brenan, J. M., Shaw, H. F., Ryerson, F. J., 1995b. Experimental evidence for the origin of lead enrichment in convergent-margin magmas. *Nature* 389, 54-56.
- Briqueu, L., Bougault, H. and Joron, J. L., 1984. Quantification of Nb, Ta, Ti and V anomalies in magmas associated with subduction zones: Petrogenetic implications. *Earth Planet. Sci. Lett.* 68, 297-308.
- Brumm, R. C., Foley, S. F., Tiepolo, M., Vannucci, R. (1998) Trace element distribution between richteritic amphiboles and silicate melts, and contrasts to their behaviour in calcic amphiboles. *Mineral. Mag.* 62A, 250-251.
- Buatier, M., Roermund, H. L. M. v., Drury, M. R., Lardeaux, J. M., 1991. Deformation and recrystallization mechanism in naturally deformed omphacites from the Sesia-Lanzo zone; geophysical consequences. *Tectonophysics* 195, 11-27.
- Cartwright, I., Barnicoat, A. C., 1999. Stable isotope geochemistry of Alpine ophiolites: A window to ocean-floor hydrothermal alteration and constraints on fluid-rock interaction during high-pressure metamorphism. *Int. J. Earth Sci.* 88, 219-235.
- Clague, D. A., Frey, F. A., Thompson, G., Rindge, S., 1981. Minor and trace element geochemistry of volcanic rocks dredged from the Galapagos spreading center: Role of crystal fractionation and mantle heterogeneity. *J. Geophys. Res.* 86, 9469-9482.
- Creaser, R. A., Heaman, L. M., Erdmer, P., 1997. Timing of high-pressure metamorphism in the Yukon-Tanana terrane, Canadian Cordillera: Constraints from U-Pb zircon dating of eclogite from the Teslin tectonic zone. *Can. J. Earth Sci.* 34, 709-715.
- Davies, J. H., Stevenson, D. J. (1992) Physical model of source region of subduction zone volcanics. *J. Geophys. Res.* 97, 2037-2070.
- Deer, W. A., Howie, R. A., Zussmann, J., 1992. An introduction to rock-forming minerals. Longmans Scientific & Technical. 696 pp.
- Dipple, G. M., Ferry, J. M., 1992. Metasomatism and fluid flow in ductile fault zones. *Contrib. Mineral. Petrol.* 112, 149-164.
- Domanik, K. J., Hervig, R. L., Peacock, S. M., 1993. Beryllium and boron in subduction zone minerals: An ion microprobe study. *Geochim. Cosmochim. Acta* 57, 4997-5010.

- Eggins, S. M., Woodhead, J. D., Kinsley, L. P. J., Mortimer, G. E., Sylvester, P., McCulloch, M. T., Hergt, J. M., Handler, M. R., 1997. A simple method for precise determination of ≥ 40 trace elements in geological samples by ICPMS using enriched isotope internal standardisation. *Chem. Geol.* 134, 311-326.
- Erambert, M., Austrheim, H., 1993. The effect of fluid and deformation on zoning and inclusion patterns in poly-metamorphic garnets. *Contrib. Mineral. Petrol.* 115, 204-214.
- Ernst, W. G., Liu, J., 1998. Experimental phase-equilibrium study of Al- and Ti-contents of calcic amphibole in MORB- A semiquantitative thermobarometer. *Am. Mineral.* 83, 952-969.
- Ferry, J. M., Gerdes, M. L. (1998) Chemically reactive fluid flow during metamorphism. *Ann. Rev. Earth Planet. Sci.* 26, 255-287.
- Fett, A., 1995. Elementverteilung zwischen Granat, Klinopyroxen und Rutil in Eklogiten- Experiment und Natur. Ph.D. dissertation, Universität Mainz.
- Fialin, M., Outrequin, M., Staub, P.-F., 1997. A new tool to treat overlaps in electron-probe microanalysis of rare-earth elements L-series X-rays. *Eur. J. Mineral.* 9, 965-968.
- Fialin, M., Remy, H., Richard, C., Wagner, C., 1999. Trace element analysis with the electron microprobe: New data and perspectives. *Am. Mineral.* 84, 70-77.
- Fitton, J. G., 1995. Coupled molybdenum and niobium depletion in continental basalts. *Earth Planet. Sci. Lett.* 136, 715-721.
- Foley, S. F., Jackson, S. E., Fryer, B. J., Greenough, J. D., Jenner, G. A. (1996) Trace element partition coefficients for clinopyroxene and phlogopite in an alkaline lamprophyre from Newfoundland by LAM-ICP-MS. *Geochim. Cosmochim. Acta* 60, 629-638.
- Force, E. R., 1980. The provenance of rutile. *J. Sediment. Petrol.* 50, 485-488.
- Franz, G., Selverstone, J., 1992. An empirical phase diagram for the clinozoisite-zoisite transformation in the system $\text{Ca}_2\text{Al}_3\text{Si}_3\text{O}_{12}(\text{OH})\text{-Ca}_2\text{Al}_2\text{Fe}^{3+}\text{Si}_3\text{O}_{12}(\text{OH})$. *Am. Mineral.* 77, 631-642.
- Froitzheim, N., Schmid, S. M., Frey, M., 1996. Mesozoic paleogeography and the timing of eclogite-facies metamorphism in the alps: A working hypothesis. *Eclogae geol. Helv.* 89, 81-110.
- Fryer, B. J., Jackson, S. E., Longrich, H. P., 1995. The design, operation and role of laser ablation microprobe coupled with an inductively coupled plasma-mass spectrometer (LAM-ICP-MS) in the Earth sciences. *Can. Mineral.* 33, 303-312.
- Getty, S. R., Selverstone, J., 1994. Stable isotopic and trace element evidence for restricted fluid migration in 2 GPa eclogites. *J. Metamorphic Geol.* 12, 747-760.
- Godard, G., Roermund, H. L. M. v., 1995. Deformation-induced clinopyroxene fabrics from eclogites. *J. Struct. Geol.* 17, 1425-1443.
- Graham, C. M., 1976. Petrochemistry and tectonic significance of Dalradian metabasaltic rocks of the SW Scottish Highlands. *J. Geol. Soc., London* 132, 61-84.
- Green, T. H., 1995. Significance of Nb/Ta as an indicator of geochemical processes in the crust-mantle system. *Chem. Geol.* 120, 347-359.
- Green, T. H., Pearson, N. J., 1987. An experimental study of Nb and Ta partitioning between Ti-rich minerals and silicate melts at high pressure and temperature. *Geochim. Cosmochim. Acta* 51, 55-62.
- Guidotti, C. V., Sassi, F. P., 1998. Miscellaneous isomorphous substitutions in Na-K white micas: A review, with special emphasis to metamorphic micas. *Rend. Lin., Sci. Fis. Nat.* 9, 57-78.
- Haggerty, S. E., 1991. Oxide mineralogy of the upper mantle. In: Lindsley, D.H. (Ed), *Oxide minerals: Petrological and and magnetic significance. Reviews in Mineralogy* 25, 355-416.

- Heinrich, C. A., 1982. Kyanite-eclogite to amphibolite facies evolution of hydrous mafic and pelitic rocks, Adula nappe, Central Alps. *Contrib. Mineral. Petrol.* 81, 30-38.
- Heinrich, C. A. (1983) Die regionale Hochdruckmetamorphose der Aduladecke, Zentralalpen, Schweiz. Ph.D., ETH Zürich.
- Heinrich, C. A., 1986. Eclogite facies regional metamorphism of hydrous mafic rocks in the Central Alpine Adula Nappe. *J. Petrol.* 27, 123-154.
- Hickmott, D. D., Shimizu, N., 1990. Trace element zoning in garnet from the Kwoiek Area, British Columbia: Disequilibrium partitioning during garnet growth. *Contrib. Mineral. Petrol.* 104, 619-630.
- Hickmott, D. D., Sorensen, S. S. & Rogers, P. S. Z., 1992. Metasomatism in a subduction complex: Constraints from microanalysis of trace elements in minerals from garnet amphibolite from the Catalina Schist. *Geology* 20, 347-350.
- Hofmann, A. W., White, W. M., 1983. Ba, Rb and Cs in the earth's mantle. *Z. Naturforsch.* 38a, 256-266.
- Holness, M. B., 1997. Fluid flow paths and mechanisms of fluid infiltration in carbonates during contact metamorphism: The Beinn an Dubhaich aureole, Skye. *J. Metamorphic Geol.* 15, 59-70.
- Holness, M. B., Graham, C. M., 1995. P-T-X effects on equilibrium carbonate-H₂O-CO₂-NaCl dihedral angles: Constraints on carbonate permeability and the role of deformation during fluid infiltration. *Contrib. Mineral. Petrol.* 119, 301-313.
- Horn, I., Hinton, R. W., Jackson, S. E., Longerich, H. P., 1997. Ultra-trace element analysis of NIST SRM 616 using laser ablation microprobe-inductively coupled plasma-mass spectrometry (LAM-ICP-MS): A comparison with secondary ion mass spectrometry (SIMS). *Geostand. Newsl.* 21, 191-203.
- Hurford, A. J., Carter, A., 1991. The role of fission track dating in discrimination of provenance. In: Morton, A. C., Todd, S. P., Haughton, P. D. W. (Eds.), *Developments in sedimentary provenance studies*. Geological Society Special Publication 57, 67-78.
- Icenhower, J., London, D. (1995) An experimental study of element partitioning among biotite, muscovite, and coexisting peraluminous silicic melt at 200 MPa (H₂O). *Am. Mineral.* 80, 1229-1251.
- Ishikawa, T., Nakamura, E. (1994) Origin of the slab component in arc lavas from across-arc variation of B and Pb isotopes. *Nature* 370, 205-208.
- Ishikawa, T., Tera, F. (1997) Source, composition and distribution of the fluid in the Kurile mantle wedge: Constraints from across-arc variations of B/Nb and B isotopes. *Earth Planet. Sci. Lett.* 152, 123-138
- Ito, E., Harris, H., Anderson, A. T., 1983. Alteration of oceanic crust and geologic cycling of chlorine and water. *Geochim. Cosmochim. Acta* 47, 1613-1624.
- Jackson, S. E., Longerich, H. P., Dunning, G. R., Fryer, B. J., 1992. The application of laser ablation microprobe inductively coupled plasma-mass spectrometry to in situ trace element determinations in minerals. *Can. Mineral.* 30, 1049-1064.
- Jamtveit, B., Bucher-Nurminen, K., Austrheim, H., 1990. Fluid controlled eclogitization of granulites in deep crustal shear zones, Bergen arcs, Western Norway. *Contrib. Mineral. Petrol.* 104, 184-193.
- Jenner, G. A., Foley, S. F., Jackson, S. E., Green, T. H., Fryer, B. J., 1993. Determination of partition coefficients for trace elements in high pressure-temperature experimental run products by laser ablation microprobe-inductively coupled plasma-mass spectrometry (LAM-ICP-MS). *Geochim. Cosmochim. Acta* 58, 5099-5103.
- Jochum, K. P., Hofmann, A. W., 1997. Constraints on earth evolution from antimony in mantle-derived rocks. *Chem. Geol.* 139, 39-49.

- Jochum, K. P., Hofmann, A. W., Seufert, H. M., 1993. Tin in mantle-derived rocks: Constraints on Earth evolution. *Geochim. Cosmochim. Acta.* 57, 3585-3595.
- Jochum, K. P., Verma, S. P., 1996. Extreme enrichment of Sb, Tl and other trace elements in altered MORB. *Chem. Geol.* 130, 289-299.
- Kretz, R., Campbell, J. L., Hoffman, E. L., Hartree, R., Teesdale, W. J., 1999. Approaches to equilibrium in the distribution of trace elements among the principal minerals in a high-grade metamorphic terrane. *J. Metamorphic Geol.* 17, 41-59.
- Kurz, W., Neubauer, F., Dachs, E., 1998a. Eclogite meso- and microfabrics: Implications for the burial and exhumation history of eclogites in the Tauern Window (eastern Alps) from P-T-d paths. *Tectonophysics* 285, 183-209.
- Kurz, W., Neubauer, F., Genser, J., Dachs, E., 1998b. Alpine geodynamic evolution of passive and active continental margin sequences in the Tauern Window (eastern Alps, Austria, Italy): A review. *Geologische Rundschau* 87, 225-242.
- Lardeaux, J. M., Caron, J.-M., Nisio, P., Péquignot, G., Boudeulle, M., 1986. Microstructural criteria for reliable thermometry in low temperature eclogites. *Lithos* 19, 187-203.
- LaTourrette, T., Hervig, R. L., Holloway, J. R., 1995. Trace element partitioning between amphibole, phlogopite, and basanite melt. *Earth Planet. Sci. Lett.* 135, 13-30.
- Leake, B. E., Wooley, A. R., Arps, C. E. S., Birch, W. D., Gilbert, M. C., Grice, J. D., Hawthorne, F. C., Kato, A., Kisch, H. J., Krivovichev, V. G., Linthout, K., Laird, J., Mandarino, J. A., Maresch, W. V., Nickel, E. H., Rock, N. M. S., Schumacher, J. C., Smith, D. C., Stephenson, N. C. N., Ungaretti, L., Whittaker, E. J. W., Youzhi, G., 1997. Nomenclature of Amphiboles: Report of the subcommittee on amphibole of the International Mineralogical Association, Commission on New Minerals and Mineral Names. *Can. Mineral.* 35, 219-246.
- Lihou, J. C., Mange-Rajetzky, M. A., 1996. Provenance of the Sardona Flysch, eastern Swiss Alps: Example of high-resolution heavy mineral analysis applied to an ultrastable assemblage. *Sediment. Geol.* 105, 141-157.
- Longerich, H. P., Guenther, D., Jackson, S. E., 1996. Elemental fractionation in laser ablation inductively coupled plasma mass spectrometry. *Fresenius J. Anal. Chem.* 355, 538-542.
- Manning, C. E., 1998. Fluid composition at the blueschist-eclogite transition in the model system Na₂O-MgO-Al₂O₃-SiO₂-H₂O-HCl. *Schweiz. Mineral. Petrogr. Mitt.* 78, 225-242.
- Matthews, A., Liati, A., Mposkos, E., Skarpelis, N. (1996) Oxygen isotope geochemistry of the Rhodope polymetamorphic terrain in northern Greece: Evidence for preservation of pre-metamorphic isotopic compositions. *Eur. J. Mineral.* 8, 1139-1152.
- May, T. W., Wiedmeyer, R. H., 1998. A table of polyatomic interferences in ICP-MS. *Atomic Spectroscopy* 19, 150-155.
- McCulloch, M. T., Gamble, J. A. (1991) Geochemical and geodynamical constraints on subduction zone magmatism. *Earth. Planet. Sci. Lett.* 102, 358-374.
- McDonough, W. F., 1991. Partial melting of subducted oceanic crust and isolation of its residual eclogitic lithology. *Phil. Trans. R. Soc. Lond. A* 335, 407-418.
- McDonough, W. F., 1999. How well do we know the siderophile element signature of the silicate earth?. *EOS* 80, 250.
- McDonough, W. F., Sun S. (1995) The composition of the Earth. *Chem. Geol.* 120, 223-253.

- Melson, W. G., Byerly, G. R., Nelen, J. A., O'Hearn, T., Wright, T. L., Vallier, T., 1977. A catalog of the major element chemistry of abyssal glasses. *Smithsonian Contrib. Earth Sci.* 19, 31-60.
- Melzer, S., Gottschalk, M., Heinrich, W., 1998. Experimentally determined partitioning of Rb between richterites and aqueous (Na, K)-chloride solutions. *Contrib. Mineral. Petrol.* 133, 315-328.
- Melzer, S., Wunder, B., 1999. Experimentally determined K-Rb-Cs exchange coefficients between micas, amphiboles and aqueous chloride solutions between 0.2 and 4 GPa. *EOS* 80, 361.
- Messiga, B., Kienast, J. R., Rebay, G., Riccardi, M. P., Tribuzio, R., 1999. Cr-rich magnesiochloritoid eclogites from the Monviso ophiolites (Western Alps, Italy). *J. Metamorphic Geol.* 17, 287-299.
- Messiga, B., Tribuzio, R., Bottazzi, P., Ottolini, L., 1995. An ion microprobe study on trace element composition of clinopyroxenes from blueschist and eclogitized Fe-Ti-gabbros, Ligurian Alps, northwestern Italy: Some petrologic considerations. *Geochim. Cosmochim. Acta* 59, 59-75.
- Meyre, C., de Capitani, C., Partzsch, J. H., 1997. A ternary solid solution model for omphacite and its application to geothermobarometry of eclogites from the Middle Adula nappe (Central Alps, Switzerland). *J. Metamorphic Geol.* 15, 687-700.
- Meyre, C., de Capitani, C., Zack, T., Frey, M., 1999. Petrology of high-pressure metapelites from the Adula nappe (Central Alps, Switzerland). *J. Petrol.* 40, 199-213.
- Meyre, C., Frey, M., 1998. Eclogite facies metamorphism and deformation of the middle Adula nappe (Central Alps, Switzerland): Excursion to Trescolmen. *Schweiz. Mineral. Petrogr. Mitt.* 78, 355-362.
- Meyre, C., Puschig, A. R., 1993. High-pressure metamorphism and deformation at Trescolmen, Adula nappe, Central Alps. *Schweiz. Mineral. Petrogr. Mitt.* 73, 277-283.
- Mezger, K., Hanson, G. N., Bohlen, S. R., 1989. High-precision U-Pb ages of metamorphic rutile: Application to cooling history of high-grade terranes. *Earth Planet. Sci. Lett.* 96, 106-118.
- Miller, C., Stosch, H.-G., Hoernes, S., 1988. Geochemistry and origin of eclogites from the type locality Koralpe and Saualpe, Eastern Alps, Austria. *Chem. Geol.* 67, 103-118.
- Miller, C., Thöni, M., 1995. Origin of eclogites from the Austroalpine Ötztal basement (Tirol, Austria): Geochemistry and Sm-Nd vs. Rb-Sr isotope systematics. *Chem. Geol.* 122, 199-225.
- Moriguti, T., Nakamura, E. (1998) Across-arc variation of Li isotopes in lavas and implications for crust/mantle recycling at subduction zones. *Earth Planet. Sci. Lett.* 163, 167-174.
- Morimoto, N., Fabries, J., Ferguson, A.K., Ginzburg, I.V., Ross, M., Seifert, F.A., Zussman, J., 1988. Nomenclature of pyroxene. *Am. Mineral.* 73, 1123-1133.
- Morton, A. C., 1991. Geochemical studies of detrital heavy minerals and their application to provenance analysis. In: Morton, A. C., Todd, S. P., Haughton, P. D. W. (Eds.), *Developments in sedimentary provenance studies. Geological Society Special Publication* 57, 31-45.
- Muehlenbachs, K. (1986) Alteration of the oceanic crust and the $\delta^{18}\text{O}$ history of seawater. In: Valley, J. W., Taylor, H. P. Jr., O'Neill, J. R. (eds) *Stable isotopes in high temperature geological processes. Rev. Mineral.* 16, 425-444.
- Münker, C., 1998. Nb/Ta fractionation in a Cambrian arc/back arc system, New Zealand: Source constraints and application of refined ICPMS techniques. *Chem. Geol.* 144, 23-45.
- Nabelek, P. I. (1987) General equations for modeling fluid/rock interaction using trace elements and isotopes. *Geochim. Cosmochim. Acta* 51, 1765-1769.
- Nabelek, P. I., Labotka, T. C. (1993) Implications of geochemical fronts in the Notch Peak contact-metamorphic aureole, Utah, USA. *Earth Planet. Sci. Lett.* 119, 539-559.

- Nadeau, S., Philippot, P., Pineau, F. (1993) Fluid inclusion and mineral isotopic compositions (H-C-O) in eclogitic rocks as tracers of local fluid migration during high-pressure metamorphism. *Earth Planet. Sci. Lett.* 114, 431-448.
- Nagasaki, A., Enami, M., 1998. Sr-bearing zoisite and epidote in ultra-high pressure (UHP) metamorphic rocks from the Su-Lu province, eastern China: An important Sr reservoir under UHP conditions. *Am. Mineral.* 83, 240-247.
- Najorka, J., Gottschalk, M., Franz, G., Heinrich, W., 1999. Ca-Sr distribution among amphibole, clinopyroxene, and chloride-bearing solutions. *Am. Mineral.* 84, 596-606.
- Newsom, H. E., White, W. M., Jochum, K. P., Hofmann, A. W., 1986. Siderophile and chalcophile element abundances in oceanic basalts, Pb isotope evolution and growth of the Earth's core. *Earth. Planet. Sci. Lett.* 80, 299-313.
- Newsom, H. E., Sims, K. W. W., Noll, P. D., Jaeger, W. L., Maehr, S. A., Beserra, T. B., 1996. The depletion of tungsten in the bulk silicate earth: Constraints on core formation. *Geochim. Cosmochim. Acta* 60, 1155-1169.
- Nicholls, I. A., Ringwood, A. E., 1973. Effect of water on olivine stability in tholeiites and the products of silica-saturated magmas in the island-arc environment. *J. Geol.* 81, 285-300.
- Noll, P. D., Newsom, H. E., Leeman, W. P., Ryan, J. G., 1996. The role of hydrothermal fluids in the production of subduction zone magmas: Evidence from siderophile and chalcophile trace elements and boron. *Geochim. Cosmochim. Acta* 60, 587-611.
- Okay, A.I., 1995. Paragonite eclogites from Dabie Shan, China: Re-equilibration during exhumation? *J. Metamorphic Geol.* 13, 449-460.
- Oliver, N. H. S. (1996) Review and classification of structural controls on fluid flow during regional metamorphism. *J. Metam. Geol.* 14, 477-492.
- Peacock, S. M. (1993) The importance of blueschist -> eclogite dehydration reactions in subducting oceanic crust. *Geol. Soc. Am. Bull.* 105, 684-694.
- Pearce, J. A., Cann, J. R., 1973. Tectonic setting of basic volcanic rocks determined using trace element analyses. *Earth Planet. Sci. Lett.* 19, 290-300.
- Pearce, N. J. G., Perkins, W. T., Westgate, J. A., Gorton, M. P., Jackson, S. E., Neal, C. R., Chenery, S. P., 1997. A compilation of new and published major and trace element data for NIST SRM 610 and NIST SRM 612 glass reference materials. *Geostand. Newsl.* 21, 115-144.
- Pennacchioni, G., 1996. Progressive eclogitization under fluid-present conditions of pre-Alpine mafic granulites in the Austroalpine Mt Emilius Klippe (Italian Western Alps). *J. Struc. Geol.* 18, 549-561.
- Philippot, P., Roermund, H. L. M. v., 1992. Deformation processes in eclogitic rocks: Evidence for the rheological delamination of the oceanic crust in deeper levels of subduction zones. *J. Struc. Geol.* 14, 1059-1077.
- Philippot, P., Selverstone, J., 1991. Trace-element-rich brines in eclogitic veins: Implications for fluid composition and transport during subduction. *Contrib. Mineral. Petrol.* 106, 417-430.
- Plank, T., Johnson, M. (1997) Experimental study of trace-element partitioning in fluids and melts generated during sediment subduction. 7.th Annual V.M. Goldschmidt Conference, 164
- Plank, T., Langmuir, C. H. (1998) The chemical composition of subducting sediment and its consequence for the crust and mantle. *Chem. Geol.* 145, 325-394.
- Poli, S., Schmidt, M. W. (1995) H₂O transport and release in subduction zones: Experimental constraints on basaltic and andesitic systems. *J. Geophys. Res.* 100B, 22299-22314.

- Powell, R., Holland, T., Worley, B., 1998. Calculating phase diagrams involving solid solutions via non-linear equations, with examples using THERMOCALC. *J. Metamorphic Geol.* 16, 577-588.
- Preston, J., Hartley, A., Hole, M., Buck, S., Bond, J., Mange, M., Still, J., 1998. Integrated whole-rock trace element geochemistry and heavy mineral chemistry studies: Aids to the correlation of continental red-bed reservoir in the Beryl Field, UK North Sea. *Petroleum Geoscience* 4, 7-16.
- Puchelt, H., Emmermann, R., 1983. Petrogenetic implications of tholeiitic basalt glasses from the East Pacific Rise and the Galapagos Spreading Center. *Chem. Geol.* 38, 39-56.
- Putlitz, B., Matthews, A., Valley, J., Katzir, Y. (1997) Laser probe oxygen isotope studies of metagabbros (Cyclades, Greece): Implications for subduction processes. *Terra Nova Abstr. suppl.* 9, 27.
- Reid, J. E., 1998. The development and geological application of a whole-rock-LA-ICP-MS technique for the determination of high field strength elements. M.S. thesis, Memorial University of Newfoundland.
- Rice, C. M., Darke, K. E., Still, J. W., 1998. Tungsten-bearing rutile from the Kori Kollo gold mine, Bolivia. *Mineral. Mag.* 62, 421-429.
- Ringwood, A. E. (1974) Petrological evolution of island arc systems. *J. Geol. Soc. London* 130, 183-204.
- Rudnick, R. L., 1998. Rutiles in eclogites; a missing Earth reservoir found?. *Abstr. with programs- Geol. Soc. Am.* 30 (7), 207.
- Ryan, J. G., Morris, J., Tera, F., Leeman, W. P., Tsetkov, A., 1995. Cross-arc geochemical variations in the Kurile arc as a function of slab depth. *Science*. 270, 625-627.
- Santini, L., 1992. Geochemistry and geochronology of the basic rocks of the Penninic Nappes of East-Central Alps (Switzerland). Ph.D. thesis, Université de Lausanne.
- Saunders, A. D., Tarney, J., Weaver, S. D., 1980. Transverse geochemical variations across the Antarctic Peninsula: Implications for the genesis of calc-alkaline magmas. *Earth Planet. Sci. Lett.* 46, 344-360.
- Schilling, J. G., Zajac, M., Evans, R., Johnston, T., White, W., Devine, J. D., Kingsley, R., 1985. Petrologic and geochemical variations along the Mid-Atlantic Ridge from 29° N to 73° N. *Am. J. Sci.* 283, 510-586.
- Schmidt, M. W. (1993) Phase relations and compositions in tonalite as a function of pressure: An experimental study at 650° C. *Am. J. Sci.* 293, 1011-1060.
- Schmidt, M. W. (1996) Experimental constraints on recycling of potassium from subducted oceanic crust. *Science* 272, 1927-1930
- Schmidt, M. W., Poli, S., 1998. Experimental based water budgets for dehydrating slabs and consequences for arc magma generation. *Earth Planet. Sci. Lett.* 163, 361-379.
- Schumacher, J. C. (1997) Appendix 2: The estimation of the proportion of ferric iron in the electron-microprobe analysis of amphiboles. *Can. Mineral.* 35, 238-246.
- Seifert, K. E., Chang, C.-W., Brunotte, D. A. (1997) Evidence from ocean drilling program Leg 149 mafic igneous rocks for oceanic crust in the Iberia abyssal plain ocean-continent transition zone. *J. Geophys. Res.* 102, 7915-7928.
- Shannon, R. D., 1976. Revised effective ionic radii and systematic studies of interatomic distances in halides and chalcogenides. *Acta Cryst. A* 32, 751-767.
- Shibata, T., Nakamura, E. (1997) Across-arc variations of isotope and trace element compositions from Quaternary basaltic volcanic rocks in northeastern Japan: Implications for interaction between subducted oceanic slab and mantle wedge. *J. Geophys. Res.* 102, 8051-8064.
- Sircombe, K. N., 1996. Provenance of heavy detrital minerals in coastal sands and sedimentary rocks of Eastern Australia using the SHRIMP ion probe. *Abstr. with programs- Geol. Soc. Am.* 28(7), 279.

- Skulski, T., Minarik, W., Watson, E.B., 1994. High-pressure experimental trace-element partitioning between clinopyroxene and basaltic melts. *Chem. Geol.* 117, 127-147.
- Sorensen, S. S., Grossman, J. N., 1989. Enrichment of trace elements in garnet amphibolites from a paleo-subduction zone: Catalina Schist, California. *Geochim. Cosmochim. Acta* 53, 3155-3177.
- Sorensen, S. S., Grossman, J. N., Perfit, M. R. (1997) Phengite-hosted LILE enrichment in eclogite and related rocks: Implications for fluid-mediated mass transfer in subduction zones and arc magma genesis. *J. Petrol.* 38, 3-34.
- Stalder, R., Foley, S. F., Brey, G. P., Horn, I., 1998. Mineral-aqueous fluid partitioning of trace elements at 900°C-1200°C and 3.0 GPa to 5.7 GPa: New experimental data set for garnet, clinopyroxene and rutile and implications for mantle metasomatism. *Geochim. Cosmochim. Acta* 62, 1781-1801.
- Staudigel, H., Hart, S. R. (1983) Alteration of basaltic glass: Mechanisms and significance of oceanic crust-seawater budget. *Geochim. Cosmochim. Acta* 47, 337-350.
- Staudigel, H., Plank, T., White, B., Schmincke, H.-U., 1996. Geochemical fluxes during seafloor alteration of the basaltic upper oceanic crust: DSDP sites 417 and 418. In: *Subduction: Top to Bottom, Geophysical Monograph* 96, 19-38.
- Stolz, A. J., Jochum, K. P., Spettel, B., Hofmann, A. W., 1996. Fluid- and melt-related enrichment in the subarc mantle: Evidence from Nb/Ta variations in island-arc basalts. *Geology* 24, 587-590.
- Stüwe, K., Powell, R. (1995) PT paths from modal proportions: Application to the Koralm Complex, Eastern Alps. *Contrib. Mineral. Petrol.* 119, 83-93.
- Sun, S., McDonough, W. F. (1989) Chemical and isotopic systematics of oceanic basalts: Implications for mantle composition and processes. In: Saunders A. D., Norry M. J. (ed) *Magmatism in the Ocean Basins*. *Geol. Soc. Spec. Publ.* 42, 313-345.
- Taylor, R. P., Jackson, S. E., Longrich, H. P., Webster, J. D. (1997) In situ trace-element analysis of individual silicate melt inclusions by laser ablation inductively coupled plasma-mass spectrometry (LAM-ICP-MS). *Geochim. Cosmochim. Acta* 61, 2559-2567.
- Taylor, S. R., McLennan, S. M. (1985) *The Continental Crust: Its composition and composition*. Blackwell
- Tera, F., Brown, L., Morris, J., Sacks, I. S. (1986) Sediment incorporation in island-arc magmas: Inferences from ¹⁰Be. *Geochim. Cosmochim. Acta* 50, 535-550.
- Tribuzio, R., Messiga, B., Vannucci, R., Bottazzi, P., 1996. Rare earth element redistribution during high-pressure low-temperature metamorphism in ophiolitic Fe-gabbros (Liguria, northwestern Italy): Implications for light REE mobility in subduction zones. *Geology* 24, 711-714.
- Volfinger, M., 1976. Effet de la température sur les distributions de Na, Rb et Cs entre la sanidine, la muscovite, la phlogopite et une solution hydrothermale sous une pression de 1 kbar. *Geochim. Cosmochim. Acta* 40, 267-282.
- Watson, E. B., 1996. Surface enrichment and trace-element uptake during crystal growth. *Geochim. Cosmochim. Acta* 60, 5013-5020.
- Watson, E. B., Lupulescu, A. (1993) Aqueous fluid connectivity and chemical transport in clinopyroxene-rich rocks. *Earth Planet. Sci. Lett.* 117, 279-294.
- Widmer, T.W., 1996. Entwässerung ozeanisch alterierter Basalte in Subduktionszonen (Zone von Zermatt- Saas Fee). Ph.D., ETH Zürich.

- Will, T., Okrusch, M., Schmädicke, E. (1998) Phase relations in the greenschist-blueschist-amphibolite-eclogite facies in the system $\text{Na}_2\text{O}-\text{CaO}-\text{FeO}-\text{MgO}-\text{Al}_2\text{O}_3-\text{SiO}_2-\text{H}_2\text{O}$ (NCFMASH), with application to metamorphic rocks from Samos, Greece. *Contrib. Mineral. Petrol.* 132, 85-102.
- Winchester, J.A., Floyd, P.A., 1977. Geochemical discrimination of different magma series and their differentiation products using immobile elements. *Chem. Geol.* 20, 325-343.
- Woodhead, J. D., Johnson R. W. (1993) Isotopic and trace-element profiles across the New Britain island arc, Papua New Guinea. *Contrib. Mineral. Petrol.* 113, 479-491.
- Yang, P., Rivers, T., Jackson, S., 1999. Crystal-chemical and thermal controls on trace-element partitioning between co-existing garnet and biotite in metamorphic rocks from Western Labrador. *Can. Mineral.* 37, 443-468.
- Yuen, D. A., Fleitout, L., Schubert, G., Froideveaux, C., 1977. Shear deformation zones along major transform faults and subducting slabs. *Geophys. J. Roy. Astron. Soc.* 54, 93-119.
- Zack, T., Foley, S. F., 1997. First laser ablation microprobe measurements of trace-element partitioning between hydrous phases in high-pressure metamorphic rocks. In: 7th An. V.M. Goldschmidt Conf., LPI Contrib. No. 921, Lunar and Planetary Institute, Houston, p. 226.
- Zack, T., Foley, S. F., Jenner, G. A. (1997) A consistent partition coefficient set for clinopyroxene, amphibole and garnet from laser ablation microprobe analysis of garnet pyroxenites from Kakanui, New Zealand. *N. Jb. Miner. Abh.* 172, 23-41.

Acknowledgments

I like to thank my advisers, Stephen Foley and Toby Rivers, for their continuous support and spirit of lively discussion. This work could not have been realized in this form without the freedom in research they always allowed me.

C.A. Heinrich and Christian Meyre are thanked for patient discussions about Adula geology with a "fishhead" like me and for donating samples. Christian Meyre is also thanked for the effective co-operation and for spending a good time with Stephen Foley and me in the field.

I. Horn, S.E. Jackson, P. Sylvester and M. Tubrett are thanked for invaluable help and innumerable advice concerning the marvellous laser ablation ICP-MS facility at Memorial University.

Furthermore I would like give a special thanks to H.-P. Meyer (Heidelberg) and A. Kronz (Göttingen) for their help with the perfectly maintained electron microprobes in their labs.

P. King and G. Hartmann (XRF), L. Hewa (solution-ICP-MS) and J. Reid (whole rock- laser ablation-ICP-MS) are thanked for conducting some of the measurements used in this study.

This work was shaped in a significant way through discussions and criticism from my colleagues and friends in the geo-community. Of course, I have to acknowledge first the veterans and active members of Foley's Pub, which are, to name only a few, M. Barth, R. Brumm, S. Buhre, D. Jacob, S. Melzer, F. Schäfer, B. Schmickler, R. Stalder and E. Zinngrebe. But I am also grateful for the time and spirit I received from members of the Geochemisches Institut (Göttingen), most of all P. Cartigny, F. Dorendorf and K. Simon and from members of the Earth Science Department of the Memorial University, which are besides others R.A. Cox, G. Dobosi, C. Petibon and P. Yang.

Help, advice, and discussions are also greatly appreciated from G.E. Bebout, F. Brenker, K. Domanik, M. Frey, D. Günther, J. Hoefs, A. Indares, G.A. Jenner, J. Mosenfelder, C. Münker, P. O'Brien, J. Partzsch, M. Pfiffner, S. Poli, S. Sorensen, V. Trommsdorff and G. Wörner.

I would also like to thank J. Halfar, M. Halfar-Formentes, J. Lezaun, M. Sachse and A. Wanke and last, but never least, my parents for the time they shared with me in the beautiful Trescolmen area.

This work was supported by the DFG (Fo 181/10-1) and NSERC.

Lebenslauf

Am 19.3.1968 wurde ich als Sohn von Käthe Zack, geborene Schnackenberg, und Dieter Zack in Bremen geboren. Von 1974 bis 1975 besuchte ich die Grundschule in Bremen, von 1975 bis 1980 die Grund- und Orientierungsschule in Ottersberg und von 1980 bis 1988 das Gymnasium in Achim. Das Abitur erlangte ich im Mai 1988. Anschließend studierte ich von 1988 bis 1990 an der Universität Heidelberg Mineralogie und Geologie und absolvierte 1990 das Vordiplom in Geologie. Danach verbrachte ich von 1990 bis 1991 ein Jahr als Austauschstudent an der University of Pennsylvania, Philadelphia, USA. Seit 1991 bin ich an der Universität Göttingen in den Fächern Mineralogie und Geologie eingeschrieben. Nach Annahme meiner Diplomarbeit mit dem Titel "Petrologische und geochemische Untersuchungen an Granatpyroxeniten aus Kakanui (Neuseeland)" erlangte ich mein Diplom in Mineralogie im April 1995. Seit 1995 beschäftige ich mich am Mineralogisch-Petrologischen Institut der Universität Göttingen und am Earth Science Department der Memorial University of Newfoundland, St. John's, Kanada unter Betreuung von Priv. Doz. Dr. Stephen F. Foley und Prof. Toby Rivers mit der hier vorliegenden Arbeit.